Chapter 6
Boiling in Micro-Channels

The subject of Chap. 6 is boiling in micro-channels. Several aspects of boiling are also considered for conventional size channels and comparison with micro-channels was carried out. Significant differences of ONB in micro-channels have been discussed compared to conventional channels. Effect of dissolved gases on boiling in water and surfactant solution was revealed. Attention was paid on pressure drop and heat transfer, critical heat flux and instabilities during flow boiling in micro-channels.

6.1 Onset of Nucleate Boiling in Conventional Size Channels

In this section the general approach used to describe the parameters corresponding to the onset of nucleate boiling (ONB) in a single channel are considered, and models and experiments are compared. The mode of ONB in parallel micro-channels is presented in Sect. 6.2. We will also look at the effect of dissolved gases on ONB during flow boiling of water and surfactant solutions in micro-channels. Section 6.3 deals with the dynamics of vapor bubble in a single micro-channel and in parallel micro-channels. Pressure drop in two-phase flow boiling in parallel micro-channels is considered in Sect. 6.4. In this section we look at a new correlation incorporating the effects of both channel size and coolant mass velocity, which shows better accuracy than prior correlations. In Sect. 6.4 heat transfer correlations in two-phase flow boiling in parallel micro-channels are examined and correlations based on the Martinelli parameter are considered. Parameters that affect the explosive boiling are discussed in Sect. 6.5. Existing critical heat flux (CHF) correlations for flow boiling of water with available databases taken from small-diameter channels are also evaluated.

L.P. Yarin, *Fluid Flow, Heat Transfer and Boiling in Micro-Channels*

6.1.1 Models for Prediction of Incipient Boiling Heat Flux and Wall Superheat

The onset of bubble nucleation usually requires that the temperature on the heated surface exceeds the saturation temperature of the liquid corresponding to a given pressure. There has been a great deal of analysis on bubble nucleation and a number of semi-empirical models of boiling incipience have been proposed during the past few decades (Carey 1992; Dhir 1998). Two general approaches were used to describe the parameters corresponding to the onset of nucleate boiling. The first is based on analysis of the behavior of a single bubble on a rough surface where the temperature of the surrounding liquid exceeds the saturation temperature. The second approach considers vapor bubbles generated in liquid (homogeneous nucleation), on a surface or at a corner (heterogeneous nucleation) based on the classical kinetics of nucleation.

The first approach developed by Hsu (1962) is widely used to determine ONB in conventional size channels and in micro-channels (Sato and Matsumura 1964; Davis and Anderson 1966; Celata et al. 1997; Qu and Mudawar 2002; Ghiaasiaan and Chedester 2002; Li and Cheng 2004; Liu et al. 2005). These models consider the behavior of a single bubble by solving the one-dimensional heat conduction equation with constant wall temperature as a boundary condition. The temperature distribution inside the surrounding liquid is the same as in the undisturbed near-wall flow, and the temperature of the embryo tip corresponds to the saturation temperature in the bubble $T_{S,b}$. The vapor temperature in the bubble can be determined from the Young–Laplace equation and the Clausius–Clapeyron equation (assuming a spherical bubble):

$$T_{S,b} - T_S = \frac{2\sigma T_S}{h_{LG}\rho_G r_b} \tag{6.1}$$

where σ is the surface tension, h_{LG} is the latent heat of vaporization, ρ_G is the vapor density, and r_b is the radius of bubble embryo assumed to be proportional to the radius of the cavity r_c.

The temperature distribution in the undisturbed fluid over the heated surface is described by the equation

$$\frac{\partial\theta}{\partial t} = \alpha\frac{\partial^2\theta}{\partial y^2} \tag{6.2}$$

where $\theta = T - T_\infty$, T_∞ is the temperature of the surrounding fluid, α is the thermal diffusivity.

Integrating Eq. (6.2) with the initial and boundary conditions

$$\begin{array}{lll} t = 0, & 0 \le y \le \delta, & \theta = 0 \\ t > 0, & y = 0, & \theta = \theta_w \end{array} \tag{6.3}$$

leads to the following expression for the liquid temperature

$$\frac{\theta}{\theta_w} = \eta + \frac{2}{\pi}\sum_{n=1}^{\infty}\frac{\cos\pi n}{n}\exp(-n^2\pi^2\mathrm{Fo})\sin\pi n\eta \tag{6.4}$$

where $\theta_w = T_w - T_\infty$, $\eta = y/\delta$, $\mathrm{Fo} = 2\alpha t/\delta^2$ is the Fourier number, δ is the thickness of thermal boundary layer, t is the time, y is the distance from the wall.

From Eqs. (6.1) and (6.4) one can find the limiting values of the cavity radius of active sizes on the heated surface

$$r_{crit} = \frac{\delta}{4}\left(1 - \frac{\theta_S}{\theta_w} \pm \sqrt{\left(1 - \frac{\theta_S}{\theta_w}\right)^2 - \frac{12.8\sigma T_S}{\rho_G h_{LG}\delta\theta_w}}\right) \tag{6.5}$$

where plus and minus signs on the right-hand side of Eq. (6.5) correspond to maximum and minimum active cavity, respectively.

It should be stressed that such models are valid only when the medium is continuous. Measurements by Ye et al. (2004) showed that bubble nucleation in water may be considered as continuous when $r_c \geq 10\,\mathrm{nm}$.

Thermodynamic and mechanical equilibrium on a curved vapor–liquid interface requires a certain degree of superheat in order to maintain a given curvature. Characteristics of homogeneous and heterogeneous nucleation can be estimated in the frame of classical theory of kinetics of nucleation (Volmer and Weber 1926; Farkas 1927; Becker and Doring 1935; Zel'dovich 1943). The vapor temperature in the bubble $T_{S,b}$ can be computed from equations (Bankoff and Haute 1957; Cole 1974; Blander and Katz 1975; Li and Cheng 2004) for homogeneous nucleation in superheated liquids

$$J_{hom} = N_0\left(\frac{kT_{S,b}}{h}\right)\exp\left(-\frac{16\pi\sigma^3}{3kT_{S,b}(P_G - P_L)}\right) \tag{6.6}$$

for heterogeneous nucleation on a surface

$$J_{het} = N_0^{2/3}\psi\left(\frac{kT_{S,b}}{h}\right)\exp\left(-\frac{16\pi\sigma^3\omega}{3kT_{S,b}(P_G - P_L)^2}\right) \tag{6.7}$$

where J is the bubble nucleation density, N_0 is the molecule number per unit volume, k is the Boltzmann constant, P_G is the pressure in a bubble, P_L is the pressure in liquid, and $h = kT_{S,b}/\left(2\sigma/\pi mB\right)^{0.5}$, where m is the mass of molecule, $B \approx 2/3$. The term ω is the geometric correction factor for the minimum work required to form the critical nucleus (for heterogeneous nucleation on a smooth surface with no cavities, $\omega = (1/2)(1+\cos\theta)$; $\psi = (1/4)(1+\cos\theta)^2(2-\cos\theta)$, θ is the contact angle).

Using the Clausius–Clapeyron equation and Eqs. (6.6) and (6.7) one can obtain the saturation temperature in the bubble $T_{S,b}$ (Li and Cheng 2004):

$$T_{S,b} - T_S = \frac{T_S}{h_{LG}\rho_G}\sqrt{\frac{16\pi\sigma^3\omega}{3kT_{S,b}\ln(N_0 kT_{S,b}\psi/J\cdot h)}}. \tag{6.8}$$

6.1.2 Comparison Between Models and Experiments

There are a number of experiments directed at studying the incipience of nucleate boiling in heated channels of hydraulic diameter $d_h = 0.04-20\,\mathrm{mm}$. The overall

Table 6.1 Onset of nucleate boiling. Characteristics of experiment

Author	Channel geometry	Hydraulic diameter (mm)	Mass flux (kg/m^2s)	Fluid	Heat flux (kW/m^2)	Pressure (MPa)
Bergles and Rohsenow (1964)	Cylindrical tube	2.387	$(2.1–19.4) \times 10^3$	Distilled water	1,890–18,900	0.261
Sato and Matsumara (1964)	Cylindrical tube	–	–	Water	100–750	0.1
Unal (1975)	Cylindrical tube	4–20	132–2,818	Water; refrigerant-22	20–1,920	0.1–15.8
Hino and Ueda (1985)	Cylindrical tube	7.0	158–1,600	Fluorocarbon R-113	11.78–46.90	0.147
Kennedy et al. (2000)	Cylindrical tube	1.17, 1.45	800–4,500	De-ionized and de-gassed water	0–4,000	0.344–1.034
Hapke et al. (2000)	Cylindrical tube	1.5	100–500	De-ionized water	50–200	0.1
Hetsroni et al. (see this book)	Cylindrical tube	1.07	49–146	Distilled water	62–162	0.1
Stoddard et al. (2002)	Annular channel	0.724–1.0	85–1,428	Fully de-gassed water	124–1,000	0.344–1.034
Su et al. (2001)	Annular channel	1.0, 1.5	45–180	Pure water	40–210	0.2–3.5
Qu and Mudawar (2002)	Rectangular channel	0.231×0.713	130–1,440	De-ionized water	200–2,000	0.12
Liu et al. (2005)	Rectangular channel	0.275×0.636	309–883	De-ionized water	100–730	0.1
Lee et al. (2004)	Trapezoidal channel	0.413	170–899	De-ionized water	1.49–500	0.161

characteristics of experiments are presented in Table 6.1. Measurements of hydrodynamic and thermal parameters corresponding to onset of nucleate boiling (ONB) were performed in circular, annular, rectangular, and trapezoidal channels, and water, refrigerant-22, and fluorocarbon R-113 were used as working fluid. ONB was recorded by various ways: analysis of the pressure drop-mass flux characteristic curve; relation between the heat flux and the wall superheat at the start point of the sharp drop in wall temperature ($\Delta T_{S,ONB} = T_{W,ONB} - T_S$, where $T_{W,ONB}$ and T_S is the temperature of the heated wall, corresponding to onset of nucleate boiling and saturation temperature, respectively); visual detection of bubble growth and departure from the heated wall. Experiments were carried out in the range of mass flux $G = 45-2{,}100\,\mathrm{kg/m^2s}$, heat flux $q = 1.49-18{,}900\,\mathrm{kW/m^2}$, and pressure $P = 0.1-15.8\,\mathrm{MPa}$.

Wall superheat

Bergles and Rohsenow (1964) studied the wall superheat that corresponded to the nucleate boiling of distilled water in a stainless steel tube of inner diameter $d = 2.387\,\mathrm{mm}$. The measurements of $\Delta T_{S,ONB} = T_{W,ONB} - T_S$ corresponding to the ONB were performed at different values of inlet temperature, T_{in}, in the range of inlet velocity $U_{in} = 3.74-19.42\,\mathrm{m/s}$, and Reynolds number corresponding to inlet parameters $\mathrm{Re} = 9 \times 10^3 - 2 \times 10^5$. Wall temperature measurements were taken at the heated length to the tube diameter ratio of $L/d = 29$ and 48. Experiments were restricted to low heat fluxes. This usually limits subcooled-boiling tests to the region of low wall superheat.

During the subcooled nucleate flow boiling of a liquid in a channel the bulk temperature of the liquid at ONB, T_B, is less than the saturation temperature, and at a given value of heat flux the difference $\Delta T_{sub,ONB} = T_S - T_B$ depends on L/d. The experimental parameters are presented in Table 6.2.

Table 6.2 shows that the ratio of $q_{ONB}/\rho U_{in} c_p$ changes relatively weakly in the range of wide variation of heat flux and inlet flow velocity. The wall superheat significantly depends on heat flux. The data of Bergles and Rohsenow (1964) are shown in Fig. 6.1. This dependence is close to $\Delta T_{S,ONB} \sim q_{ONB}^{0.5}$. The results presented by

Table 6.2 Parameters of experiments by Bergles and Rohsenow (1964)

Inlet velocity	Inlet temperature		Subcooling		Heat flux	Wall superheat	Parameter	
	$L_{ONB}/d = 29$	$L_{ONB}/d = 48$	$L_{ONB}/d = 29$	$L_{ONB}/d = 48$			$L/d = 29$	$L/d = 48$
U_{in} [m/s]	T_{in} [°C]		$\Delta T_{sub,ONB}$ [K]		q_{ONB} [MW/m^2]	$\Delta T_{S,ONB}$ [K]	$q_{ONB}/\rho_{ONB} U_{in} c_p$ [K]	
19.42	8	40	108.3	66.6	9.974	27	0.126	0.126
9.54	13	52	103.3	50	5.67	19.4	0.149	0.146
2.145	22	47	92.2	56.6	3.71	12.2	0.144	0.144

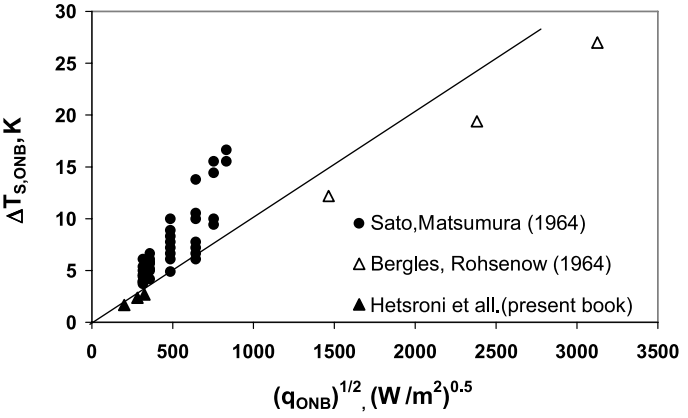

Fig. 6.1 Dependence of wall superheat on heat flux

Sato and Matsumura (1964) and the results of flow boiling in the 1.07 mm tube with average roughness of $k_s = 0.29\,\mu m$, obtained in the range of Reynolds number Re = 50–150 by Hetsroni et al. are also shown in Fig. 6.1. The values of $\Delta T_{S,ONB}$ presented by Sato and Matsumura (1964) are higher than those obtained at the same heat flux by Bergles and Rohsenow (1964), and Hetsroni et al. According to studies by Hsu (1962), Sato and Matsumura (1964), Davis and Anderson (1966), Kandlikar et al. (1997), and Liu et al. (2005) one can conclude that $\Delta T_{S,ONB} \sim q_{ONB}^{0.5}$

$$q_{ONB} = M \frac{k_L h_{LG} \rho_G}{\sigma T_S} \Delta T_{S,ONB}^2 \tag{6.9}$$

where M is constant in a wide range of $q_{ONB} = 10^3 - 10^6\,W/m^2$, and k_L, ρ_G, σ are the thermal conductivity of liquid, the vapor density, and the surface tension, respectively. For example M is $1/12$ in Hsu (1962), $1/8$ in Sato and Matsumura (1964), $1/8(1+\cos\theta)$ in Davis and Anderson (1966), where θ is contact angle, and $1/9.2$ (Kandlikar et al. 1997).

Experiments by Bergles and Rohsenow (1964) corresponded to boiling incipience in relatively short channels when subcooling of the working fluid at the ONB point was about $\Delta T_{sub,ONB} = 50-100\,K$, where $\Delta T_{sub,ONB} = T_S - T_{B,ONB}$ and $T_{B,ONB}$ is the bulk (mean mass) fluid temperature at the channel cross-section, where ONB occurs. Unal (1975) studied the incipience of boiling at relatively high values of L_{ONB}/d_h. The experimental determination of the ONB in this study has been carried out in such a way: The number of bubbles appearing on the developed films have been counted for different inlet temperatures at a constant heat flux q, pressure P, and mass flux G. It was observed that not all the bubbles were attached to the wall of the test section, but some were in the bulk of the flow. In these experiments the value of $\Delta T_{sub,ONB}$ did not exceed 4.3 K.

Heat transfer characteristics during flow boiling of water in the $d = 1.5$ mm tube were studied by Hapke et al. (2000). The measured roughness was on the order

of magnitude of 5 μm. The axial distribution of the external wall temperature was measured using the thermographic method. The temperature reached a maximum at the initial point after the single-phase liquid heating. A wall superheat occurred at this point. The local temperature varied near the initial point when the boiling started. Amplitudes of 2 K with a frequency of approximately 2 Hz were achieved. The results measured were compared with those presented by Sato and Matsumura (1964) and by Bergles and Rohsenow (1964). A satisfactory agreement existed only for heat fluxes of about $q = 50\,\mathrm{W/m^2}$. However, the wall has to be superheated to a relatively great extent to initiate the nucleate boiling in the experiments by Hapke et al. (2000) compared to those reported by Sato and Matsumura (1964) and by Bergles and Rohsenow (1964). A mass flux dependence of the wall superheat was reported by Hapke et al. (2000). Figure 6.2 shows the dependence of ΔT_S on the parameter q_{ONB}/G.

Qu and Mudawar (2002) performed experiments to measure the incipient boiling heat flux q_{ONB}, in a heat sink containing 21 rectangular micro-channels 231 μm wide and 713 μm deep. Tests were performed using de-ionized water with inlet liquid velocities of 0.13–1.44 m/s, inlet temperatures of 30, 60, and 90 °C, and outlet pressure of 0.12 MPa. Using a microscope, boiling incipience was identified when the first bubbles were detected growing at, and departing from the micro-channel wall. The authors conclude that bubble behavior at incipient boiling in micro-channels is quite different from that in large channels. At incipient boiling, a small number of nucleation sites were observed close to the exit of several micro-channels. The detachment size was comparable to that of the micro-channel cross-section for lower velocities and decreased progressively with increasing velocity. Results of these experiments are presented in Fig. 6.3. Figure 6.3 shows that the wall superheat is directly proportional to the heat flux, $\Delta T_{S,ONB} \sim q_{ONB}$.

Sato and Matsumura (1964), and Bergles and Rohsenow (1964) have proposed the equation for the incipient boiling condition in the case that surface cavities of all sizes are available for nucleation. Hino and Ueda (1985) studied incipient boiling of fluorocarbon R-113 in a stainless steel tube of $d = 7$ mm at mass velocity $G = 158{-}1{,}600\,\mathrm{kg/m^2 s}$, and inlet subcooling $\Delta T_{sub,in} = T_S - T_{in}$ ranged from 10–

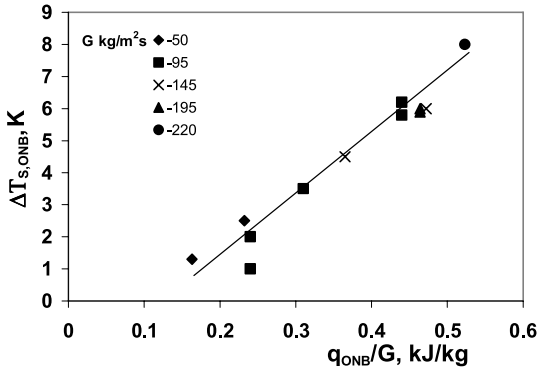

Fig. 6.2 Dependence of wall superheat $\Delta T_{S,ONB} = T_{W,ONB} - T_S$ at ONB point on the parameter q_{ONB}/G observed by Hapke et al. (2000) in the $d = 1.5$ mm tube

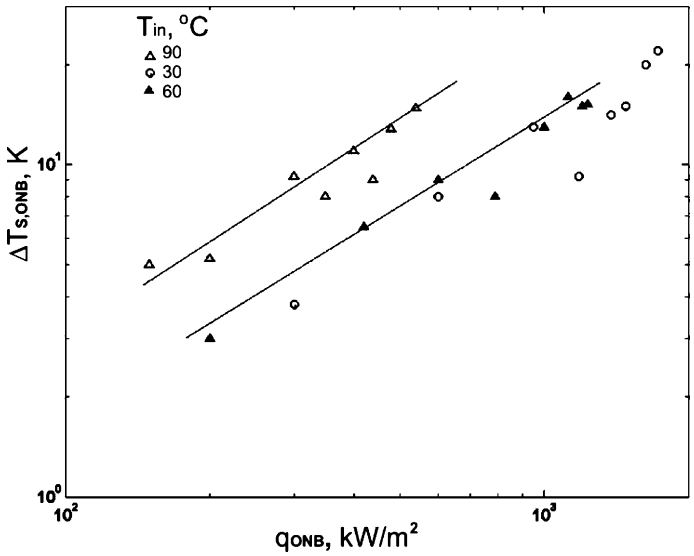

Fig. 6.3 Dependence of wall superheat on heat flux. Experiments performed by Qu and Mudawar (2002) in rectangular parallel micro-channels 231 μm wide and 713 μm deep

30 K. In the case where the upper limit of available cavity sizes was restricted to radius $r^*_{\max}$ the incipient boiling condition was expressed as follows by Hino and Ueda (1985):

$$q_{\mathrm{ONB}} = \frac{k_{\mathrm{L}}}{r^*_{\max}} \Delta T_{\mathrm{ONB}} - \frac{2\sigma k_{\mathrm{L}} T_{\mathrm{S}}}{h_{\mathrm{LG}} \rho_{\mathrm{G}} (r^*_{\max})^2} \,. \tag{6.10}$$

Figure 6.4 shows the relation between the heat flux and the wall superheat at the ONB position obtained by Hino and Ueda (1975) in the range of the largest cavity radius $r^*_{\max} = 0.22 - 0.34\,\mu\mathrm{m}$. Experimental points show that the wall superheat at the ONB position was practically independent of the mass flux and the inlet subcooling. The lines shown in this figure represent the values of Sato and Matsumura (1964), and Bergles and Rohsenow (1964). The wall superheats reported by Hino and Ueda (1975) were much greater than those predicted by Eq. (6.9).

The data of ONB in trapezoidal micro-channels of $d_{\mathrm{h}} = 41.3\,\mu\mathrm{m}$ presented by Lee et al. (2004) are shown in Fig. 6.5. Figure 6.5 illustrates a comparison of the data of the results reported by Lee et al. (2004) and prediction of Eq. (6.10) with various different values of $r^*_{\max}$. For the experimental data points in Fig. 6.5, the saturation temperature is corresponding to the local pressure at each of the ONB locations. The local pressure is estimated by assuming a linear pressure distribution in the channel between the inlet and exit ones. The system pressure may vary from case to case. For Fig. 6.5 an average system pressure of 161.7 kPa over various different cases of this study was employed. As for the wall temperature, it is assumed that the channel wall temperature is uniform as the channel is relatively short and the wall material, silicon, has relatively good thermal conductivity. The figure indi-

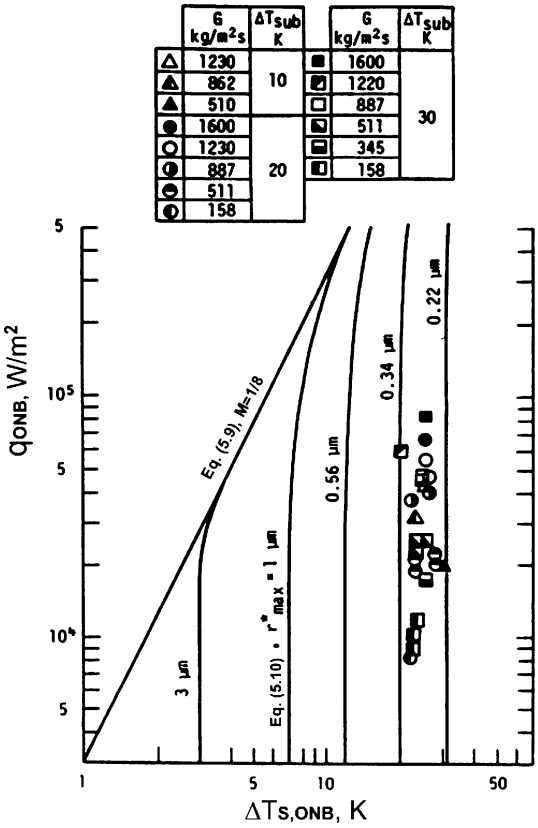

Fig. 6.4 Relation between heat flux and wall superheat at the position of incipient boiling. Reprinted from Hino and Ueda (1975) with permission

cates that most of the cavity sizes ranged from 1.5 to 4 μm. This is consistent with the maximum roughness on the side wall of the channels used in experiments. Experiments showed that for a given value of $r^*_{\max}$, wall superheat, $\Delta T_{S,ONB}$, does not depend on mass flux.

Effect of pressure

The wall superheat in Eq. (6.9) depends on saturation temperature T_S and consequently on pressure P_S:

$$\frac{\sigma T_S}{k_L \rho_G} = \psi(P_S)\,. \tag{6.11}$$

The analysis shows that Eq. (6.11) can be presented for water in the pressure range $P_S = 1-20$ bar as follows

$$\left(\frac{\sigma T_S}{k_L \rho_G}\right)^{1/2} = 7.33 P_S^{-0.5}\,. \tag{6.12}$$

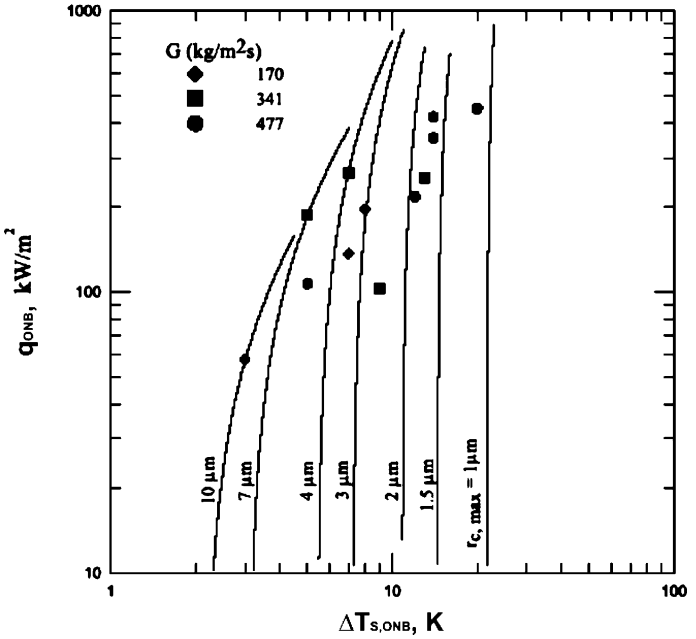

Fig. 6.5 Relationship between heat flux and wall superheat in micro-channels of $d_h = 41.3$ μm. Reprinted from Lee et al. (2004) with permission

Using Eq. (6.9) and Eq. (6.12) the wall superheat is given by

$$\Delta T_{S,ONB} = M P_S^{\alpha} (q_{ONB})^{\beta} \tag{6.13}$$

where M is constant.

Analysis of experimental data presented by Sato and Matsumura (1964), Bergles and Rohsenow (1964), Hetsroni et al. as well as theoretical analysis by Hsu (1962), Davis and Anderson (1966), Kandlikar et al. (1997) shows that the values of exponents α and β are close to $\alpha = -0.50$, $\beta = 0.50$ (Table 6.3).

Table 6.3 Exponents in Eq. (6.13)

Author	Exponents α, β		Source
	α	β	
Hsu (1962)	−0.50	0.50	Theoretical analysis
Sato, Matsumura (1964)	−0.50	0.50	α Theoretical analysis β Empirical correlation
Bergles, Rohsenow (1964)	−0.51	0.49	Empirical correlation
Davis, Anderson (1966)	−0.50	0.50	Theoretical analysis
Kandlikar (1997)	−0.50	0.50	Theoretical analysis
Hetsroni et al.	–	0.50	Empirical correlation

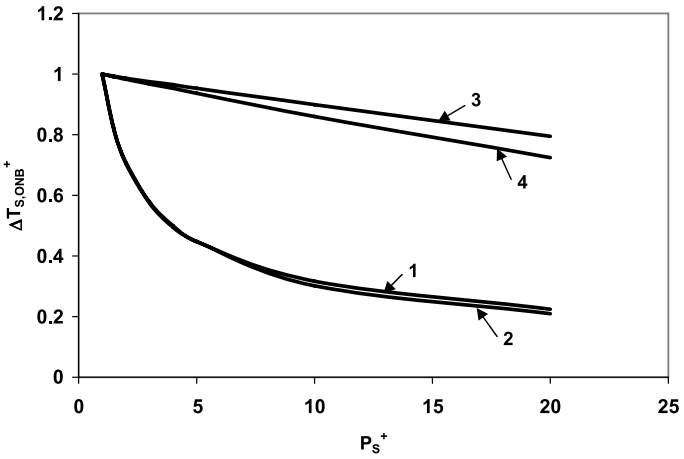

Fig. 6.6 Dependence of dimensionless wall superheat $\Delta T^{+}_{\mathrm{S,ONB}} = \Delta T_{\mathrm{ONB}}/\Delta T^{*}_{\mathrm{ONB}}$ on dimensionless pressure $P^{+}_{\mathrm{S}} = P_{\mathrm{S}}/P^{*}_{\mathrm{S}}$. *1* Hsu (1962), *2* Bergles and Rohsenow (1964), *3* Thom et al. (1965), *4* Jens and Lottes (1951)

On the other hand, Jens and Lottes (1951) and Thom et al. (1965) presented empirical correlations that showed another dependence of wall superheat on pressure. Dependence of the dimensionless wall superheat $\Delta T^{+}_{\mathrm{S,ONB}} = \Delta T_{\mathrm{ONB}}/\Delta T^{*}_{\mathrm{ONB}}$ on dimensionless pressure $P^{+}_{\mathrm{S}} = P_{\mathrm{S}}/P^{*}_{\mathrm{S}}$ is presented in Fig. 6.6 where $\Delta T^{*}_{\mathrm{ONB}}$ and P^{*}_{S} corresponds to wall superheat and pressure of 1 bar. In Fig. 6.6 the theoretical prediction based on the Hsu (1962) model, and empirical correlation of Bergles and Rohsenow (1964) are shown.

The Bergles and Rohsenow correlation (1964) is

$$\Delta T_{\mathrm{S,ONB}} = 0.555 \left(\frac{q_{\mathrm{ONB}}}{1{,}082 P^{1.156}} \right)^{P^{0.0234/2.16}} \tag{6.14}$$

where P is in bar, $\Delta T_{\mathrm{S,ONB}}$ in K, and q_{ONB} in $\mathrm{W/m^2}$.

The empirical correlation by Jens and Lottes (1951) is

$$\Delta T_{\mathrm{S,ONB}} = 25 (q_{\mathrm{ONB}})^{0.25} \exp\left(-\frac{P}{62} \right) \tag{6.15}$$

where P is in bar, $\Delta T_{\mathrm{S,ONB}}$ in K, and q_{ONB} in $\mathrm{W/m^2}$.

The empirical correlation by Thom et al. (1965) is

$$\Delta T_{\mathrm{S,ONB}} = 22.65 (q_{\mathrm{ONB}})^{0.5} \exp\left(-\frac{P}{87} \right) \tag{6.16}$$

where P is in bar, $\Delta T_{\mathrm{S,ONB}}$ in K, and q_{ONB} in $\mathrm{W/m^2}$.

It is seen that the empirical correlation by Bergles and Rohsenow (1964) agrees fairly well with prediction of theoretical analysis based on the Hsu (1962) model. Empirical correlations by Jens and Lottes (1951) and by Thom et al. (1965) show that wall superheat weakly depends on pressure.

Comparison of wall superheat predicted by classical kinetics of nucleation to experimental results

Using the properties of water Li and Cheng (2004) computed from the classical kinetics of nucleation the homogeneous nucleation temperature and the critical nucleation radius r_{cr}. The values are: $T_{S,B} = 303.7\,^{\circ}\mathrm{C}$ and $r_{crit} = 3.5$ nm. However, the nucleation temperatures of water in heat transfer experiments in micro-channels carried out by Qu and Mudawar (2002), and Hetsroni et al. (2002b, 2003, 2005) were considerably less that the homogeneous nucleation temperature of $T_{S,B} = 303.7\,^{\circ}\mathrm{C}$. The nucleation temperature of a liquid may be considerably decreased because of the following effects: dissolved gas in liquid, existence of corners in a micro-channel, surface roughness.

Liquid subcooling at ONB point

The data of liquid subcooling at ONB point presented in Table 6.4 indicate that the value of $\Delta T_{sub,ONB} = T_S - T_{B,ONB}$ changes in the wide range of $\Delta T_{sub,ONB} =$

Table 6.4 Liquid subcooling at ONB point

Author and method of ONB detection	Heat flux q_{ONB} MW/m^2	Inlet flow velocity U_{in} m/s	Pressure P MPa	Relative heated length L_{ONB}/d	Fluid subcooling $\Delta T_{sub,ONB}$ K
Unal (1975)	0.38	2.121	13.9	1250	4.3
High-speed photographic technique	0.45	2.121	15.8	1250	4.1
Bergles and	9.774	19.2	0.261	29	108.3
Rohsenow	9.774	19.2	0.261	48	66.6
(1964)	6.67	9.54	0.261	29	103.3
Dependence	5.67	9.54	0.261	48	50.0
of wall	2.145	3.74	0.261	29	92.2
superheat on heat flux	2.145	3.74	0.261	48	56.6
Kennedy et al.	1.5–4.0	1.0–4.0	1.034	137	5–12
(2000)	1.5–3.0	1.3–2.6	1.034	110	13–19
Dependence	1.5–3.0	3.5	0.69	137	4.0
of pressure	1.5–3.0	1.3	0.69	110	4.0
drop on mass	1.5–3.0	2.0	0.344	137	5.0
flux	1.5–3.0	4.3	0.344	110	5.0

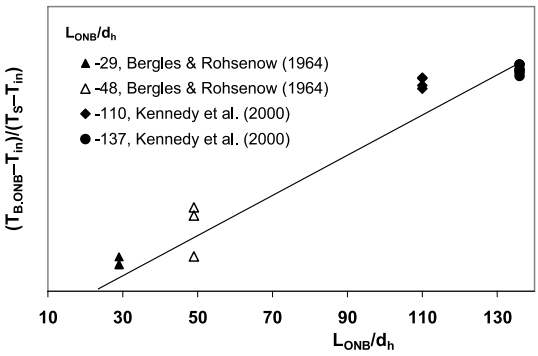

Fig. 6.7 Relationship of $(T_{\mathrm{B,ONB}} - T_{\mathrm{in}})/(T_{\mathrm{S}} - T_{\mathrm{in}})$ on $L_{\mathrm{ONB}}/d_{\mathrm{h}}$

4.0−108.3 K, where $T_{\mathrm{B,ONB}}$ is the average mass liquid temperature at the cross-section where ONB occurs.

Figure 6.7 shows the relationship of $(T_{\mathrm{B,ONB}} - T_{\mathrm{in}})/(T_{\mathrm{S}} - T_{\mathrm{in}})$ on $L_{\mathrm{ONB}}/d_{\mathrm{h}}$. The results obtained by different investigators indicate that in the range of $q_{\mathrm{ONB}} = 1.5{-}9.8\,\mathrm{MW/m^2}$ the value of $(T_{\mathrm{B,ONB}} - T_{\mathrm{in}})/(T_{\mathrm{S}} - T_{\mathrm{in}})$ depends only on the parameter $L_{\mathrm{ONB}}/d_{\mathrm{h}}$.

For qualitative analysis of the conditions at which the ONB phenomenon was studied experimentally in conventional size channels, as well as in micro-channels the parameter $D = \Delta T_{\mathrm{sub,ONB}}/T_{\mathrm{S}}$ may be used. Depending on the value of D the channels can be subdivided into two groups: (1) $D < 1$, and (2) $D \ll 1$. When the value of D was in the range 0.125–0.25, as in experiments by Bergles and Rohsenow (1964), the onset of nucleate boiling occurred at values of the bulk temperature, $T_{\mathrm{B,ONB}}$, significantly less than the saturation temperature. It should be noted that at low values of $T_{\mathrm{B,ONB}}$ the Prandtl number of liquid is large enough. As a result the thin thermal layer formed over the channel wall. When $D \ll 1$, the onset of nucleate boiling occurred at values of the bulk temperature, $T_{\mathrm{B,ONB}}$, that were close to the saturation temperature. Experiments by Unal (1975), Kennedy et al. (2000), and by Liu et al. (2005) were carried out under such conditions. For example, in experiments by Kennedy et al. (2000) the value of D was in the range 0.011–0.043. Figure 6.8 illustrates the fluid temperature distribution depending on the relation of $D = \Delta T_{\mathrm{sub,ONB}}/T_{\mathrm{S}}$. The dark area corresponds to the region where the local fluid temperature T exceeds the saturation temperature T_{S}. In this region the maximum probability of the bubble embryo formation takes place.

6.1.3 Effect of Inlet Velocity on Wall Superheat

The point of ONB located at the channel exit corresponds to minimum heat flux at which the boiling incipience is possible for the channel of the given length. Kennedy et al. (2000) presented the measurements that were carried out at different values of the inlet average velocity U_{in}, whereas the inlet temperature T_{in}, was constant.

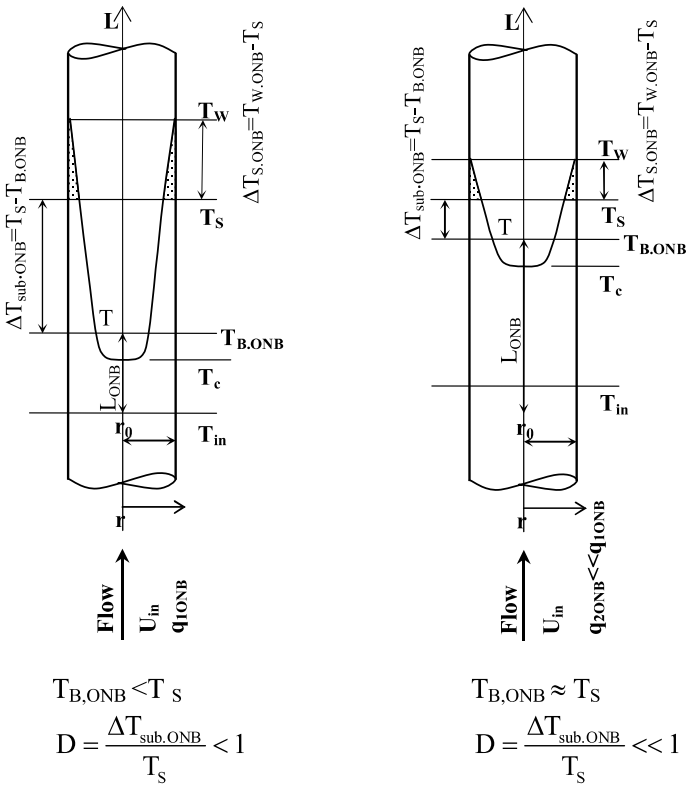

Fig. 6.8 Fluid temperature distribution depending on the relation of $D = \Delta T_{\text{sub,ONB}}/T_S$

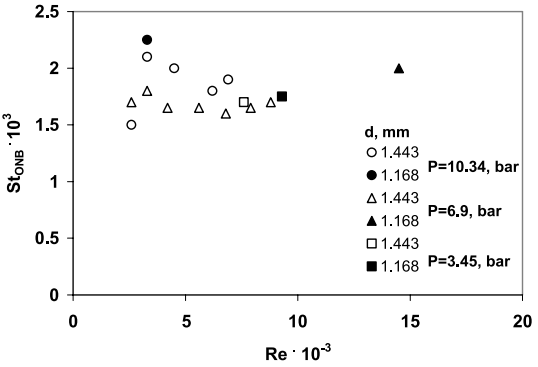

Fig. 6.9 Dependence of the boiling Stanton number at ONB point. Experiments by Kennedy et al. (2000)

Figure 6.9 illustrates the dependence of the boiling Stanton number at ONB point, $\text{St}_{\text{ONB}} = q_{\text{ONB}}/[\rho_L U_{\text{in}} c_p (T_S - T_{\text{in}})]$, on the Reynolds number, $\text{Re} = U_{\text{in}} d_h/\nu$. One can see that the value of the St_{ONB} does not change significantly in the range of $\text{Re} \sim 0.4 \times 10^4 - 1.6 \times 10^4$, i.e., the value of q_{ONB} depends on the inlet average velocity when its temperature is constant.

To estimate the value of the bulk liquid temperature at ONB in conventional size channels, as well as in micro-channels the energy and continuity equations should be considered.

Energy and continuity equations for cylindrical channels are:

$$\rho u c_{\mathrm{p}} \frac{\partial T}{\partial x} + \rho v c_{\mathrm{p}} \frac{\partial T}{\partial y} = \frac{k}{y} \frac{\partial}{\partial y} \left(y \frac{\partial T}{\partial y} \right) + k \frac{\partial^2 T}{\partial x^2} \tag{6.17}$$

$$\frac{\partial (\rho u)}{\partial x} + \frac{1}{y} \frac{\partial (\rho u)}{\partial y} = 0 \tag{6.18}$$

where c_{p} and k are specific heat and thermal conductivity of the liquid, respectively, and u, v are streamwise and spanwise components of the velocity.

The boundary conditions for Eqs. (6.17) and (6.18) read as

$$\begin{array}{ll} x = 0\,, & u = U_{\mathrm{in}}\,, \quad \rho = \rho_{\mathrm{in}}\,, \quad T = T_{\mathrm{in}} \\ x > 0 & \begin{cases} y = 0\,, & \frac{\partial T}{\partial y} = 0 \\ y = r_0\,, & -\lambda \frac{\partial T}{\partial y} = q \end{cases} \end{array} \tag{6.19}$$

where r_0 is the tube radius, q is the heat flux on the wall.

Restricting our consideration analysis of the developed flow we rewrite Eqs. (6.17) and (6.18) in the form

$$\rho u c_{\mathrm{p}} \frac{\partial (T - T_{\mathrm{in}})}{\partial x} = \frac{k}{y} \frac{\partial}{\partial y} \left(y \frac{\partial T - T_{\mathrm{in}}}{\partial y} \right) + k \frac{\partial^2 (T - T_{\mathrm{in}})}{\partial x^2} \tag{6.20}$$

$$\frac{\partial \rho u}{\partial x} = 0\,. \tag{6.21}$$

Multiplying Eq. (6.21) on $c_{\mathrm{p}}(T - T_{\mathrm{in}})$ and summing this equation with Eq. (6.20) we obtain

$$\frac{\partial \rho u c_{\mathrm{p}} (T - T_{\mathrm{in}})}{\partial x} = \frac{k}{y} \frac{\partial}{\partial y} \left(y \frac{\partial (T - T_{\mathrm{in}})}{\partial y} \right) + k \frac{\partial^2 (T - T_{\mathrm{in}})}{\partial x^2}\,. \tag{6.22}$$

Integration of Eq. (6.22) gives

$$\frac{\partial}{\partial x} \int_0^{r_0} \rho u c_{\mathrm{p}} (T - T_{\mathrm{in}}) y \,\mathrm{d}y = k y \left. \frac{\partial (T - T_{\mathrm{in}})}{\partial y} \right|_0^{r_0} + k \frac{\partial^2}{\partial x^2} \int_0^{r_0} (T - T_{\mathrm{in}}) y \,\mathrm{d}y\,. \tag{6.23}$$

Omitting in Eq. (6.23) the last term that allows for axial heat transfer, Eq. (6.23) may be expressed:

$$\frac{\partial}{\partial x} \int_0^{r_0} \rho u c_{\mathrm{p}} (T - T_{\mathrm{in}}) y \,\mathrm{d}y = q r_0\,. \tag{6.24}$$

Integration of Eq. (6.24) from $x = 0$ to $x = L_{\mathrm{ONB}}$ gives

$$\frac{\partial}{\partial x} \int_0^{r_0} \rho u_{\mathrm{ONB}} c_{\mathrm{p}} (T_{\mathrm{ONB}} - T_{\mathrm{in}}) y \,\mathrm{d}y = q_{\mathrm{ONB}} r_0 L_{\mathrm{ONB}}\,. \tag{6.25}$$

Introducing the mean mass temperature gives

$$T_{\mathrm{B,ONB}} = \frac{1}{2\rho U_{\mathrm{in}} c_{\mathrm{p}} r_0^2} \int_0^{r_0} \rho u c_{\mathrm{p}} T_{\mathrm{ONB}} y \, \mathrm{d}y \,. \tag{6.26}$$

Equation (6.26) may be presented in the form

$$\frac{q_{\mathrm{ONB}}}{\rho U_{\mathrm{in}} c_{\mathrm{p}} (T_{\mathrm{B.ONB}} - T_{\mathrm{in}})} \frac{2L_{\mathrm{ONB}}}{r_0} = 1 \,. \tag{6.27}$$

Equation (6.27) was obtained for circular channels. Rectangular channels with four or three conductive walls are shown in Fig. 6.10.

The thermal balance equation for rectangular channels with four or three heated walls shown in Fig. 6.10 are:

$$\iint_{\mathrm{S}} \rho u c_{\mathrm{p}} (T_{\mathrm{B,ONB}} - T_{\mathrm{in}}) \, \mathrm{d}y \, \mathrm{d}z = q_{\mathrm{ONB}} L_{\mathrm{ONB}} \cdot 4(a+b) \tag{6.28}$$

and

$$\iint_{\mathrm{S}} \rho u c_{\mathrm{p}} (T_{\mathrm{B,ONB}} - T_{\mathrm{in}}) \, \mathrm{d}y \, \mathrm{d}z = q_{\mathrm{ONB}} L_{\mathrm{ONB}} \cdot 2(2a+b) \tag{6.29}$$

where S is the area of channels cross-section:

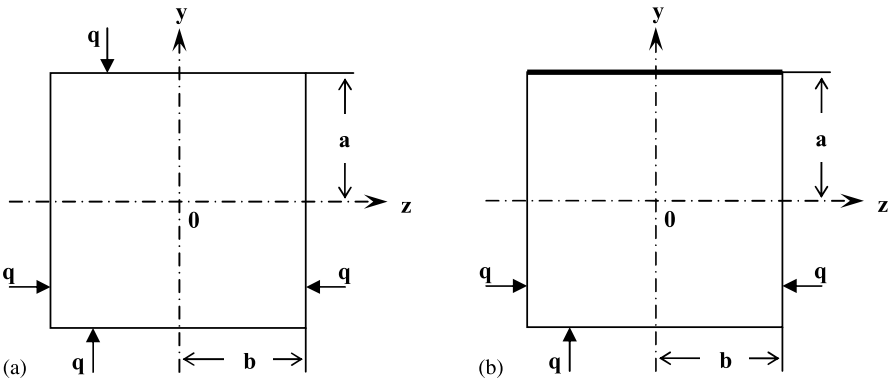

Fig. 6.10 Rectangular channels: (**a**) four heated walls, (**b**) three heated walls

In the terms of mean mass temperature Eqs. (6.28) and (6.29) take the form

$$\frac{q_{\mathrm{ONB}}}{\rho U_{\mathrm{in}} c_{\mathrm{p}} (T_{\mathrm{B,ONB}} - T_{\mathrm{in}})} \frac{L_{\mathrm{ONB}} (a+b)}{ab} = 1 \tag{6.30}$$

and

$$\frac{q_{\mathrm{ONB}}}{\rho U_{\mathrm{in}} c_{\mathrm{p}} (T_{\mathrm{B,ONB}} - T_{\mathrm{in}})} \frac{L_{\mathrm{ONB}} (a+b)}{2ab} = 1 \,. \tag{6.31}$$

If the value of $T_{B,ONB} \approx T_S$, ($D \ll 1$) the integral characteristics for the circular channels, the rectangular channels with four and three heated walls, respectively, are:

$$\frac{q_{ONB}}{\rho U_{in} c_p (T_S - T_{in})} \frac{2L_{ONB}}{r_0} = I_{c,ONB} \tag{6.32}$$

$$\frac{q_{ONB}}{\rho U_{in} c_p (T_S - T_{in})} \frac{L_{ONB}(a+b)}{ab} = I_{4,ONB} \tag{6.33}$$

$$\frac{q_{ONB}}{\rho U_{in} c_p (T_S - T_{in})} \frac{L_{ONB}(2a+b)}{2ab} = I_{3,ONB}\,. \tag{6.34}$$

The bulk temperature $T_{B,ONB}$ is close to saturation temperature T_S, when the values calculated using Eqs. (6.32), (6.33) and (6.34) do not differ significantly from unity. In Fig. 6.11 the experimental results reported by Kennedy et al. (2000) are presented as the dependence of the value $I_{c,ONB}$ (Eq. 6.32) on the Peclet number. The data may be described by the single line of $I_{c,ONB} = 0.96$. In this case the bulk temperature $T_{B,ONB}$, at ONB point should not differ significantly from T_S. Experimental results given in Table 6.4 support this statement.

The onset of nucleate boiling in the flow of water through a micro-channel heat sink was investigated by Liu et al. (2005). The rectangular micro-channels of $d_h = 384\,\mu m$ and length of 25.4 mm were used. Holes were drilled into the bottom of the copper block to house eight cartridge heaters that can provide heating through three walls. Onset of nucleate boiling was identified with a high-speed imaging system. To complement the incipient heat flux results identified from the visualization approach, the micro-channel wall temperatures and pressure drop along the micro-channels were analyzed. Experimental parameters obtained in this study are presented in Fig. 6.12 as the dependence of the value $I_{3,ONB}$ on the Peclet number. In this case the parameter $I_{3,ONB} \sim 0.93$, and T_b should also not differ significantly from T_S. Unfortunately, the experimental data of T_b were not reported by Liu et al. (2005).

Parameters $I_{c,ONB}$, $I_{3,ONB}$, and $I_{4,ONB}$ change in the range of $0 < T < 1$. They account for a specific temperature field in heated micro-channels and are criteria for the relative micro-channel length. Note, if $D < 1$ the value of parameter I is significantly less than unity. The paper by Celata et al. (1997) reports the results of experimental research of the onset of subcooled water boiling in the circular

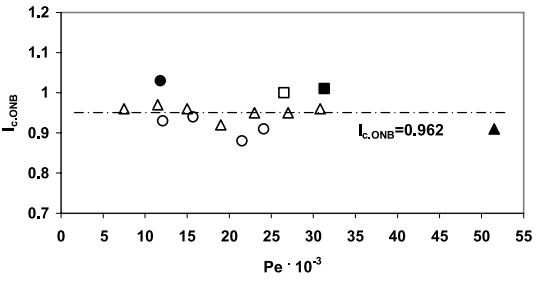

Fig. 6.11 Dependence of the value $I_{c,ONB}$ on the Peclet number (the legend is given in Fig. 6.9). Experiments by Kennedy et al. (2000)

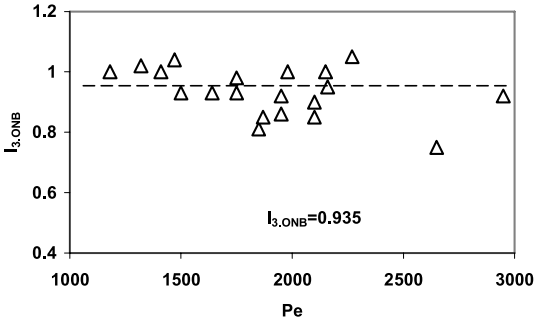

Fig. 6.12 Dependence of the value $I_{3,\mathrm{ONB}}$ on the Peclet number. Experiments by Liu et al. (2005)

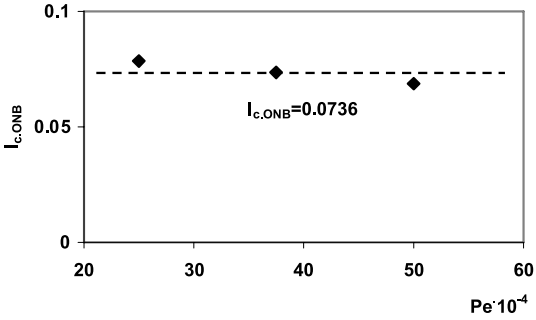

Fig. 6.13 Value of I_c as a function of the Peclet number. Experiments by Celata et al. (1997)

channel with $d = 8\,\mathrm{mm}$, and $L = 100\,\mathrm{mm}$. Test conditions were as follows: $U_{\mathrm{in}} = 5{-}10\,\mathrm{m/s}$, $P_{\mathrm{out}} = 1.0{-}2.5\,\mathrm{MPa}$, $T_{\mathrm{in}} = 30{-}60\,^{\circ}\mathrm{C}$, inlet subcooling $\Delta T_{\mathrm{sub,in}} = T_{\mathrm{S}} - T_{\mathrm{in}}$ from 120 to 194 K, $q_{\mathrm{ONB}} = 3{-}11\,\mathrm{MW/m^2}$. Figure 6.13 shows the value of $I_{\mathrm{c,ONB}}$ as a function of the Peclet number. The authors did not report liquid subcooling at ONB. In this study the parameter was $I_{\mathrm{c,ONB}} \sim 0.074$. According to an estimation based on such a small value of $I_{\mathrm{c,ONB}}$ one can conclude that onset of nucleate boiling in experiments by Celata et al. (1997) occurred at high liquid subcooling.

The wall superheat that corresponds to bubble formation in liquid flow can be estimated using an approach that is not connected to the mechanism of bubble formation. Such tentative estimation makes it possible to consider only the low level of wall superheat. According to Kays and Krawford (1993) the temperature distribution in turbulent flow and $\mathrm{Pr} \sim 1$ is

$$\frac{T_{\mathrm{W}} - T}{T_{\mathrm{W}} - T_{\mathrm{c}}} = \left(\frac{r_0 - r}{r_0}\right)^{1/7} \tag{6.35}$$

where T is the current fluid temperature, and T_{c} is the liquid temperature at the tube axis.

From the analytical solution based on the thermal boundary approach:

$$T_{\mathrm{w}} - T_{\mathrm{c}} = \frac{q}{\rho c_{\mathrm{p}} U} \frac{1}{\sqrt{f/2}} \left(5\,\mathrm{Pr} + 5\ln(5\,\mathrm{Pr}+1) + 2.5\ln\frac{\mathrm{Pr}\sqrt{f/2}}{60}\right) \tag{6.36}$$

where $f = 2\tau_w/(\rho U^2)$, τ_w is the wall shear stress.

Dependence of wall superheat on inlet fluid velocity

For $D \ll 1$, $T_{B,ONB} \approx T_S$ and

$$\Delta T_{S,ONB} = T_{W,ONB} - T_S \,. \tag{6.37}$$

Under these conditions the wall superheat depends weakly on the Reynolds number (Kennedy et al. 2000).

The same conclusion is evident from results obtained by Hino and Ueda (1975) and presented above in Fig. 6.4. The conclusion that ΔT_S is almost unaffected by inlet flow velocity as at $D \ll 1$ as at $D < 1$ was established from experiments carried out in the channels of diameters about $d = 1-10$ mm. What has been commonly observed at incipient boiling for subcooled flow in channels of this size is that small bubbles nucleate, grow and collapse while still attached to the wall, as a thin bubble layer formed along the channel wall.

6.1.4 Effect of Inlet Parameters on Incipient Boiling Heat Flux

Effect of inlet velocity

Qualitative analysis of the Eqs. (6.32), (6.33), and (6.34) makes it possible to illustrate the salient features of the dependence q_{ONB} on U_{in}. They could be approximated by the following lines shown in Fig. 6.14a. The solid line corresponds to the case of $T_{in} \ll T_S$ ($D < 1$), the dotted line corresponds to the case of $T_{in} \approx T_S$ ($D \ll 1$). Experimental results reported by Liu et al. (2005) (see Fig. 6.14b) agree qualitatively with analytical prediction. The same tendency was also observed by Qu and Mudawar (2002).

Effect of inlet temperature on q_{ONB}

From Eqs. (6.32), (6.33) and (6.34) one can conclude that incipient boiling heat flux q_{ONB} depends on the inlet temperature T_{in}. Such a behavior is shown in Fig. 6.15a. Note that at the same value of T_{in} the value of q_{ONB} increases with increasing inlet velocity. Experimental data by Liu et al. (2005) shown in Fig. 6.15b agree qualitatively with analysis.

6.1.5 Incipience of Boiling in Surfactant Solutions

Under some conditions boiling incipience in surfactant solutions may be quite different from that in Newtonian fluids. Hetsroni et al. (2007) presented results for

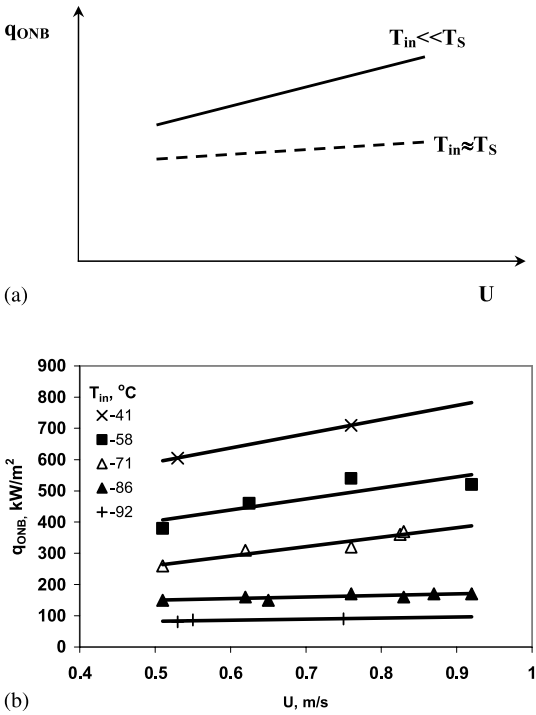

Fig. 6.14 Variation of incipient boiling heat flux with inlet flow velocity: (**a**) analytical predictions, (**b**) experimental data by Liu et al. (2005)

natural convection boiling in narrow horizontal annular channels of the gap size 0.45–2.2 mm for Alkyl (8-16) degraded solutions, i.e., solutions that were used after 6 to 10 runs.

For degraded Alkyl (8-16) solutions boiling occurred at wall superheat higher than that observed in fresh solutions and water. Incipience of boiling in both water and fresh surfactant solutions was accompanied by formation of small bubbles on the heated surface. However, a significant difference in the behavior of boiling patterns was observed. The formation of big vapor clusters took place before boiling incipience in degraded Alkyl (8-16) solutions in the range of concentrations $C = 10-600$ ppm (weight part per million). This process is shown in Fig. 6.16a–c. The burst of such a cluster is shown in Fig. 6.16d. The cluster formation was accompanied by high wall superheat ($T_W - T_S$) in heat flux controlled experiments, where T_W is the temperature measured on the heated wall, and T_S is the saturation temperature measured in the vessel. It should be stressed that these clusters were not gas (air) bubbles. The desorption of the dissolved gases formed bubbles of gas and a limited amount of bubbles containing gas–water vapor mixture. As a result, boiling incipience occurred at a heated wall temperature below that of saturation temperature. In the present study such a phenomenon was not observed. We also measured fluid temperature T_f in the annular space between the heated tube and the inner wall of glass tube by a thermocouple. This temperature exceeded over 4–12 K the saturation temperature depending on solution concentration. Finally, the collapse

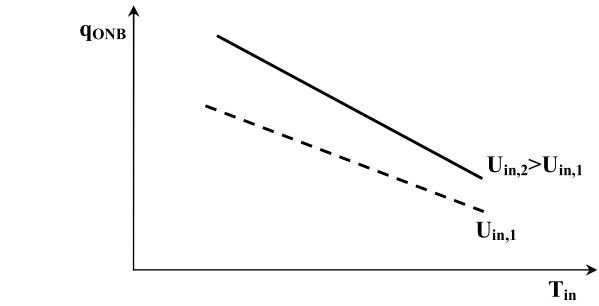

(a)

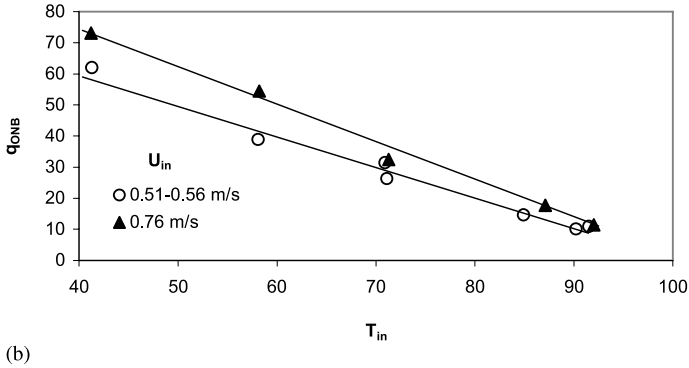

(b)

Fig. 6.15 Variation of incipient boiling heat flux with inlet flow temperature: (**a**) analytical predictions, (**b**) experimental data by Liu et al. (2005)

of the cluster led to a reduction in wall superheat and the saturated boiling regime occurred. For water boiling we did not observe the bubble coalescence at very small scales. For pool boiling of surfactant solutions bubble coalescence was observed. There were clusters of small bubbles, which rose from the cavity. These bubbles were adjacent to each other and the cluster neck was not observed. The bursting of vapor clusters before boiling incipience of degraded cationic surfactant Habon G solution was also observed by Hetsroni et al. (2002b).

Data were taken for both increasing and decreasing heat fluxes. The total mass of the liquid in the test facility remained constant, thus no fresh liquid was introduced to "top off" the system. For water boiling in the gap sizes of 0.45, 1.2, 2.2, and 3.7 mm, the Bond numbers, $\mathrm{Bn} = \delta(\sigma/g(\rho_\mathrm{L} - \rho_\mathrm{G}))^{-0.5}$, were 0.185, 0.493, 0.9 and 1.52, respectively, where δ is the gap size, σ is the surface tension, g is the acceleration due to gravity, and ρ_L and ρ_G are the liquid and the vapor densities. Boiling of surfactant solutions was investigated in a gap size of 0.45 and 2.2 mm in the range of Bond numbers $\mathrm{Bn} = 0.26-1.26$.

The results obtained at $\mathrm{Bn} = 1.26$ are presented in Fig. 6.17, for different concentrations of surfactant solutions. The onset of boiling corresponds to the curve ABCD for the runs with increasing heat flux. It follows the curve DCA for decreas-

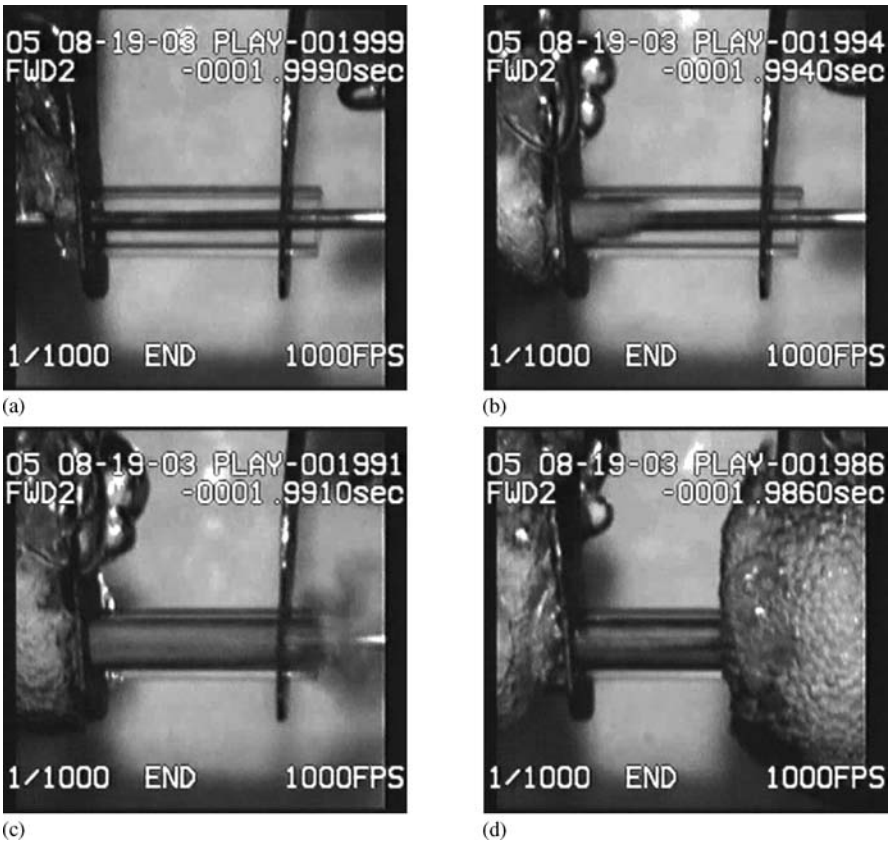

Fig. 6.16 Boiling incipience in degraded solutions. Reprinted from Hetsroni et al. (2007) with permission

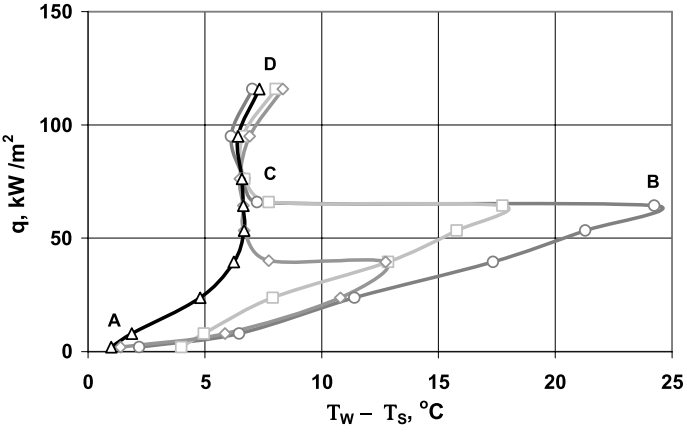

Fig. 6.17 Boiling hysteresis in degraded Alkyl (8-16) solutions. (○) $C = 300$ ppm, (□) $C = 100$ ppm, (◇) $C = 25$ ppm, (△) $C = 10$ ppm. Reprinted from Hetsroni et al. (2007) with permission

ing heat flux. The measurements were repeated several times and the same phenomena were observed. Point B stands for the condition at which the fluid starts to boil when the heat flux is increasing (the typical process is shown in Fig. 6.16a–d). Zhang and Manglik (2005) concluded that hysteresis occurred due to high wettability, which takes place at very high concentrations, $C > C_{CMC}$, where C_{CMC} is the critical micelle concentration. It should be stressed that in the present study hysteresis was observed in restricted boiling of degraded solutions as for pre-CMC solutions ($C < 300$ ppm) as for post-CMC solutions. It is speculated that molecules of degraded surfactant are more amenable to formation of a surfactant monolayer, which renders the interface less flexible and results in the dampening of interfacial motion. For Alkyl (8-16) hysteresis occurs only in degraded solutions.

6.2 Onset of Nucleate Boiling in Parallel Micro-Channels

6.2.1 Physical Model of the Explosive Boiling

Flow and boiling in parallel micro-channels occur under conditions of significant hydrodynamic and thermal heterogeneity due to finite lateral size of the heat sink, as well as interaction between the steams in individual channels connected by inlet and outlet collectors. Some data on such flows are presented by Ozawa et al. (1989), Peles (1999), and Peles et al. (2001). The temperature field of the heat sinks involving 13 to 26 micro-channels with hydraulic diameters of 0.10–0.22 mm under conditions of low quality flow boiling was studied by Hetsroni et al. (2002a, 2002b, 2003). The results showed that the wall temperature of the channels located at the central part of the heat sink was higher than that of the channels located at the peripheral part. The successive images obtained using high-speed video visualization showed that flow patterns in a given channel were quasi-periodic. The onset of nucleate boiling was established when the first bubbles were observed. This process is accompanied by pressure drop and temperature fluctuations, so that the boiling incipience is a local phenomenon. As discussed previously, the vapor accumulated in the inlet plenum. That leads to the increase of inlet temperature to a value close to T_S. According to analysis presented in the previous section, $T_{B,ONB}$ is close to the saturation temperature T_S, and wall superheat ΔT_S, since the onset of nucleation boiling is much lower than that calculated from the classical kinetics of nucleation for homogeneous nucleation in superheated fluid. For example, the wall superheat was about 4 K for flow boiling in the 26 micro-channels of $d_h = 0.103$ mm at $q = 220\,\mathrm{kW/m^2}$ and $U_{in} = 0.14\,\mathrm{m/s}$ (Hetsroni et al. 2003).

Visual observation in the studies by Hetsroni et al. (2002a,b, 2003), Qu and Mudawar (2002) proved bubble behavior at incipient boiling in micro-channels ($d_h < 1$ mm) and concluded that it was quite different from that in larger channels. After nucleation, bubbles first grew to detachment size before departing into the liquid flow. The detachment size was comparable to that of the micro-channel

cross-section for lower velocities and decreased progressively with increasing velocity. The detached bubbles moved to the downstream plenum where they collapsed. These visual observations proved that boiling incipience in the micro-channel heat sink was accompanied by both bubble growth and departure.

A physical model of ONB for the explosive boiling and dryout, was suggested. In order to understand why dryout occurred even at a low value of vapor quality x, it is important to keep in mind that the liquid film does not cover the entire heated surface of the micro-channel, and two-phase flow is characterized by an unsteady cyclic behavior. The following assumptions are made in the development of the model:

1. The bubble nucleation occurs at the location where the wall temperature exceeds the saturation temperature.
2. The heat flux is uniform and constant along the inner wall of the micro-channel.
3. All energy entering the fluid is used to vaporize the liquid. The temperatures of the liquid and vapor remain at saturation temperature.
4. After the bubble venting the liquid remains attached to the wall as droplets or clusters of droplets. It evaporates during the period of the cycle.
5. The thermal inertia of the wall is negligible, i.e., we assumed no phase shift between temperature of the channel wall and the heater.

Figure 6.18 shows a representation of the explosive boiling process. The bubble is assumed to nucleate at the ONB point (Fig. 6.18a). Then the bubble quickly grows to the channel size and an elongated bubble is formed. During this process some amount of liquid remains in front of the bubble (Fig. 6.18b). Figure 6.18c shows bubble venting. During this process the bubble expands not only in the upstream but also in the downstream direction. An interesting result is that a single bubble cyclically growing and collapsing away from the outlet manifold is capable of inducing a mean unidirectional fluid flow. This trend was also reported by Ory et al. (2000).

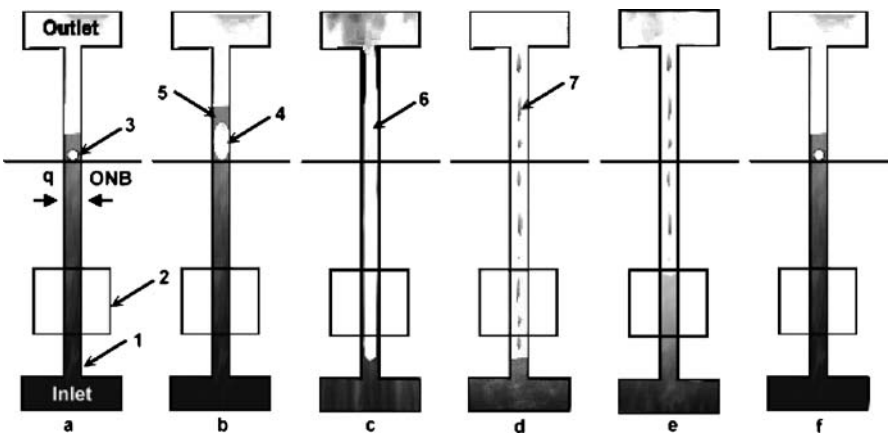

Fig. 6.18 Scheme of explosive boiling: *1* micro-channel, *2* main area of visual observation, *3* ONB point, *4* elongated cylindrical bubble, *5* liquid in front of the bubble, *6* vapor, *7* liquid droplets and clusters. Reprinted from Hetsroni et al. (2005) with permission

Figure 6.18d shows the appearance of liquid droplets or clusters of liquid droplets on the wall after the bubble venting. The pressure in the micro-channel decreases and water starts to move into it from the inlet manifold (Fig. 6.18e). Figure 6.18f shows the start of a new cycle.

6.2.2 *Effect of Dissolved Gases on ONB During Flow Boiling of Water and Surfactant Solutions in Micro-Channels*

Desorption of the dissolved gases formed bubbles of gas and a limited amount of bubbles containing gas–water vapor mixture. As a result, boiling incipience occurred at a channel wall temperature below the saturation temperature. Steinke and Kandlikar (2004a) studied flow boiling in six parallel micro-channels, each having hydraulic diameter of 0.207 mm. During the flow boiling studies with water in these micro-channels, nucleation was observed at a surface temperature of $T_W = 90.5\,^{\circ}C$ for the dissolved oxygen content of 8.0 parts per million (ppm) at a pressure of $P = 1$ bar.

Comparison between water flow and surfactant solution was investigated by Klein et al. (2005). The experimental facility was designed and constructed as illustrated schematically in Fig. 6.19.

The test module consisted of inlet and outlet manifolds that were jointed to the test chip (Fig. 6.20). The tested chip with heater is shown in Fig. 6.21. It was made from a square shape 15×15 mm and 0.5 mm thick silicon wafer, which was later bonded to a 0.53 mm thick Pyrex cover. On one side of the silicon wafer 26 micro-channels were etched, with triangular shaped cross-sections, with a base of 0.21 mm

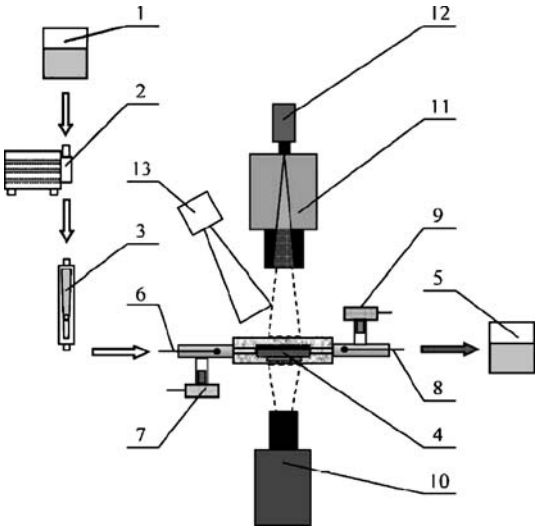

Fig. 6.19 Schematic view of the experimental facility. *1* Inlet tank, *2* mini-gear pump, *3* rotameter, *4* test module, *5* exit tank, *6* inlet thermocouple, *7* inlet pressure gauge, *8* outlet thermocouple, *9* outlet pressure gauge, *10* high-speed IR camera, *11* microscope, *12* high-speed CCD camera, *13* external light source. Reprinted from Klein et al. (2005) with permission

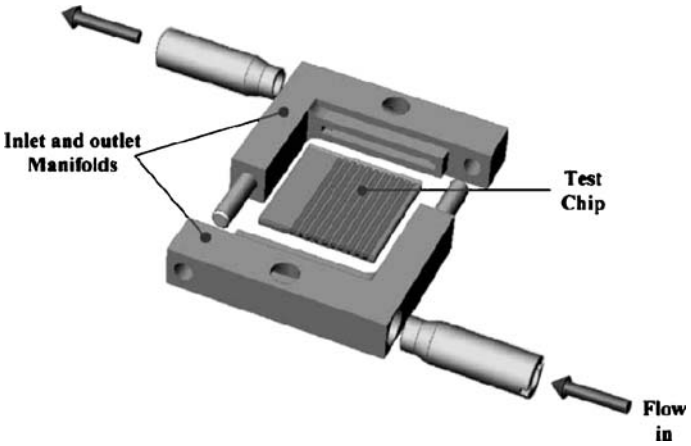

Fig. 6.20 Test module. Reprinted from Klein et al. (2005) with permission

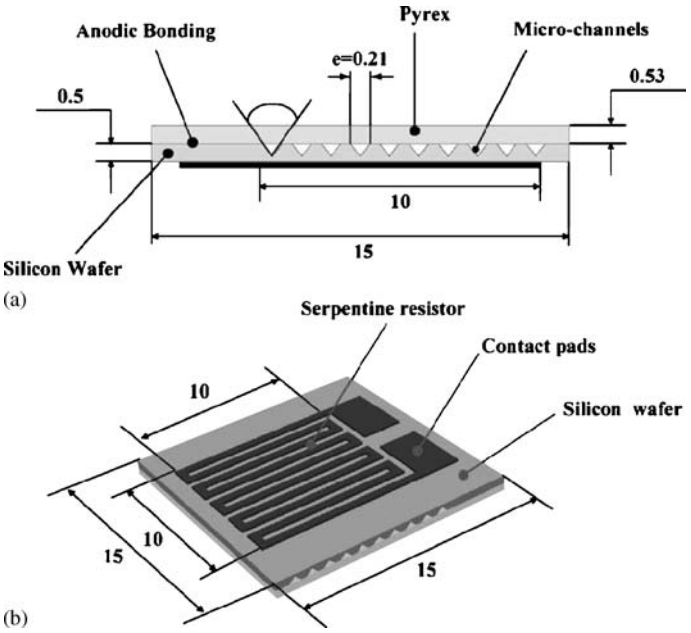

Fig. 6.21 Test chip with heater: (**a**) cross-section, (**b**) heater. Reprinted from Klein et al. (2005) with permission

and a base angle of 54.7°. Using a microscopic lens, IR measurements can be taken up to 800 Hz with a 30 μm spatial resolution. The surfactant used was of the Alkyl polyglucosides (APG) type.

Figure 6.22 shows the effect of APG additives on the dynamic and the static surface tension for different mass concentrations, measured at 75 and 95 °C. The

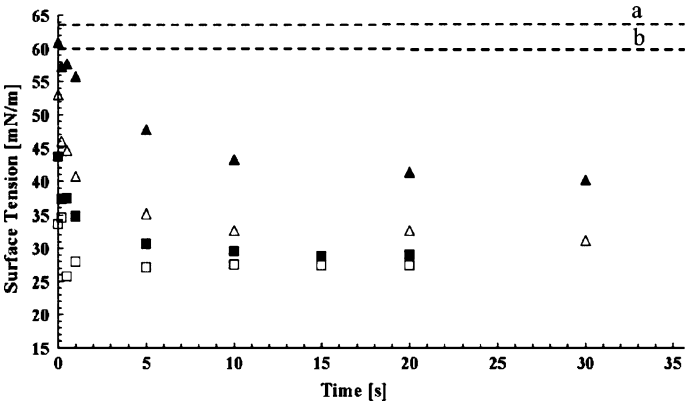

Fig. 6.22 Surface tension of the APG solutions. Concentration and solution temperature (°C): $C =$ 100 ppm, *filled triangles* (▲) represent 75 °C, *empty triangles* (△) represent 95 °C; $C = 300$ ppm, *filled squares* (■) represent 75 °C, *empty squares* (□) represent 95 °C. Reprinted from Klein et al. (2005) with permission

dashed lines a,b represent the surface tension value for pure water at 75 and 95 °C. Solid points represent the APG data at 75 °C and the hollow points represent the APG data at 95 °C. Note that an increase in concentration decreases surface tension down to a value of 31 mN/m, compared to 59.9 mN/m for pure water.

The temperatures on the heater $T_{W,ONB}$, and heat fluxes q_{ONB} corresponding to onset of nucleate boiling in water and surfactant solution that contain dissolved gases are presented in Table 6.5.

As can be seen in Table 6.5, ONB in APG solution of concentration $C = 100$ ppm took place at significantly higher surface temperatures. It should be noted that the ONB in surfactant solutions may not be solely associated with static surface tension Sher and Hetsroni (2002). Other parameters such as heat flux, mass flux, kind of surfactant, surface materials, surface treatments, surface roughness, dynamic surface tension and contact angle need to be considered as well.

Table 6.5 Onset of nucleate boiling in fluids that contain dissolved gases. Reprinted from Klein et al. (2005) with permission

De-ionized water			APG-100 ppm, surfactant solution		
Mass flux (kg/m^2 s)	q_{ONB} (W/cm^2)	$T_{W,ONB}$ (°C)	Mass flux (kg/m^2 s)	q_{ONB} (W/cm^2)	$T_{W,ONB}$ (°C)
37.9	5.2	81.6	39.4	7.7	107.3
57.7	8.2	91.6	57.2	9.3	101.4
84.9	9.9	81.6	83.3	15.9	116.6
116.2	16.2	96.6	117.6	23.2	120.3
172.3	21.0	91.6	171.2	32.3	121.1

6.2.3 Effect of Roughness

On roughened surface boiling enhancement occurs due to the increased number of active cavities that promote bubble nucleation and provide more and larger sites for bubble growth. However, during boiling the effect of surface roughness may diminish generally due to phenomenon known as "aging". Cavities formed by roughening the surface were often not stable vapor traps and reentrant cavities may be used as a vapor trap for conventional size channels. Effect of reentrant cavities on boiling in micro-channels was studied by Kosar et al. (2005) and by Kuo and Peles (2007). Intensified nucleation activity was observed in the micro-channels with reentrant cavities accompanied by significantly better uniformity of nucleation site distribution. Significant reductions in the wall superheat required to initiate boiling were measured in structured surface micro-channels compared to the plain-wall micro-channel.

6.3 Dynamics of Vapor Bubble

6.3.1 The State of the Art of the Problem

The bubble dynamics was a subject of numerous theoretical investigations starting from pioneering work by Rayleigh (1917). The results of the study of bubble growth in superheated liquid, as well as their response to different disturbances are collected in a number of monographs and surveys devoted to mechanisms of two-phase media and the theory of heat transfer and boiling (Kutateladze 1963; Nigmatulin 1991; Carey 1992; Dhir 1998; Nakoryakov et al. 2000).

There are many criteria for bubble shape or bubble detachment suggested for the description of bubble growth dynamics. The distinct feature of bubble dynamics is that contact angle deviates from the static value due to the fast growth. The well-known Fritz equation (1936) predicts bubble departure diameter for contact angle of 48°. This agrees well with the experimental data at atmospheric pressure. Hsu and Graham (1961) assumed a contact angle of 53.1°. Han and Griffith (1965) presented a theory and experimental results of bubble growth of pool boiling at low heat flux. Bubble departure was considered by the authors and it was found that the Fritz relation works as the non-equilibrium bubble contact angle. Most of the previous research on single bubble growth has been performed using a constant wall heat flux created by heating a metallic block beneath the bubble (Staniszewski 1959; Han and Griffith 1965; Cole and Shulman 1966; van Stralen 1966). The effect of pressure for contact angle of 48° was described by Cole and Shulman (1966).

Analytical analyses for the growth of a single bubble have been performed for simple geometrical shapes, using a simplified heat transfer model. Plesset and Zwick (1954) solved the problem by considering the heat transfer through the bubble interface in a uniformly superheated fluid. The bubble growth equation was obtained

from the conduction through the thermal boundary layer around the bubble. The interface cooling effect was also reported by Zuber (1961) and Mikic et al. (1970).

Zeng et al. (1993) proposed that the dominant forces leading to bubble detachment could be the unsteady growth force and buoyancy force. In order to derive an accurate detachment criterion from a force balance, all forces should be accurately known. If a mechanism is not known precisely, then approximate expressions, one or two fitted parameters and comparison with experiments might offer a solution. Such fitting procedures have indeed been applied (Klausner et al. 1993; Mei et al. 1995a; Helden et al.1995).

Mei et al. (1995b) developed a numerical model for vapor bubble growth in saturated pool boiling and demonstrated that the bubble growth rate is reduced due to the resulting temperature gradients beneath the nucleation site. Thorncroft et al. (1998) carried out experimental investigations of bubble growth and detachment in vertical up flow and down flow boiling. They observed that the growth data fit a power law ranging from about $t^{0.33}$ to $t^{0.5}$, where t is the time. The models of bubble growth and correlations for the bubble radius are discussed by Thorncroft et al. (2001).

Robinson and Judd (2001) considered four regions of bubble growth: surface tension controlled region, transition domain, inertial controlled growth and heat transfer controlled growth. A theory has been developed that is able to accommodate both spatial and temporal variations in the temperature and velocity fields in the liquid surrounding the bubble as it grows. Overall agreement between the theory and experimental data is very good. Bubble growth and variation of bubble lifetime and size with flux, subcooling, heat flux and pressure were examined by Prodanovic et al. (2002).

Nucleate pool boiling experiments with constant wall temperature were performed by Lee et al. (2003) using R-11 and R-113 for saturated boiling conditions. The geometry of the bubble was obtained from the images. The bubble growth rate was proportional to $t^{0.2}$, which was slower than the growth rate proposed in previous studies. Detachment of a vapor bubble from a plane, solid wall has been studied theoretically by Geld (2004). The vapor–liquid interface shape was approximated by a truncated sphere. The forces related to gravity and surface energy densities were found to be major contributors to departure time.

Boiling incipience and vapor bubble growth dynamics in aqueous surfactant solutions were studied using high-speed photography by Wu and Yang (1992). The bubble growth period was observed to increase slightly, while the waiting period and the time interval between two consecutive bubbles were reduced drastically. The experimental results of bubble dynamics for pure water and 100 ppm SDS solution at relatively low heat flux of $23\,\mathrm{kW/m^2}$ were presented by Yang and Maa (2003). It was shown that the departure diameter decreases considerably with addition of surfactant. Bubble growth in saturated pool boiling in water and surfactant solution was studied by Hetsroni et al. (2006a). It was shown that at relatively low heat fluxes on the wall ($q \leq 10\,\mathrm{kW/m^2}$), shape, lifetime and the volume of bubble growth in surfactant solution did not differ significantly with those in water. The time behavior of contact angle of bubble growth in surfactant solution is qualitatively similar to that of water.

At high enough heat flux of $q \geq 50\,\mathrm{kW/m^2}$, the boiling in surfactant solution, when compared to pure water, was observed to be more vigorous. Surfactant promotes activation of nucleation sites. The bubbles appeared in clusters. The lifetime of each bubble in the cluster is shorter than that of a single water bubble. The detachment diameter increases with increasing heat flux, whereas analysis of bubble growth in surfactant solution reveals the opposite effect: the detachment diameter of the bubble decreases with increasing heat flux.

These studies consider the dynamics of a single bubble that grows in infinity space, which is filled by superheated liquid. Under these conditions the bubble expansion depends on inertia forces or on intensity of heat transfer. In the case when inertia forces are dominant the bubble radius grows linearly in time (Carey 1992):

$$r(t) = \left(\frac{2}{3}\frac{T_\infty - T_\mathrm{S}}{T_\mathrm{S}}\frac{h_\mathrm{LG}\rho_\mathrm{G}}{\rho_\mathrm{L}}\right)^{1/2} t \tag{6.38}$$

where T_∞ and T_S are the ambient and saturated temperature, h_LG is the latent heat of evaporation, and ρ_G and ρ_L are the vapor and liquid density, respectively.

When the heat transfer is dominant, bubble radius is directly proportional to the square root of time

$$r(t) = 2C\sqrt{\alpha t} \tag{6.39}$$

where $C = \mathrm{Ja}\sqrt{3/\pi}$, $\mathrm{Ja} = (T_\infty - T_\mathrm{S})\rho_\mathrm{L}c_\mathrm{pL}/\rho_\mathrm{G}h_\mathrm{LG}$ is the Jacob number, and α is the liquid thermal diffusivity.

The bubble dynamics in a confined space, in particular in micro-channels, is quite different from that in infinity still fluid. In micro-channels the bubble evolution depends on a number of different factors such as existence of solid walls restricting bubble expansion in the transversal direction, a large gradient of the velocity and temperature field, etc. Some of these problems were discussed by Kandlikar (2002), Dhir (1998), and Peng et al. (1997). A detailed experimental study of bubble dynamics in a single and two parallel micro-channels was performed by Lee et al. (2004) and Li et al. (2004).

6.3.2 Dimensional Analysis

From the physical point of view it is possible to suggest that the rate of bubble growth in micro-channel is determined by the following parameters:

1. Physical properties of the fluid and its vapor: ρ_G, ρ_L, μ_L, k_L, c_pL, σ, h_LG
2. Average inlet flow velocity: U
3. Micro-channel characteristic size: d_*
4. Initial diameter of the bubble: d_0 (6.40)
5. Wall superheat: $\Delta T_\mathrm{S} = T_\mathrm{w} - T_\mathrm{S}$
6. Heat flux on the wall: q
7. Acceleration due to the gravity: g
8. Time: t

In accordance with (6.40) one can present the functional equation for rate of bubble growth as follows

$$\frac{\mathrm{d}r}{\mathrm{d}t} = f(q, h_{\mathrm{LG}}, \rho_{\mathrm{L}}, \rho_{\mathrm{G}}, \mu_{\mathrm{L}}, k_{\mathrm{L}}, c_{\mathrm{pL}}, d_0, d_*, \sigma, \Delta T_{\mathrm{S}}, g, t, U) \tag{6.41}$$

where $\mathrm{d}r/\mathrm{d}t$ is the rate of bubble growth, t is the time.

Using dimensions of length L, mass M, time τ, temperature T, and energy J, one can obtain dimensions of parameters on the right-hand side of Eq. (6.41):

$$\begin{aligned} &q\ [J\tau^{-1}L^{-2}],\ h_{\mathrm{LG}}\ [JM^{-1}],\ \rho_{\mathrm{L}}\ [ML^{-3}],\ \rho_{\mathrm{G}}\ [ML^{-3}],\ \mu_{\mathrm{L}}\ [ML^{-1}T^{-1}], \\ &k_{\mathrm{L}}\ [J\tau^{-1}L^{-1}T^{-1}],\ c_{\mathrm{pL}}\ [JM^{-1}T^{-1}],\ U\ [L\tau^{-1}],\ d_0\ [L],\ d_*\ [L],\ \sigma\ [M\tau^{-2}], \\ &T_{\mathrm{S}}\ [T],\ g\ [L\tau^{-2}],\ t\ [\tau]. \end{aligned} \tag{6.42}$$

Among the dimensional variables of the problem, five parameters have independent dimensions and Eq. (6.41) may be written in dimensionless form. Choosing parameters p_{L}, c_{pL}, U, ΔT_{S}, d_* and taking into account π-theorem (Sedov 1993), Eq. (6.41) can be represented as:

$$\Pi = \varphi(\Pi_1, \Pi_2, \ldots \Pi_9) \tag{6.43}$$

where $\Pi = \frac{\dot{r}}{U}$, $\Pi_1 = \frac{q}{\rho_{\mathrm{L}} U c_{\mathrm{pL}} \Delta T_{\mathrm{S}}}$, $\Pi_2 = \frac{h_{\mathrm{LG}}}{c_{\mathrm{pL}} \Delta T_{\mathrm{S}}}$, $\Pi_3 = \frac{\rho_{\mathrm{G}}}{\rho_{\mathrm{L}}}$, $\Pi_4 = \frac{\mu_{\mathrm{L}}}{\rho U d_*}$, $\Pi_5 = \frac{k_{\mathrm{L}}}{\rho_{\mathrm{L}} c_{\mathrm{pL}} U d_*}$, $\Pi_6 = \frac{d_0}{d_*}$, $\Pi_7 = \frac{\sigma}{\rho U^2 d_*}$, $\Pi_8 = \frac{g d_*}{U^2}$, $\Pi_9 = \frac{\tau U}{d_*}$, $\dot{r} = \frac{\mathrm{d}r}{\mathrm{d}t}$.

Analysis of experimental data presented by Lee et al. (2004) revealed that parameters Π_3–Π_9 did not change significantly. Parameter Π_2 depends mainly on the wall superheat, $\Delta T_{\mathrm{S}} = T_{\mathrm{W}} - T_{\mathrm{S}}$. It should be noted that the value of wall temperature T_{W} in experimental investigations was obtained from the measurements, whereas the value of saturation temperature T_{S} was calculated using the dependence of T_{S} on saturation pressure P_{S}. Assuming linear pressure distribution along the micro-channel Lee et al. (2004) presented two approaches to calculate T_{S}. The first of them is based on the local pressure at the nucleate boiling incipience. The second one is based on the average value of the pressure in the micro-channel $P_{\mathrm{S}} = (P_{\mathrm{in}} + P_{\mathrm{out}})/2$. Depending on the method of calculation of saturation temperature, the results differ. We assumed that $\Pi_2 \approx \mathrm{const}$. Thus, one can consider Π_1 as the dimensionless parameter that determines the rate of bubble growth in the linear regime:

$$\frac{\mathrm{d}r}{\mathrm{d}t} = \varphi(\Pi_1)\,. \tag{6.44}$$

6.3.3 Experimental Data

Single micro-channel

Data by Lee et al. (2004) and Li et al. (2004) contain the results related to bubble dynamics in a single micro-channel and two parallel ones. The experimen-

tal setup used by Lee et al. (2004) consisted of the test section, a syringe pump, a heating module and a flow visualization system. The test section was a 5 mm wide silicon strip, etched with the micro-channel on its top surface. The top surface dimension was 5×20 mm. Figure 6.23 displays the top and cross-section views of the test section. The top and bottom widths of the trapezoid channel are 102.8 and 59.12 μm, respectively, and the channel depth is 30.1 μm resulting in a hydraulic diameter of 41.3 μm. The channel length is 28 mm leading to a length-to-diameter ratio of 678. Only the central 20 mm was heated. The rms roughness of the bottom surface was 206 nm, while it was 82 nm for the side wall.

The results are presented in Table 6.6 (the data related to flow regimes at which the wall temperature T_w was less than saturated, are excluded from this table).

According to Eq. (6.44) such a behavior may be analyzed using parameter Π_1. In the range of $\Pi_1 = 0.00791-0.0260$ linear behavior of the bubble radius was observed, when $\Pi_1 > 0.0260$ exponential bubble growth took place (Fig. 6.24).

Table 6.6 also demonstrates extraordinarily high bubble growth rates of 94.63, 72.8 and 95.3 μm/ms. For these three cases, the growth rates are two orders of magnitude higher than the other cases. The authors noted that it is unclear why the bubble growth rate for such cases is much higher than the other cases.

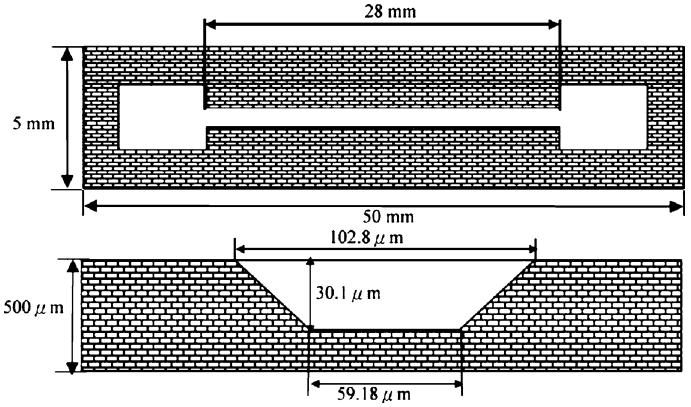

Fig. 6.23 The top and cross-section views of the test section with a trapezoid micro-channel (length shown not in scale). Reprinted from Lee et al. (2004) with permission

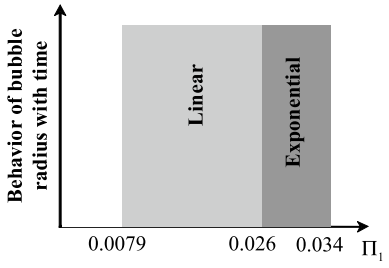

Fig. 6.24 Behavior of bubble radius with time. The values of Π_1 were calculated from experimental results presented by Lee et al. (2004)

Table 6.6 Behavior of bubble radius with time. Data by Lee et al. (2004)

Number	Heat flux q [W/m^2]	Mass flux G [kg/m^2 s]	Bubble growth rate $\mathrm{d}r/\mathrm{d}t$ [μm/ms]	Parameter $\Pi_1 = \frac{q}{\rho_L U c_{pL} \Delta T_S}$	Behavior of bubble radius with time
1	103,000	341	94.63	0.00791	
2	189,000	341	0.24	0.0260	
3	264,000	341	0.32	0.0259	
4	255,000	341	0.22	0.0135	
5	107,000	477	7.09	0.0106	
6	218,000	477	72.8	0.0019	Linear
7	353,000	477	0.54	0.0124	
8	415,000	477	0.10	0.0145	
9	449,000	477	0.10	0.0110	
10	57,600	170	2.62	0.0267	
11	137,000	170	95.3	0.0272	Exponential
12	196,000	170	4.91	0.0339	

Parallel micro-channels

The bubble dynamics under conditions corresponding to flow in two parallel trapezoidal micro-channels with hydraulic diameter 47.7 μm was studied by Li et al. (2004). The bubbles in two parallel micro-channels generally grow similarly to that in a single micro-channel. The authors reported on the presence of two-phase flow instability.

Hetsroni et al. (2003) studied bubble growth in 26 parallel triangular micro-channels of $d_h = 103\,\mu\mathrm{m}$ and length of 10 mm. When incipient boiling superheat is achieved, the vapor bubble nucleates and grows rapidly. The bubble is initially a small sphere and then the axisymmetric growth in a narrow channel takes place. Temporal variation of bubble size is shown in Fig. 6.25. Figure 6.25a,b shows the variation of bubble size in the streamwise direction L_p, and in the spanwise direction L_n, respectively. From these figures one can conclude that at time $t = 0.375$ s the maximum length of the bubble in the streamwise direction L_p is about eight times larger than that in the spanwise direction L_n.

The observed ratio $f = L_p/L_n$, is quite different from that reported for subcooled flow boiling of water in tubes of 17–22 mm inner diameter. Prodanovic et al. (2002) reported that this ratio was typically around 0.8 for experiments at 1.05–3 bar. The situation considered in experiments carried out by Hetsroni et al. (2003) is however different as the bubbles undergo a significant volume change and the flow is unstable. Ory et al. (2000) studied numerically the growth and collapse of a bubble in a narrow tube filled with a viscous fluid. The situation considered in that study is also quite different from experiments by Hetsroni et al. (2003) as, in that case, heat was added to the system impulsively, rather than continuously as we do here.

Visual observation of bubble growth in parallel triangular micro-channels showed that the majority of the first bubbles were observed on the channel bottom wall, though a few bubbles did appear on the side walls. After nucleation, bubbles first

grew to detachment size before departing into the liquid flow. The detached bubbles moved to the downstream plenum.

Bubble velocity

Figure 6.26 shows the velocity of displacement of the bubble tail in the streamwise direction U_b (m/s) versus bubble lifetime t, at fixed conditions as described

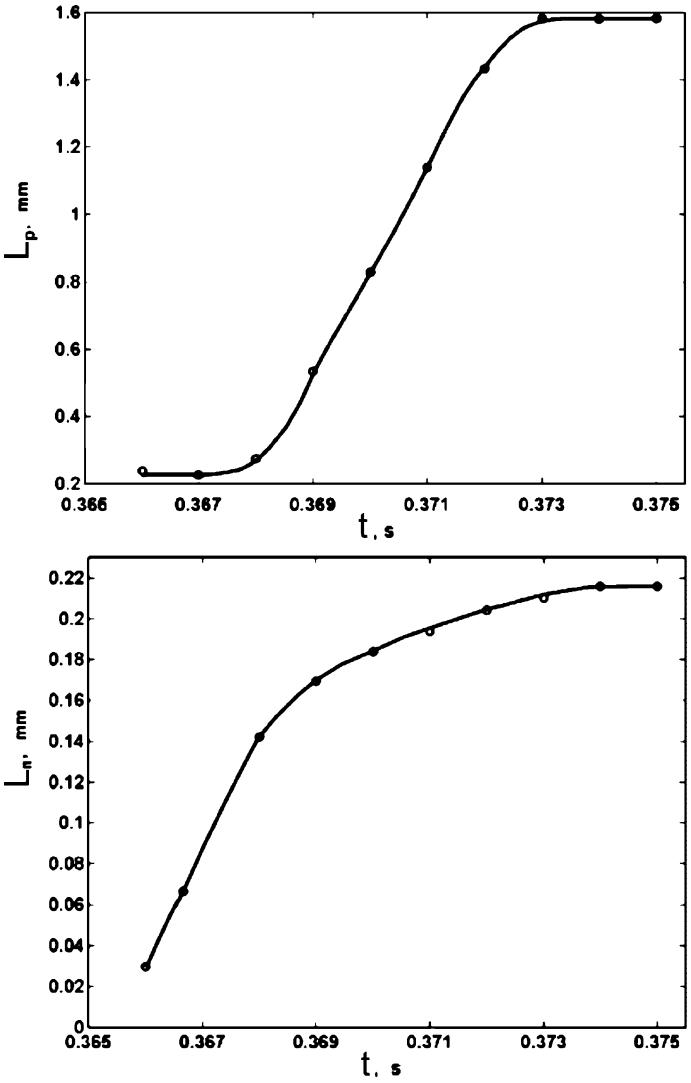

Fig. 6.25 Temporal variation of vapor bubble size: (**a**) streamwise direction, L_p (**b**) spanwise direction, L_n. $U_{LS} = 0.046$ m/s, $q = 8 \times 10^4$ W/m^2. Reprinted from Hetsroni et al. (2003) with permission

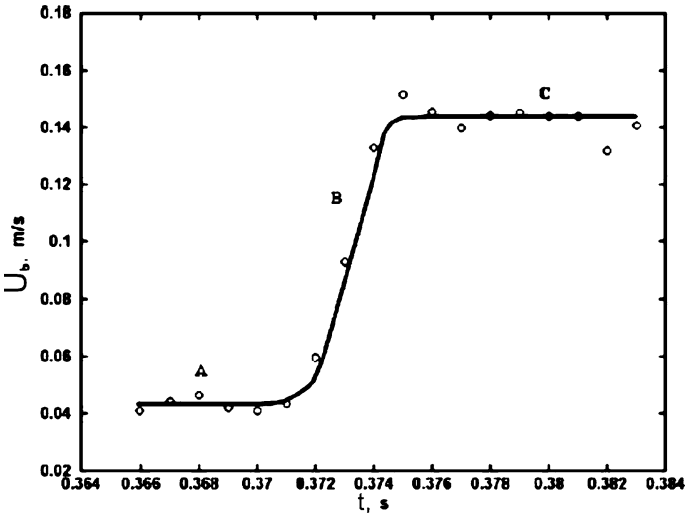

Fig. 6.26 Velocity of bubble displacement. $U_{LS} = 0.046\,\mathrm{m/s}$, $q = 80\,\mathrm{kW/m^2}$. Reprinted from Hetsroni et al. (2003) with permission

above, i.e., $q = 8 \times 10^4\,\mathrm{W/m^2}$, $U_{LS} = 0.046\,\mathrm{m/s}$. One may conclude that the velocity of bubble displacement varies, depending on the given range of lifetime. In region A the boiling process during the time of about 0.005 s from the appearance of the first bubble, ONB, the bubble velocity is equal to the superficial liquid velocity. It should be noted that the term ONB, known as the onset of nucleate boiling, was "borrowed" from the terminology of subcooled flow boiling in larger tubes. Region B is characterized by a sharp increase in the bubble velocity. One may conclude that the bubble is accelerated in the streamwise flow direction. Figure 6.26 shows that in this region the bubble velocity increases about threefold, during a time interval of about 0.003 s. After the time when U_b reaches maximum value it remains constant, as shown in Fig. 6.26, region C.

Such a behavior agrees with results reported by Agostini et a. (2008). It was found that the elongated bubble velocity increased with increasing bubble length until a plateau was reached. An analytical model has been proposed that is able to predict this trend.

The collision of elongated bubbles has been studied by Revellin et al. (2008) along adiabatic glass micro-channels of 509 and 709 μm internal diameters for refrigerant R-134a. A model for the collision of elongated bubbles in micro-channels was proposed to predict the bubble length distribution at the exit of the micro-evaporator.

In micro-channels bubbles cause a significant volume change (relative to the channel size). As a result, pressure fluctuations were observed. The temporal behavior of the pressure drop is shown in Fig. 6.27. The data were obtained at $q = 220\,\mathrm{kW/m^2}$ and $U_{LS} = 0.14\,\mathrm{m/s}$. Such a behavior is a result of vapor formation in each micro-channel.

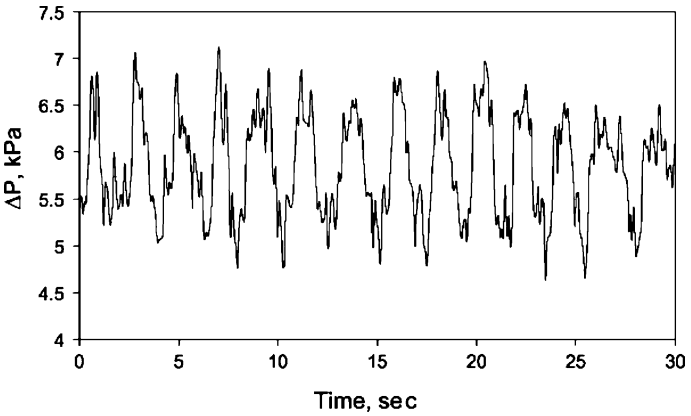

Fig. 6.27 Pressure drop fluctuations. $U_{LS} = 0.14$ m/s, $q = 220$ kW/m^2. Reprinted from Hetsroni et al. (2003) with permission

The pressure spike introduces a disruption in the flow. Depending on the local conditions, the excess pressure inside the bubble may overcome the inertia of the incoming liquid and the pressure in the inlet manifold, and cause a reverse flow of varying intensity depending on the local conditions. There are two ways to reduce the flow instabilities: reduce the local liquid superheat at the ONB and introduce a pressure drop element at the entrance of each channel, Kandlikar (2006). Kakac and Bon (2008) reported that density-wave oscillations were observed also in conventional size channels. Introduction of additional pressure drop at the inlet (small diameter orifices were employed for this purpose) stabilized the system.

A simultaneous visualization and measurement study has been carried out by Wang et al. (2008) to investigate effects of inlet/outlet configurations on flow boiling instabilities in parallel micro-channels having a length of 30 mm and a hydraulic diameter of 186 μm. It was found that nearly steady flow boiling existed in the parallel micro-channels through an inlet restriction.

6.4 Pressure Drop and Heat Transfer

6.4.1 Pressure Drop in Two-Phase Flow Boiling

The measurements show that the pressure drop in circular and rectangular micro-channels depend strongly on the mass and heat fluxes (Tran et al. 2000; Yu et al. 2002; Shuai et al. 2003).

The flow patterns (expansion of the bubbly, slug and annular regions of flow) affect the local pressure drop, as well as the pressure oscillations in micro-channels (Kandlikar et al. 2001; Wu and Cheng 2003a,b, 2004; Qu and Mudawar 2003; Hetsroni et al. 2005; Lee and Mudawar 2005a).

The influence of inlet conditions on stability of flow boiling in micro-channels was analyzed by Brutin and Tadrist (2004). The set-up with rectangular micro-channel $500 \times 4{,}000\,\mu m$ was used to study flow boiling at two kinds of upstream conditions, which corresponded to constant liquid velocity at channel entrance (confinement condition) and constant velocity at the syringe outlet. The flow characteristics corresponding to steady and unsteady regimes were studied and the Reynolds number that subdivided these states was found.

Hwan and Kim (2006) investigated the pressure drop in circular stainless steel tubes with inner diameter of 244, 430, and 792 μm. These data show that mass flux strongly affects two-phase pressure drop in micro-channels of different diameters.

A detailed analysis of several correlations for calculating pressure drop in boiling flow was carried out by Qu and Mudawar (2003a). They tested two groups of correlations, the first of them corresponds to boiling flow in conventional channels (Collier and Thome 1994; Lockhart and Martinelli 1949), and the second ones to boiling in conventional size channels and micro-channels (Mishima and Hibiki 1996; Tran et al. 2000; Lee and Lee 2001a; Yu et al. 2002; Qu and Mudawar 2003a).

In the study by Qu and Mudawar (2003a) experiments were performed to measure pressure drop in two-phase micro-channel heat sink containing 21 parallel $231 \times 713\,\mu m$ micro-channels. The pressure drop in the micro-channel two-phase region ΔP_{tp} was expressed as the sum of acceleration and friction components:

$$\Delta P_{tp} = \Delta P_{tp,a} + \Delta P_{tp,f} \tag{6.45}$$

where $\Delta P_{tp,a}$ is the acceleration component of two-phase pressure drop, and $\Delta P_{tp,f}$ is the friction component of two-phase pressure drop.

The predictive capability of the proposed correlation for all operating conditions of the study by Qu and Mudawar (2003a) was illustrated. The mean absolute error (MAE) of each correlation

$$\mathrm{MAE} = \frac{1}{N}\sum \frac{\left|\Delta P_{pred} - \Delta P_{exp}\right|}{\Delta P_{exp}} 100\% \tag{6.46}$$

was used to discuss the results, where N is the number of experimental data. The comparison showed that the MAE for the first group of correlations, denoted as Eqs. (1) to (6) in the study of Qu and Mudawar (2003a), was in the range of $\mathrm{MAE} = 29-378\%$. The correlations of the second group, Eqs. (7) to (11), are presented in Table 6.7.

In Table 6.7, C is the Martinelli–Chisholm constant, f is the friction factor, f_f is the friction factor based on local liquid flow rate, f_{fo} is the friction factor based on total flow rate as a liquid, G is the mass velocity in the micro-channel, L is the length of micro-channel, P is the pressure, ΔP is the pressure drop, $P_{tp,a}$ is the acceleration component of two-phase pressure drop, $\Delta P_{tp,f}$ is the frictional component of two-phase pressure drop, v is the specific volume, x_e is the thermodynamic equilibrium quality, X_{vt} is the Martinelli parameter based on laminar liquid-turbulent vapor flow, X_{vv} is the Martinelli parameter based on laminar liquid-laminar vapor flow, α is the void fraction, μ is the viscosity, ρ is the density, Φ_f^2 is the two-phase frictional

multiplier based on local liquid flow rate, Φ_{fo}^2 is the two-phase frictional multiplier based on total flow considered as a liquid, Re_g is the Reynolds number based on local vapor flow, Re_{fo} is the Reynolds number based on total flow as a liquid; the subscripts are f for liquid, frictional, g for vapor, in for test module inlet, out for test module outlet, pred for predicted, and tp for two-phase.

It should be noted that for convenience in Table 6.7 we used the same nomenclature as in original paper by Qu and Mudawar (2003a).

Figures 6.28 and 6.29 show the comparison of pressure drop data with predictions of conventional size/micro-channels correlations ((7)–(11), Table 6.7).

A new approach was developed by Lee and Mudawar (2005a) to improve the accuracy of pressure drop prediction in two-phase micro-channels. Since the bubbly and churn flow patterns are rarely detected in high-flux micro-channel flow, the separated flow model was deemed more appropriate than the homogeneous.

It was assumed that the added complexity of two-phase flow in a micro-channel is the result of interactions between liquid inertia, the liquid viscous force, and surface tension. Two key measures of these interactions are the Reynolds and Weber numbers based on liquid properties:

$$Re_L = \frac{U d_h}{\nu_L} \tag{6.47}$$

and

$$We_L = \frac{G^2 d_h}{\sigma \rho_L} \tag{6.48}$$

The two-phase pressure drop multiplier

$$\Phi_L^2 = 1 + \frac{C}{X} + \frac{1}{X^2} \tag{6.49}$$

is modified with a new dimensionless parameter defined as

$$C = C_1 Re_L^{c_2} We_L^{c_3} \tag{6.50}$$

where C_1, C_2, C_3 are parameters presented in Eqs. (6.51–6.52).

To enhance the predictive capability of the new correlation, both the present R-134a data and prior micro-channel water data of Qu and Mudawar (2003a) were examined. Large differences between the thermophysical properties of the two coolants were deemed highly effective at broadening the application range of the new correlation. Another key difference between the two data sets is both the liquid and vapor flows are laminar for the water data, while low viscosity rendered the vapor flow turbulent for R-134a. Typical micro-channel operating conditions rarely produced turbulent liquid flow. Therefore, two separate correlations were derived for C, based on the flow states of the liquid and vapor,

$$C_{vv} = 2.16 Re_L^{0.047} We_L^{0.60} \text{ (laminar liquid–laminar vapor)} \tag{6.51}$$

$$C_{vt} = 1.45 Re_L^{0.25} We_L^{0.23} \text{ (laminar liquid–turbulent vapor)} \tag{6.52}$$

Table 6.7 Pressure drop correlations. Reprinted from Qu and Mudawar (2003a) with permission

Author	Component of ΔP	Definitions	Max average error
Misima, Hibiki (1996) (7)	$\Delta P_{\mathrm{tp,f}} = \frac{L_{\mathrm{tp}}}{x_{\mathrm{e,out}}} \int_0^{x_{\mathrm{e,out}}} \frac{2f_{\mathrm{f}}G^2(1-x_{\mathrm{e}})^2\nu_{\mathrm{f}}}{d_{\mathrm{h}}} \Phi_{\mathrm{f}}^2 \, \mathrm{d}x_{\mathrm{e}}$ $\Delta P_{\mathrm{tp,a}} = G^2\nu_{\mathrm{f}}\left[\frac{x_{\mathrm{e,out}}^2}{\alpha_{\mathrm{out}}}\left(\frac{\nu_{\mathrm{g}}}{\nu_{\mathrm{f}}}\right) + \frac{(1-x_{\mathrm{e,out}})^2}{1-\alpha_{\mathrm{out}}} - 1\right]$	$\Phi_{\mathrm{f}}^2 = 1 + \frac{C}{X_{\mathrm{vv}}} + \frac{1}{X_{\mathrm{vv}}^2}$, $X_{\mathrm{vv}} = \left(\frac{\mu_{\mathrm{f}}}{\mu_{\mathrm{g}}}\right)^{0.5}\left(\frac{1-x_{\mathrm{e}}}{x_{\mathrm{e}}}\right)^{0.5}\left(\frac{\nu_{\mathrm{f}}}{\nu_{\mathrm{g}}}\right)^{0.5}$ $\alpha_{\mathrm{out}} = \left[1 + \left(\frac{1-x_{\mathrm{e,out}}}{x_{\mathrm{e,out}}}\right)\left(\frac{\nu_{\mathrm{f}}}{\nu_{\mathrm{g}}}\right)^{2/3}\right]^{-1}$ $C = 21\left[1 - \exp(-0.319 \cdot 10^3 d_{\mathrm{h}})\right]$	13.9
Tran et al. (2000) (8)	$\Delta P_{\mathrm{tp,f}} \frac{2f_{f0}G^2\nu_{\mathrm{f}}}{d_{\mathrm{h}}} \frac{L_{\mathrm{tp}}}{x_{\mathrm{e,out}}} \int_0^{x_{\mathrm{e,out}}} \Phi_{\mathrm{fo}}^2 \, \mathrm{d}x_{\mathrm{e}}$ $\Delta P_{\mathrm{tp,a}} = G^2\nu_{\mathrm{f}}\left[\frac{x_{\mathrm{e,out}}^2}{\alpha_{\mathrm{out}}}\left(\frac{\nu_{\mathrm{g}}}{\nu_{\mathrm{f}}}\right) + \frac{(1-x_{\mathrm{e,out}})^2}{1-\alpha_{\mathrm{out}}} - 1\right]$	$\Phi_{f0}^2 = 1 + \left(4.3\Gamma^2 - 1\right) \cdot \left[N_{\mathrm{conf}} x_{\mathrm{e}}^{0.875}(1-x_{\mathrm{e}})^{0.875} + x_{\mathrm{e}}^{1.75}\right]$ $\Gamma = \left(\frac{\nu_{\mathrm{g}}}{\nu_{\mathrm{f}}}\right)^{0.5}\left(\frac{\mu_{\mathrm{g}}}{\mu_{\mathrm{f}}}\right)^{0.5}$ $\alpha_{\mathrm{out}} = \left[1 + \left(\frac{1-x_{\mathrm{e,out}}}{x_{\mathrm{e,out}}}\right)\left(\frac{\nu_{\mathrm{f}}}{\nu_{\mathrm{g}}}\right)^{2/3}\right]^{-1}$ $N_{\mathrm{conf}} = \left[\frac{\sigma}{g(\rho_{\mathrm{f}}-\rho_{\mathrm{g}})}\right]^{0.5}/d_{\mathrm{h}}$	828.3
Lee, Lee (2001a) (9)	$\Delta P_{\mathrm{tp,f}} = \frac{L_{\mathrm{tp}}}{x_{\mathrm{e,out}}} \int_0^{x_{\mathrm{e,out}}} \frac{2f_{\mathrm{f}}G^2(1-x_{\mathrm{e}})^2\nu_{\mathrm{f}}}{d_{\mathrm{h}}} \Phi_{\mathrm{f}}^2 \, \mathrm{d}x_{\mathrm{e}}$ $\Delta P_{\mathrm{tp,a}} = G^2\nu_{\mathrm{f}}\left[\frac{x_{\mathrm{e,out}}^2}{\alpha_{\mathrm{out}}}\left(\frac{\nu_{\mathrm{g}}}{\nu_{\mathrm{f}}}\right) + \frac{(1-x_{\mathrm{e,out}})^2}{1-\alpha_{\mathrm{out}}} - 1\right]$	$\Phi_{\mathrm{f}}^2 = 1 + \frac{C}{X_{\mathrm{vt}}} + \frac{1}{X_{\mathrm{vt}}^2}$, $X_{\mathrm{vt}} = \left(\frac{f_{\mathrm{f}}\mathrm{Re}_{\mathrm{g}}^{0.25}}{0.079}\right)^{0.5}\left(\frac{1-x_{\mathrm{e}}}{x_{\mathrm{e}}}\right)\left(\frac{\nu_{\mathrm{f}}}{\nu_{\mathrm{g}}}\right)^{0.5}$ $\alpha_{\mathrm{out}} = \left[1 + \left(\frac{1-x_{\mathrm{e,out}}}{x_{\mathrm{e,out}}}\right)\left(\frac{\nu_{\mathrm{f}}}{\nu_{\mathrm{g}}}\right)^{2/3}\right]^{-1}$ $C = 6.185 \cdot 10^{-2}\mathrm{Re}_{f0}^{0.726}$	19.1
Yu et al. (2002) (10)	$\Delta P_{\mathrm{tp,f}} = \frac{L_{\mathrm{tp}}}{x_{\mathrm{e,out}}} \int_0^{x_{\mathrm{e,out}}} \frac{2f_{\mathrm{f}}G^2(1-x_{\mathrm{e}})^2\nu_{\mathrm{f}}}{d_{\mathrm{h}}} \Phi_{\mathrm{f}}^2 \, \mathrm{d}x_{\mathrm{e}}$ $\Delta P_{\mathrm{tp,a}} = G^2\nu_{\mathrm{f}}\left[\frac{x_{\mathrm{e,out}}^2}{\alpha_{\mathrm{out}}}\left(\frac{\nu_{\mathrm{g}}}{\nu_{\mathrm{f}}}\right) + \frac{(1-x_{\mathrm{e,out}})^2}{1-\alpha_{\mathrm{out}}} - 1\right]$	$\Phi_{\mathrm{f}}^2 = \frac{1}{X_{\mathrm{vt}}^{1.9}} X_{\mathrm{vt}} = \left(\frac{f_{\mathrm{f}}\mathrm{Re}_{\mathrm{g}}^{0.25}}{0.046}\right)^{0.5}\left(\frac{1-x_{\mathrm{e}}}{x_{\mathrm{e}}}\right)\left(\frac{\nu_{\mathrm{f}}}{\nu_{\mathrm{g}}}\right)^{0.5}$ $\alpha_{\mathrm{out}} = \left[1 + \left(\frac{1-x_{\mathrm{e,out}}}{x_{\mathrm{e,out}}}\right)\left(\frac{\nu_{\mathrm{f}}}{\nu_{\mathrm{g}}}\right)^{2/3}\right]^{-1}$	48.0
Qu, Mudawar (2003a) (11)	$\Delta P_{\mathrm{tp,f}} = \frac{L_{\mathrm{tp}}}{x_{\mathrm{e,out}}} \int_0^{x_{\mathrm{e,out}}} \frac{2f_{\mathrm{f}}G^2(1-x_{\mathrm{e}})^2\nu_{\mathrm{f}}}{d_{\mathrm{h}}} \Phi_{\mathrm{f}}^2 \, \mathrm{d}x_{\mathrm{e}}$ $\Delta P_{\mathrm{tp,a}} = G^2\nu_{\mathrm{f}}\left[\frac{x_{\mathrm{e,out}}^2}{\alpha_{\mathrm{out}}}\left(\frac{\nu_{\mathrm{g}}}{\nu_{\mathrm{f}}}\right) + \frac{(1-x_{\mathrm{e,out}})^2}{1-\alpha_{\mathrm{out}}} - 1\right]$	$\Phi_{\mathrm{f}}^2 = 1 + \frac{C}{X_{\mathrm{vv}}} + \frac{1}{X_{\mathrm{vv}}^2}$, $X_{\mathrm{vv}} = \left(\frac{\mu_{\mathrm{f}}}{\mu_{\mathrm{g}}}\right)^{0.5}\left(\frac{1-x_{\mathrm{e}}}{x_{\mathrm{e}}}\right)^{0.5}\left(\frac{\nu_{\mathrm{f}}}{\nu_{\mathrm{g}}}\right)^{0.5}$ $\alpha_{\mathrm{out}} = \left[1 + \left(\frac{1-x_{\mathrm{e,out}}}{x_{\mathrm{e,out}}}\right)\left(\frac{\nu_{\mathrm{f}}}{\nu_{\mathrm{g}}}\right)^{2/3}\right]^{-1}$ $C = 21\left[1 - \exp(-0.319 \cdot 10^3 d_{\mathrm{h}})\right] \cdot (0.00418G + 0.0613)$	12.4

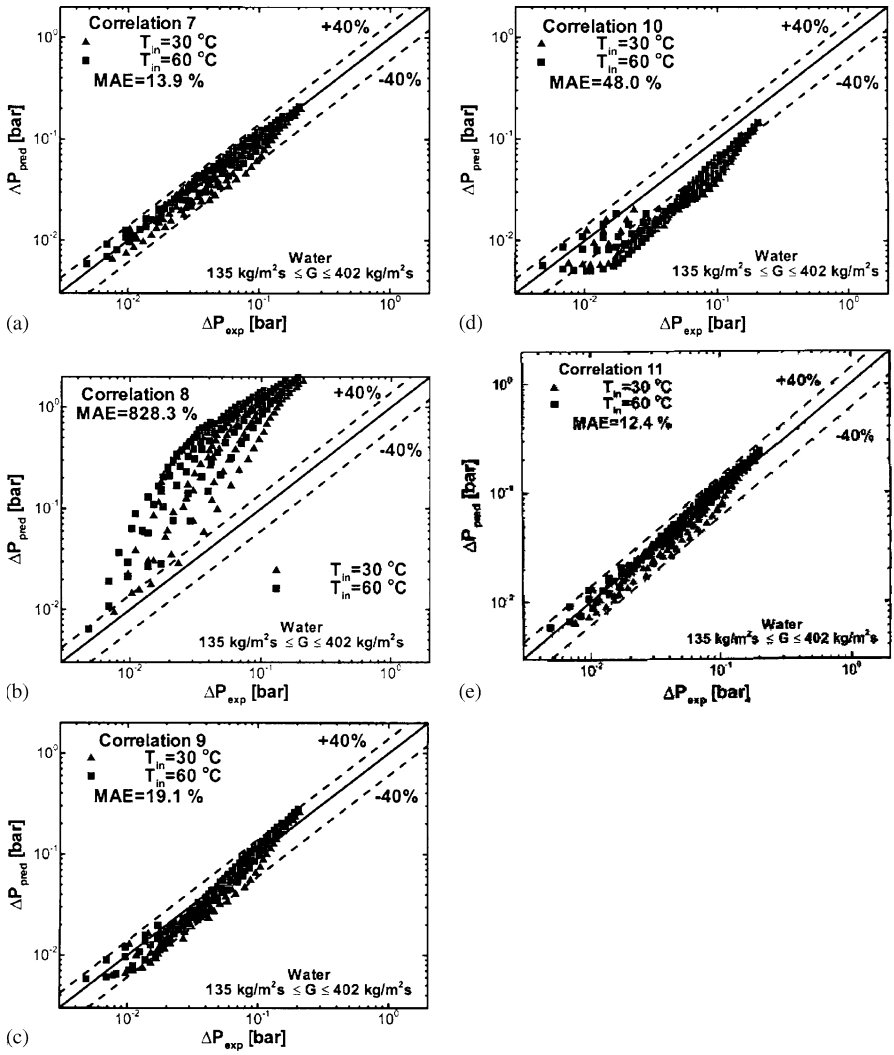

Fig. 6.28 Comparison of pressure drop data with predictions of mini/micro-channel correlations of (**a**) Mishima and Hibiki (1996), (**b**) Tran et al. (2000), (**c**) Lee and Lee (2001a,d) and Yu et al. (2002), (**e**) Qu and Mudawar (2003a). Reprinted from Qu and Mudawar (2003a) with permission

Notice the stronger effect of surface tension where both liquid and vapor are laminar. Figure 6.30a shows good agreement of the pressure drop predictions based on the new correlation with the R-134a data, both in terms of MAE (mean absolute error) and the general trend. The largest deviation is concentrated in the low mass flux and low heat flux region where both the heat loss (which influences the accuracy of the heat flux used in the pressure drop model) and the flow rate measurement uncertainty are greatest. Figure 6.30b shows the present correlation is also very effective at predicting the micro-channel water data of Qu and Mudawar (2003a).

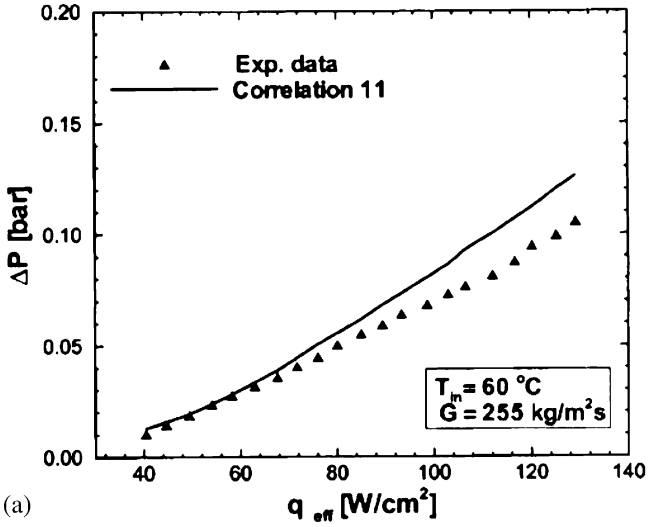

(a)

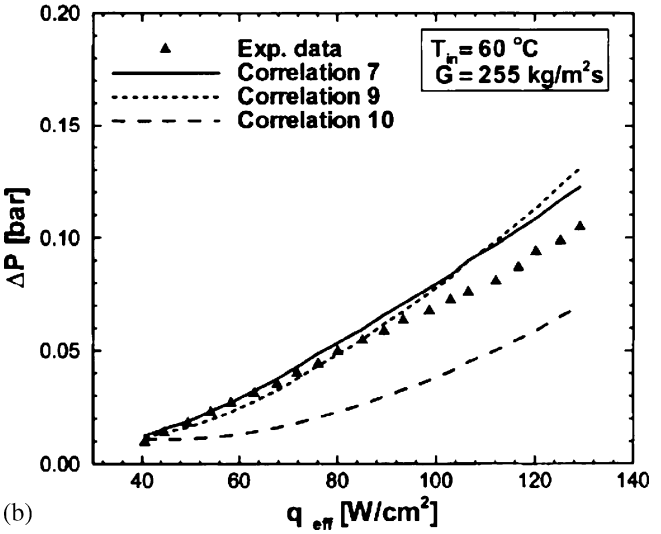

(b)

Fig. 6.29 Comparison of pressure drop data with correlation predictions for $T_{\text{in}} = 60\,^{\circ}\text{C}$ and $G = 255\,\text{kg/m}^2\text{s}$. (**a**) correlation (11), (**b**) correlations (7)–(10). Reprinted from Qu and Mudawar (2003a) with permission

Quiben and Thome (2007a,b) presented an experimental and analytical investigation of two-phase pressure drops during evaporation in horizontal tubes. Experiments were performed under diabatic conditions in tubes of $d = 8$ and 13 mm in the range of vapor quality $x = 0-1$, mass velocity $G = 70-700\,\text{kg/m}^2\text{s}$, heat flux $q = 6.0-57.5\,\text{kW/m}^2$. The test fluids were R-134a, R-22 and R-410A. The results

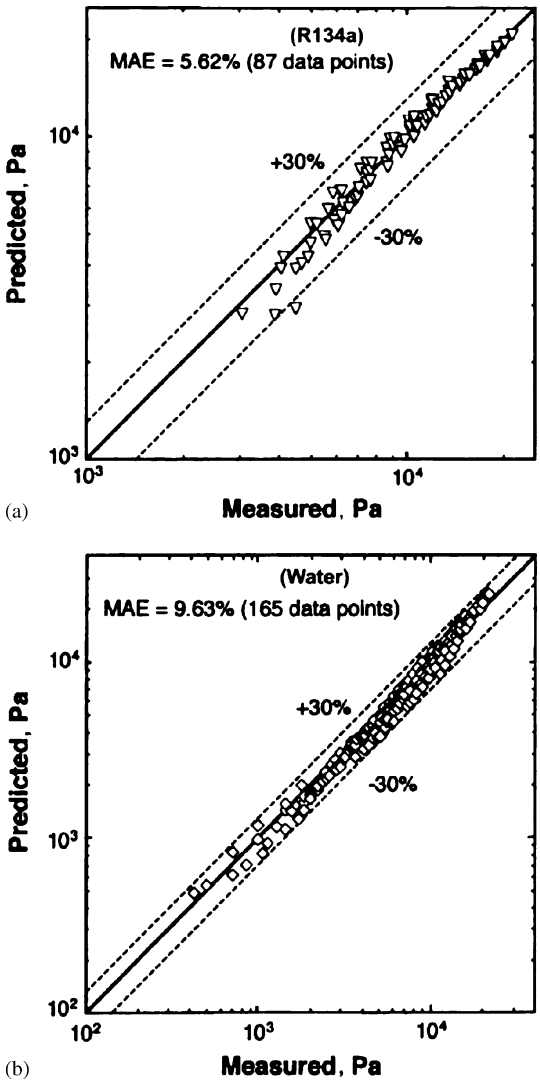

Fig. 6.30 Comparison of correlation predictions with (**a**) R-134a (Lee and Mudawar (2005a)) and (**b**) water Qu and Mudawar's (2003a) micro-channel water data. Reprinted from Lee and Mudawar (2005a) with permission

showed that while the fluid, diameter and mass velocity had a strong effect over the entire range of vapor quality, the heat flux influenced the pressure drop only for a particular range vapor qualities near and after the onset dryout. An analytical study was undertaken in order to develop a new two-phase prediction method. A model has been developed following a phenomenological approach and the interfacial structure between the phases was taken into account. The flow pattern effects are particularly important at low flow rates (stratification effects) and high vapor qualities (dryout effects). This model works well in annular flow and captures the position of the pressure drop peak under condition of dryout at high vapor quality.

6.4.2 Heat Transfer in Two-Phase Flow Boiling

The heat transfer coefficient of boiling flow through a horizontal rectangular channel with low aspect ratio (0.02–0.1) was studied by Lee and Lee (2001b). The mass flux in these experiments ranged from 50 to 200 $\mathrm{kg/m^2\,s}$, maximum heat flux was 15 $\mathrm{kW/m^2}$, and the quality ranged from 0.15 to 0.75, which corresponds to annular flow. The experimental data showed that under conditions of the given experiment, forced convection plays a dominant role.

The detail experimental study of flow boiling heat transfer in two-phase heat sinks was performed by Qu and Mudawar (2003b). It was shown that the saturated flow boiling heat transfer coefficient in a micro-channel heat sink is a strong function of mass velocity and depends only weakly on the heat flux. This result, as well as the results by Lee and Lee (2001b), indicates that the dominant mechanism for water micro-channel heat sinks is forced convective boiling but not nucleate boiling.

Heat transfer characteristics for saturated boiling were considered by Yen et al. (2003). From this study of convective boiling of HCFC123 and FC72 in micro-tubes with inner diameter 190, 300 and 510 μm one can see that in the saturated boiling regime, the heat transfer coefficient monotonically decreased with increasing vapor quality, but independent of mass flux.

The convective and nucleate boiling heat transfer coefficient was the subject of experiments by Grohmann (2005). The measurements were performed in micro-tubes of 250 and 500 μm in diameter. The nucleate boiling metastable flow regimes were observed. Heat transfer characteristics at the nucleate and convective boiling in micro-channels with different cross-sections were studied by Yen et al. (2006). Two types of micro-channels were tested: a circular micro-tube with a 210 μm diameter, and a square micro-channel with a 214 μm hydraulic diameter. The heat transfer coefficient was higher for the square micro-channel because the corners acted as effective nucleation sites.

Several popular macro-channel correlations and recently recommended small-channel correlations were examined by Lee and Mudawar (2005b). Predictions were adjusted for the three-sided wall heating and rectangular geometry using the following relation:

$$h_{\mathrm{tp}} = h_{\mathrm{tp,cor}} \frac{\mathrm{Nu}_3}{\mathrm{Nu}_4} \tag{6.53}$$

where $h_{\mathrm{tp,cor}}$ is the value predicted from a correlation for uniform circumferential heating, and Nu_3 and Nu_4 are the single-phase Nusselt numbers for laminar flow with three-sides and four-sides wall heating, respectively (Shah and London 1978).

$$\mathrm{Nu}_3 = 8.235(1 - 1.883\beta + 3.767\beta^2 - 5.814\beta^3 + 5.361\beta^4 - 2.0\beta^5) \tag{6.54}$$

and

$$\mathrm{Nu}_4 = 8.235(1 - 2.042\beta + 3.085\beta^2 - 2.477\beta^3 + 1.058\beta^4 - 0.186\beta^5) \tag{6.55}$$

where β is the ratio of the channel depth to width.

Figure 6.31 compares the measured heat transfer coefficient by Lee and Mudawar (2005b) in two-phase flow of R-134a to predictions based on previous studies. The predictive accuracy of a correlation was measured by the mean absolute error, defined as

$$\mathrm{MAE} = \frac{1}{N}\sum\left[\frac{\left|h_{\mathrm{tp,pred}} - h_{\mathrm{tp,exp}}\right|}{h_{\mathrm{tp,exp}}} \times 100\%\right]. \tag{6.56}$$

Figure 6.31 shows all correlations yield poor predictions evidenced by their large MAE values.

Experiments by Lee and Mudawar (2005b) reveal the range of parameters at which heat transfer is controlled by nucleate boiling or annular film evaporation. The first of these processes occurs only at low qualities ($x < 0.05$) corresponding to very low heat fluxes; the second one at moderate ($0.05 < x < 0.55$) or high ($x > 0.55$) qualities that correspond to high enough heat fluxes. New correlations were suggested by Lee and Mudawar (2005b). They are based on the Martinelli parameter X and account for micro-channel effects not represented in the prior correlations.

Table 6.8 summarizes the new correlations for the three quality regions. The low and high-quality regions are based solely on the Martinelli parameter while the mid-range includes the effects of Bo and $\mathrm{We_{fo}}$ as well. Overall, convection to liquid is important for both the low and mid-quality regions, while convection to vapor becomes important for the high-quality region. For the latter, the low viscosity of R-134a vapor yields vapor Reynolds numbers corresponding to turbulent flow at high-heat flux conditions despite the small hydraulic diameter of the micro-channel. Thus, the single-phase vapor term in the high quality correlation must allow for both laminar or turbulent vapor flow.

Table 6.8 shows that the effect of the Martinelli parameter is important for each of the three quality ranges. The present correlations show the heat transfer coefficient is

Table 6.8 Two-phase flow boiling in micro-channels. Heat transfer coefficient. Reprinted from Lee and Mudawar (2005b) with permission

x_e	Correlation	Data	MAE (%)
0–0.05	$h_{\mathrm{tp}} = 3.856X^{0.267}h_{\mathrm{sp,L}}$ $X^2 = \frac{(\mathrm{d}p/\mathrm{d}z)_{\mathrm{L}}}{(\mathrm{d}p/\mathrm{d}z)_{\mathrm{G}}}$, $h_{\mathrm{sp,L}} = \frac{\mathrm{Nu}_3 k_{\mathrm{L}}}{d_{\mathrm{h}}}$ $X_{\mathrm{vv}} = \left(\frac{\mu_{\mathrm{L}}}{\mu_{\mathrm{G}}}\right)^{0.5}\left(\frac{1-x_e}{x_e}\right)^{0.5}\left(\frac{\nu_{\mathrm{L}}}{\nu_{\mathrm{G}}}\right)^{0.5}$ $X_{\mathrm{vt}} = \left(\frac{f_{\mathrm{L}}\mathrm{Re}_{\mathrm{G}}^{0.25}}{0.079}\right)^{0.5}\left(\frac{1-x_e}{x_e}\right)^{0.5}\left(\frac{\nu_{\mathrm{L}}}{\nu_{\mathrm{G}}}\right)^{0.5}$ $\mathrm{Re_G} = \frac{Gx_e d_{\mathrm{h}}}{\mu_{\mathrm{G}}}$	50 Water data points	11.6
0.05–0.55	$h_{\mathrm{tp}} = 436.48\mathrm{Bo}^{0.522}\mathrm{We}_{\mathrm{L}}^{0.351}X^{0.665}h_{\mathrm{sp,L}}$ $\mathrm{Bo} = \frac{q}{Gh_{\mathrm{LG}}}$, $\mathrm{We_{fo}} = \frac{\nu_{\mathrm{L}}G^2 d_{\mathrm{h}}}{\sigma}$	83 R-134a data points 157 Water data points	11.9
0.55–1.0	$h_{\mathrm{tp}} = \max\left\{(108.6X^{1.665}h_{\mathrm{sp,G}}), h_{\mathrm{sp,G}}\right\}$ $h_{\mathrm{sp,G}} = \frac{\mathrm{Nu}_3 k_{\mathrm{G}}}{d_{\mathrm{h}}}$ for laminar gas flow $h_{\mathrm{sp,G}} = 0.023\mathrm{Re}_{\mathrm{G}}^{0.8}\,\mathrm{Pr}_{\mathrm{G}}^{0.4}$ for turbulent gas flow	28 R-134a data points	16.1

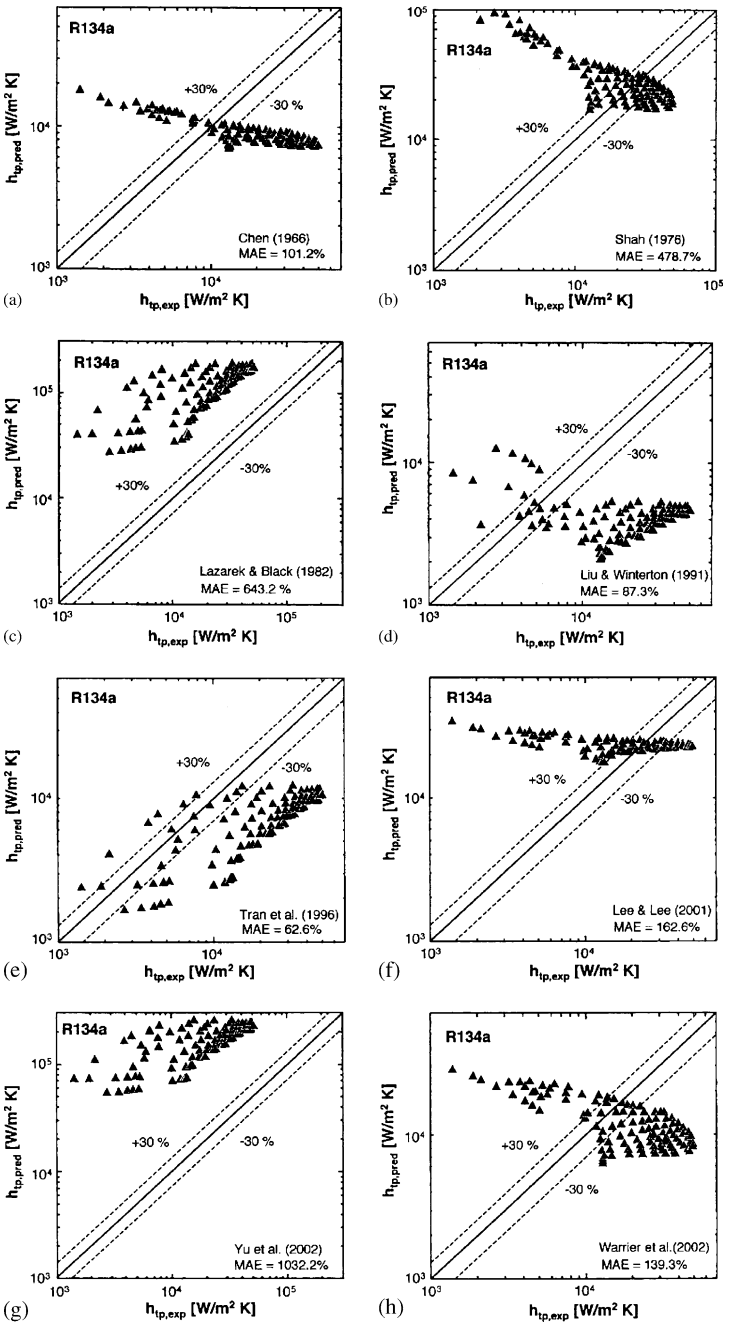

Fig. 6.31 Comparison of R-134a heat transfer coefficient data with predictions based on Chen (1966), Shah (1982), Lazarek and Black (1982), Liu and Winterton (1991), Tran et al. (1996), Lee et al. (2001b), Yu et al. (2002) and Warrier et al. (2002). Reprinted from Lee and Mudawar (2005b) with permission

proportional to the Martinelli parameter raised to a positive exponent, whereas prior macro-channel correlations employ a negative exponent for the same parameter.

In this table the parameters are defined as follows: Bo is the boiling number, d_h is the hydraulic diameter, f is the friction factor, h is the local heat transfer coefficient, k is the thermal conductivity, Nu is the Nusselt number, Pr is the Prandtl number, q is the heat flux, v is the specific volume, X is the Martinelli parameter, X_{vt} is the Martinelli parameter for laminar liquid–turbulent vapor flow, X_{vv} is the Martinelli parameter for laminar liquid–laminar vapor flow, x_e is thermodynamic equilibrium quality, z is the streamwise coordinate, μ is the viscosity, ρ is the density, σ is the surface tension; the subscripts are L for saturated fluid, LG for property difference between saturated vapor and saturated liquid, G for saturated vapor, sp for single-phase, and tp for two-phase.

Figure 6.32 illustrates good agreement between predictions based on the correlation scheme suggested by Lee and Mudawar (2005b) and both the R-134a and water data. An overall MAE of 12.26% indicates good predictive capability, especially with most of the data falling within a ±30% error range and capturing the correct data trend.

The work by Steinke and Kandlikar (2004b) focused on the obtaining heat transfer data during flow boiling in micro-channels. An experimental investigation was performed for flow boiling using water in six parallel, horizontal micro-channels

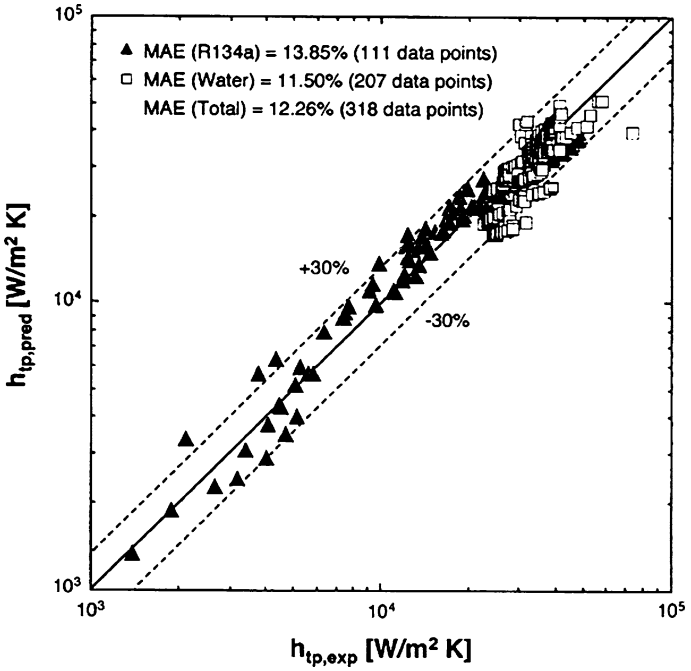

Fig. 6.32 Comparison of heat transfer coefficient data for R-134s and water with predictions based on Lee and Mudawar correlation. Reprinted from Lee and Mudawar (2005b) with permission

with a hydraulic diameter of 207 μm. The channels had a slightly trapezoidal cross-section, with the top and bottom widths differing by about 15 μm. The average channel dimensions are 214 μm wide by 200 μm deep and 57.15 mm long. The range of parameters are mass flux from 157 to 1,782 $\mathrm{kg/m^2\,s}$, heat flux from 5 to 930 $\mathrm{kW/m^2}$, inlet temperature of 22 °C, quality from subcooled to 1.0, and atmospheric pressure at the exit.

$$h_{\mathrm{tp}} = 0.6683\mathrm{Co}^{-0.2}(1-x)^{0.8} f_2 h_{\mathrm{L}} + 1{,}058\mathrm{Bo}^{0.7}(1-x)^{0.8} F \cdot h_{\mathrm{L}} \tag{6.57}$$

$$\mathrm{Co} = \left(\frac{\rho_{\mathrm{G}}}{\rho_{\mathrm{L}}}\right)^{0.5} \left(\frac{1-x}{x}\right)^{0.8} \tag{6.58}$$

$$\mathrm{Bo} = \frac{q}{G h_{\mathrm{LG}}} \tag{6.59}$$

where Co is the convection number given in Eq. (6.58), Bo is the boiling number given in Eq. (6.59), f_2 is the multiplier, h_{L} is the heat transfer coefficient with all liquid flow, and x is the quality. The F number for water is 1.0 and the f_2 is multiplier is 1.0 for micro-channel flow.

The empirical correlation (6.57) predicts a heat transfer coefficient about two times higher than that measured by Qu and Mudawar (2003b) during flow boiling of water ($x < 0.15$) and during flow boiling of R-134a ($x = 0.4$–0.8). Correlation (6.57) also overpredicts the experimental data obtained by Yen et al. (2003) during convective boiling of HCFC123 and FC72 in $d = 190\,\mu\mathrm{m}$ tubes in the range of $x = 0.4$–0.9.

6.4.3 Critical Heat Flux of Flow Boiling

Available data sets for flow boiling critical heat flux (CHF) of water in small-diameter tubes are shown in Table 6.9. There are 13 collected data sets in all. Only taking data for tube diameters less than 6.22 mm, and then eliminating duplicate data and those not meeting the heat balance calculation, the collected database included a total of 3,837 data points (2,539 points for saturated CHF, and 1,298 points for subcooled CHF), covering a wide range of parameters, such as outlet pressures from 0.101 to 19.0 MPa, mass fluxes from 5.33 to $1.34 \times 10^5\,\mathrm{kg/m^2 s}$, critical heat fluxes from 0.094 to 276 $\mathrm{MW/m^2}$, hydraulic diameters of channels from 0.330 to 6.22 mm, length-to-diameter ratios from 1.00 to 975, inlet qualities from −2.35 to 0, and outlet thermal equilibrium qualities from −1.75 to 1.00.

Zhang et al. (2006) compared some correlation with each database. The comparison results are tabulated in Table 6.10. Mean deviation is defined as $(1/N) \times \sum \left|(q_{\mathrm{crit,exp}} - q_{\mathrm{crit,cal}})/q_{\mathrm{crit,exp}}\right| \times 100\%$, a bold font in Table 6.10 denoting the smallest of mean deviations predicted by four correlations including a new correlation, and an underlined font being the smallest except for the correlation by Zhang et al. (2006).

Figure 6.33 compared graphically the predicted CHF values by the Bowring (1972) correlation, the Katto (1984) correlation and the Shah (1987) correlation

Table 6.9 Collected database for flow boiling CHF of water in small-diameter tubes. Reprinted from Zhang et al. (2006) with permission

Symb.	Reference	d_h [mm]	l/d_h	P_0 [MPa]	G [kg/m^2 s]	x_{in}[%]	x_{out}[%]	$q_{crit,exp}$ [MW/m^2]
○	Thompson and Macbeth (1964)	1.02–5.74	11.7–792	0.103–19.0	13.0–1.57×10^4	−235 to −0.031	−44.8 to 99.9	0.113–21.4
△	Lowdermilk et al. (1958)	1.30–4.78	25.0–250	0.101–0.690	27.1–3.42×10^4	−29.1 to −0.032	−3.02 to 99.1	0.167–41.6
▽	Becker et al. (1965)	3.93–6.07	164.8–382	1.13–6.97	470–5.45×10^3	−67.5 to −23.4	0.086–9,607	1.59–5.66
◫	Griffel (1965)	6.22	147	6.89–10.3	1.85×10^3–1.39×10^4	−91.4 to −6.38	−7.07 to 30.4	2.60–7.81
⬡	Nariai et al. (1987, 1989)	1.00–3.00	3.33–50.0	0.101–1.05	4.30×10^3–2.99×10^4	−31.5 to −3.07	−18.3 to 5.55	4.50–66.1
⬡	Inasaka and Nariai (1989)	3.00	33.3	0.290–1.05	4.30×10^3–2.99×10^4	−31.5 to −12.5	−18.3 to −3.99	7.30–44.5
◁	Inasaka (1993)	1.00–3.00	3.17–50.4	0.101	6.71×10^3–2.09×10^4	−15.6 to −6.66	−13.2 to 1.10	4.64–67.0
□	Celata et al. (1993)	2.5	40	0.585–2.61	1.12×10^4–4.00×10^4	−46.1 to −18.7	−35.6 to 0.6	1.21–60.6
⬠	Vandervort et al. (1994)	0.330–2.67	1.66–26.2	0.131–2.28	5.03×10^3–4.18×10^4	−28.2 to −1.91	−22.6 to 28.4	4.60–124
◍	Lezzi et al. (1994)	1.00	239–975	1.90–7.20	7.76×10^2–2.74×10^4	−64.4 to 0	64.3–0.976	0.285–2.36
◇	Kureta (1997)	1.00–6.00	1.00–113	0.101	5.33–1.91×10^4	−17.2 to 0.032	−14.6 to 99.5	0.0935–158
◈	Roach et al. (1999)	1.13–1.45	110–141	0.336–1.04	256–1.04×10^4	−27.9 to −13.1	36.2–97.4	0.860–3.70
▷	Mudawar and Bowers (1999)	0.406–2.54	2.36–34.2	0.250–17.2	5.00×10^3–1.34×10^5	−189 to −11.7	−175 to −6.23	9.40–276
	Total (13 databases)	0.330–6.22	1.00–975	0.101–19.0	5.33–1.34×10^5	−235 to 0	−175 to 99.9	0.0935–276

Table 6.10 Assessment of CHF correlations for flow boiling of water. Reprinted from Zhang et al. (2006) with permission

Reference	Mean deviation [%]						
	Correlations for saturated CHF				Correlations for subcooled CHF		
	Bowring (1972)	Katto and Ohno (1984)	Shah (1987)	Zhang et al. (2006)	Inasaka and Nariai (1987)	Celata et al. (1993)	Hall and Mudawar (2000)
Thompson and Macbeth (1964)	**12.3**	15.2	12.6	17.8	18.7	21.8	7.68
Lowdermilk et al. (1958)	32.4	21.9	15.7	**11.2**	30.3	13.2	32.7
Becker et al. (1965)	**5.51**	7.14	10.0	11.5			
Griffel (1965)	5.61	5.47	**4.43**	17.2	4.48	21.3	5.97
Nariai et al. (1987, 1989)	73.8	35.7	**21.8**	29.0	16.4	31.4	17.8
Inasaka and Nariai (1989)	81.2	37.1			9.25	17.1	7.48
Inasaka (1993)			**14.3**	38.3	18.9	28.0	21.7
Celata et al. (1993)					23.2	28.7	14.8
Vandervort et al. (1994)	82.5	16.9	42.9	**16.7**	17.3	24.6	29.6
Lezzi et al. (1994)	32.3	**7.84**	15.3	9.40			
Kureta (1997)	52.5	51.9	37.9	**20.2**	42.7	47.0	35.6
Roach et al. (1999)	18.6	33.5	**16.4**	18.0			
Mudawar and Bowers (1999)					83.5	38.7	18.8
Total (13 databases)	29.3	26.4	20.6	**16.8**	30.5	30.1	19.2

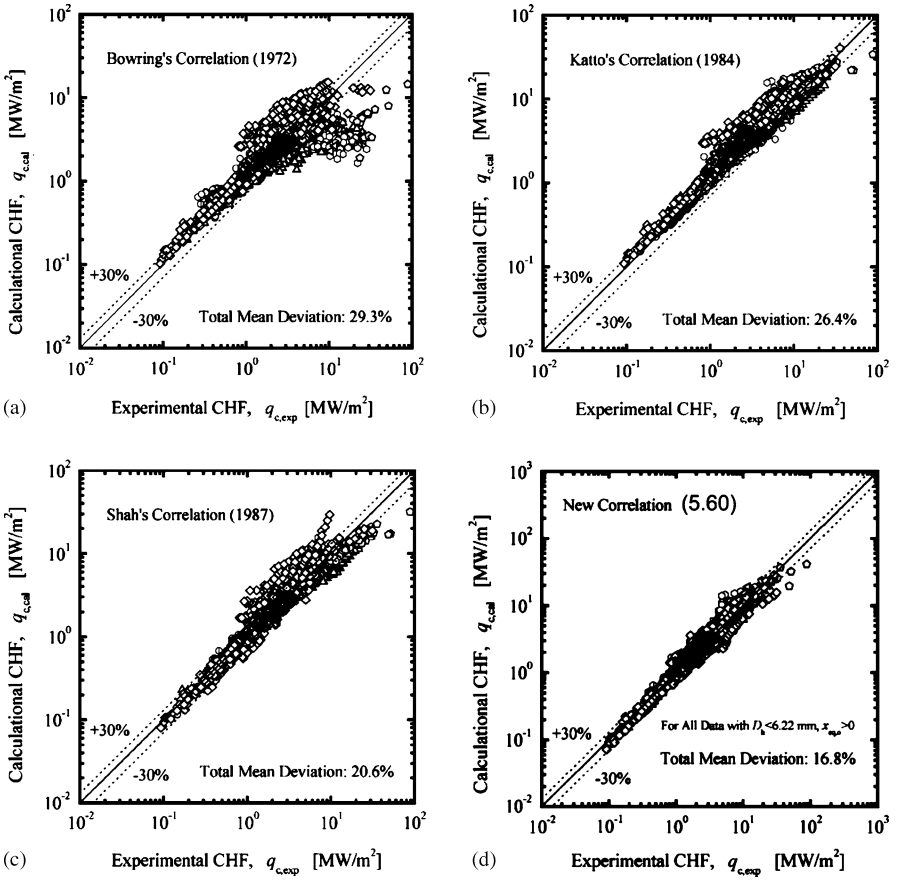

Fig. 6.33 Evaluation of correlations with saturated CHF data. (**a**) Bowring correlation (1972), (**b**) Shah correlation (1987), (**c**) Katto correlation (1984), (**d**) Zhang et al. correlation (2006). Reprinted from Zhang et al. (2006) with permission

with the experimental values, respectively. Symbols for each data set are depicted in Table 6.9. For low CHF values, shown in Fig. 6.33a, the Bowring (1972) relation correlated generally well with the experimental CHF values, although there is a slight overprediction. For high CHF values, however, the Bowring (1972) relation fails to correlate the experimental CHF values. A large scatter of predictions can be observed and many of them tend to deviate systematically from the experimental values. Figure 6.33b shows the behavior of the Katto (1984) correlation. Although the relation correlates all the data successfully within a relatively small scatter, it seems that there exist some slight overpredictions for most of the CHF data. Figure 6.33c shows the evaluation of the Shah (1987) correlation. For low CHF values, the predictions by the Shah (1987) correlation have a very small scatter and most are centered within the error band of $\pm 30\%$. For high CHF values, the Shah (1987) correlation tends to predict CHF with some scatter. The best agreement with experi-

mental data on saturated CHF is the correlation by Zhang et al. (2006) (Fig. 6.33d):

$$\mathrm{Bo} = 0.0352\left[\mathrm{We} + 0.0119\left(\frac{L}{d_\mathrm{h}}\right)^{2.31}\left(\frac{\rho_\mathrm{G}}{\rho_\mathrm{L}}\right)^{0.361}\right]^{-0.295} \times\left[\left(\frac{L}{d_\mathrm{h}}\right)^{-0.311}\left(2.05\left(\frac{\rho_\mathrm{L}}{\rho_\mathrm{L}}\right)^{0.170} - x_\mathrm{in}\right)\right] \tag{6.60}$$

where $\mathrm{Bo} = q_\mathrm{crit}/(h_\mathrm{LG}G)$ is the boiling number, $\mathrm{We} = (G^2 d_\mathrm{h})/(\sigma\rho_\mathrm{L})$ is the Weber number, q_crit is the critical heat flux, h_LG is the latent heat of evaporation, G is the mass flux, x_in is the thermodynamical equilibrium quality at inlet, ρ_G and ρ_L are the density of saturated vapor and liquid, respectively, d_h is the hydraulic diameter, L is the heated length, and σ is the surface tension.

Hall and Mudawar (2000) provided a comprehensive review of the current state of the knowledge of subcooled CHF for water flow boiling in channels, and designed a statistical correlation with five parameters based on almost all available subcooled CHF databases in the literature:

$$\mathrm{Bo} = \frac{C_1\mathrm{We}^{C_2}(\rho_\mathrm{L}/\rho_\mathrm{G})^{C_3}[1 - C_4(\rho_\mathrm{L}/\rho_\mathrm{G})^{C_5}x_\mathrm{in}]}{1 + 4C_1C_4\mathrm{We}^{C_2}(\rho_\mathrm{L}/\rho_\mathrm{G})^{C_3+C_5}(L/d_\mathrm{h})} \tag{6.61}$$

where the Weber number $\mathrm{We} = G^2 d_\mathrm{h}/(\rho_\mathrm{L}\sigma)$, $C_1 = 0.0722$, $C_2 = -0.312$, $C_3 = -0.644$, $C_4 = 0.900$, and $C_5 = 0.724$. The correlation was developed using a total of 4,860 data points and predicted CHF with a rms error of 14.3% in the following parametric ranges: $0.1 < P_0 < 20$ MPa, $0.25 < d_\mathrm{h} < 15.0$ mm, $2 < L/d_\mathrm{h} < 200$, $300 < G < 30{,}000\,\mathrm{kg/m^2\,s}$, $-2.00 < x_\mathrm{in} < 0.00$, and $-1.00 < x_\mathrm{out} < 1.00$.

A theoretical model for the prediction of the critical heat flux of refrigerants flowing in heated, round micro-channels has been developed by Revellin and Thome (2008). The model is based on the two-phase conservation equations and includes the effect of the height of the interfacial waves of the annular film. Validation has been carried out by comparing the model with experimental results presented by Wojtan et al. (2006), Qu and Mudawar (2004), Bowers and Mudawar (1994), Lazareck and Black (1982). More than 96% of the data for water and R-113, R-134a, R-245fa were predicted within ±20%.

6.5 Explosive Boiling of Water in Parallel Micro-Channels

The thermohydrodynamical processes of boiling in a micro-channel heat sink were subject to a number of experimental investigations performed during the last decade. Periodic wetting and rewetting phenomena were observed by Hetsroni et al. (2003, 2005), Zhang et al. (2002), Steinke and Kandlikar (2004a), and Kandlikar and Balasubramanian (2004). Flow boiling of water in parallel silicon micro-channels with trapezoidal cross-sectional area with hydraulic diameters of 158.8 and 82.8 μm, was

studied by Wu and Cheng (2003a,b, 2004). Long period fluctuations in fluid pressure, fluid temperature, and fluid mass flux were measured.

6.5.1 Quasi-Periodic Boiling in a Certain Single Micro-Channel of a Heat Sink

In the study by Hetsroni et al. (2006b) the test module was made from a square-shaped silicon substrate 15×15 mm, 530 μm thick, and utilized a Pyrex cover, 500 μm thick, which served as both an insulator and a transparent cover through which flow in the micro-channels could be observed. The Pyrex cover was anodically bonded to the silicon chip, in order to seal the channels. In the silicon substrate parallel micro-channels were etched, the cross-section of each channel was an isosceles triangle. The main parameters that affect the explosive boiling oscillations (EBO) in an individual channel of the heat sink such as hydraulic diameter, mass flux, and heat flux were studied. During EBO the pressure drop oscillations were always accompanied by wall temperature oscillations. The period of these oscillations was very short and the oscillation amplitude increased with an increase in heat input. This type of oscillation was found to occur at low vapor quality.

Period between successive events

Figure 6.34 shows the dependence of the dimensionless period of phase transformations (i.e., the time between bubble venting), t^*, on boiling number Bo ($t^* = t/Ud_h$,

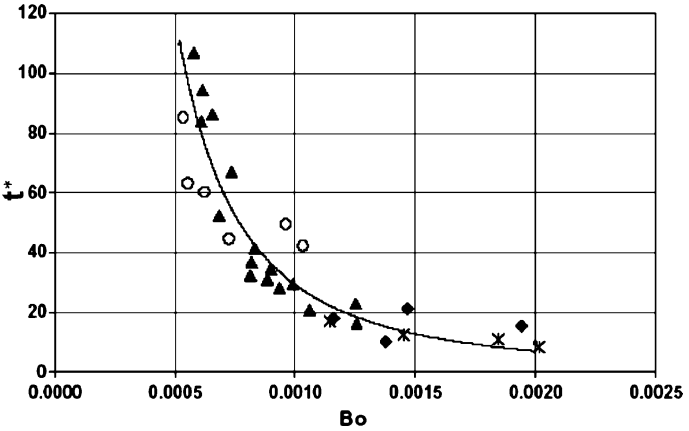

Fig. 6.34 Dependence of dimensionless time interval between cycles on boiling number: circles (○) represent $d_h = 100$ μm, water, triangles (▲) represent $d_h = 130$ μm, water, diamonds (◇) represent $d_h = 220$ μm, water, star (∗) represents $d_h = 220$ μm, ethanol. Reprinted from Hetsroni et al. (2006b) with permission

$\mathrm{Bo} = q/Gh_{\mathrm{LG}}$, where t is the period between successive events, U is the mean velocity of single-phase flow in the micro-channel, d_{h} is the hydraulic diameter of the channel, q is heat flux, m is mass flux, h_{LG} is the latent heat of vaporization). The dependence t^* on Bo can be approximated, with a standard deviation of 16%, by

$$t^* = 0.000030\mathrm{Bo}^{-2}. \tag{6.62}$$

6.5.2 The Initial Thickness of the Liquid Film

The term initial liquid film thickness is defined as the average thickness of fluid, evenly distributed during period t, over the surface of the circular micro-channel, after venting of the elongated bubble. This surface is located downstream of the ONB and may be characterized by the heated length L, and hydraulic diameter d_{h}, assuming that during the period t the liquid film has disappeared due to evaporation. The heat removed from the wall surface is the same as that required for the liquid film evaporation during the period t. The heat balance is:

$$\pi\delta d_{\mathrm{h}} L\rho_{\mathrm{L}} = q\pi d_{\mathrm{h}} Lt/h_{\mathrm{LG}} \tag{6.63}$$

where ρ_{L} is the liquid density.

The average liquid thickness δ, can be calculated as:

$$\delta = qt/\rho_{\mathrm{L}} h_{\mathrm{LG}}. \tag{6.64}$$

Figure 6.35 shows dependence of the dimensionless initial liquid thickness of water and ethanol δ^*, on the boiling number Bo, where $\delta^* = \delta U/\nu$, U is the mean velocity of single-phase flow in the micro-channel, and ν is the kinematic viscosity of the

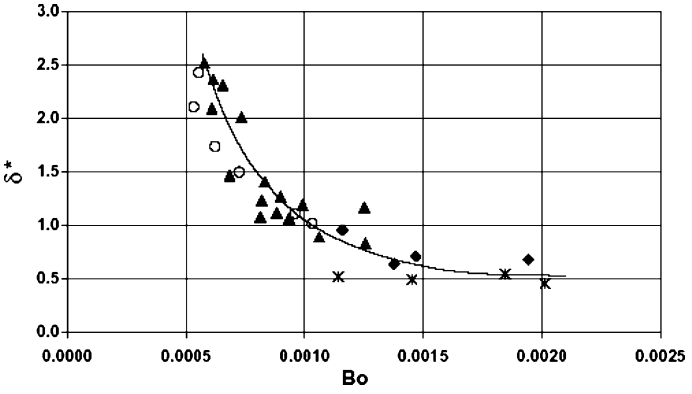

Fig. 6.35 Dependence of dimensionless initial film thickness on boiling number: *circles* (○) represent $d_{\mathrm{h}} = 100\,\mu$m, water, *triangles* (▲) represent $d_{\mathrm{h}} = 130\,\mu$m, water, *diamonds* (♦) represent $d_{\mathrm{h}} = 220\,\mu$m, water, *star* (∗) represents $d_{\mathrm{h}} = 220\,\mu$m, ethanol. Reprinted from Hetsroni et al. (2006b) with permission

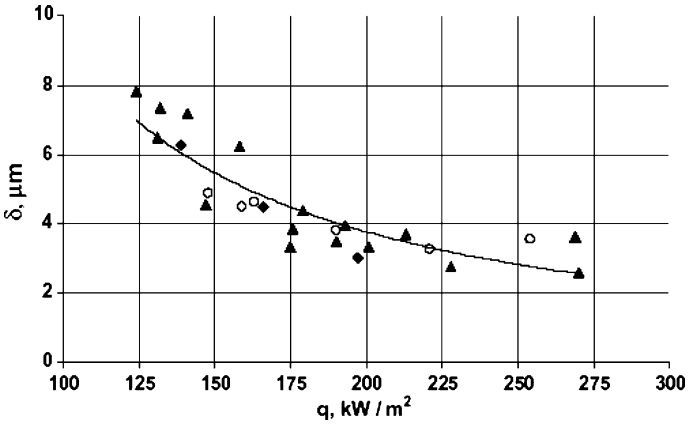

Fig. 6.36 Variation of initial film thickness for water versus heat flux: *circles* (○) represent d_h = 100 μm, water, *triangles* (▲) represent d_h = 130 μm, water, *diamonds* (♦) represent d_h = 220 μm, water. Reprinted from Hetsroni et al. (2006b) with permission

liquid at saturation temperature. The dependence of δ^* on Bo can be approximated, with a standard deviation of 18%, by

$$\delta^* = 0.00015\mathrm{Bo}^{-1.3}. \tag{6.65}$$

The initial thickness of the liquid film is a key parameter of the explosive boiling. This point may be discussed in some detail with regard to the beginning of the critical heat flux (CHF) regime. The variation of the initial thickness of the film of water versus the heat flux is provided in Fig. 6.36. For explosive boiling the film thickness decreases with increasing heat flux from 125 to 270 $\mathrm{kW/m^2}$ from about 8 to 3 μm. This range of values is on the same order of magnitude as those given by Moriyama and Inoue (1996) and by Thome et al. (2004) for R-113 in small spaces (100–400 μm). Decreasing liquid film thickness with increasing heat flux is a distinct feature of dryout during explosive boiling. Under these conditions at which the instantaneous temperature of the heater surface exceeds 125 °C, the value of δ was in the range of (3 ± 0.6) μm. This value may be considered as minimum initial film thickness. If the liquid film reached the minimum initial film thickness $\delta_{\min}$, CHF regime occurred. According to Thome et al. (2004) $\delta_{\min}$ is assumed to be on the same order of magnitude as the surface roughness. The values of the minimum initial film thickness calculated by Thome et al. (2004) for R-113 at saturation temperature 47.2 °C was in the range of 1.5–3.5 μm.

6.5.3 System that Contains a Number of Parallel Micro-Channels

Hetsroni et al. (2006b) also studied the effect of EBO in individual channels on the average characteristics of the whole heat sink: total pressure drop and tempera-

ture fluctuations on the heater, and the heat transfer coefficient. The high-frequency oscillations in individual micro-channels are superimposed and lead to total low-frequency pressure drop and temperature oscillations of the system.

Fluctuation of pressure drop, fluid and heated wall temperatures

The experimental investigations of boiling instability in parallel micro-channels have been carried out by simultaneous measurements of temporal variations of pressure drop, fluid and heater temperatures. The channel-to-channel interactions may affect pressure drop between the inlet and the outlet manifold as well as associated temperature of the fluid in the outlet manifold and heater temperature. Figure 6.37 illustrates this phenomenon for pressure drop in the heat sink that contains 13 micro-channels of $d_h = 220\,\mu m$ at mass flux $G = 93.3\,kg/m^2\,s$ and heat flux $q = 200\,kW/m^2$. The temporal behavior of the pressure drop in the whole boiling system is shown in Fig. 6.37a. The considerable oscillations were caused by the flow pattern alternation, that is, by the liquid/two-phase alternating flow in the micro-channels. The pressure drop FFT is presented in Fig. 6.37b. Under

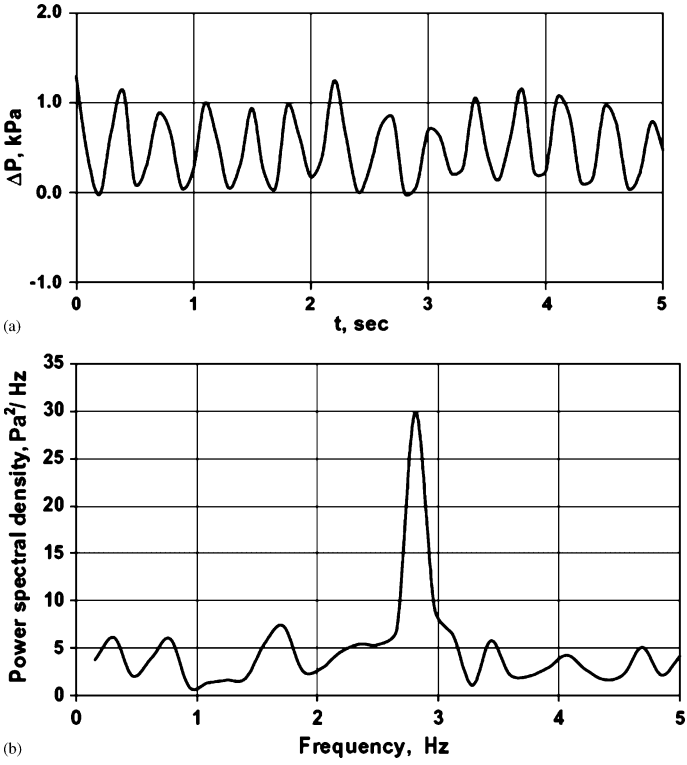

Fig. 6.37 Time variation of pressure drop at $q = 200\,kW/m^2$: (**a**) pressure drop fluctuations, (**b**) pressure drop amplitude spectrum. Reprinted from Hetsroni et al. (2006b) with permission

condition of the given experiment the period of pressure drop fluctuation is about $t = 0.36$ s. The results differ significantly from those reported by Wu and Cheng (2004). In the range of average values of mass flux $G = 112-146\,\mathrm{kg/m^2s}$ and heat flux $q = 135-226\,\mathrm{kW/m^2}$ these authors observed much longer oscillation period (from $t = 15.4$ to 202 s). In experiments conducted by Wu and Cheng (2004), the water in the pressure tank was moved by the compressed nitrogen gas to the test section. According to the authors when the boiling occurred in the test section, the pressure drop across the test was suddenly increased due to generation of vapor bubbles. This increase in pressure drop caused a decrease in mass flux. The long period pressure drop fluctuations may be connected to the period of increasing or decreasing of incoming mass flux. The former depends not only on boiling in the micro-channels of heat sinks, but also on the nitrogen pressure in the water tank and the total length of the pipe connecting the water tank to the test section. In our ex-

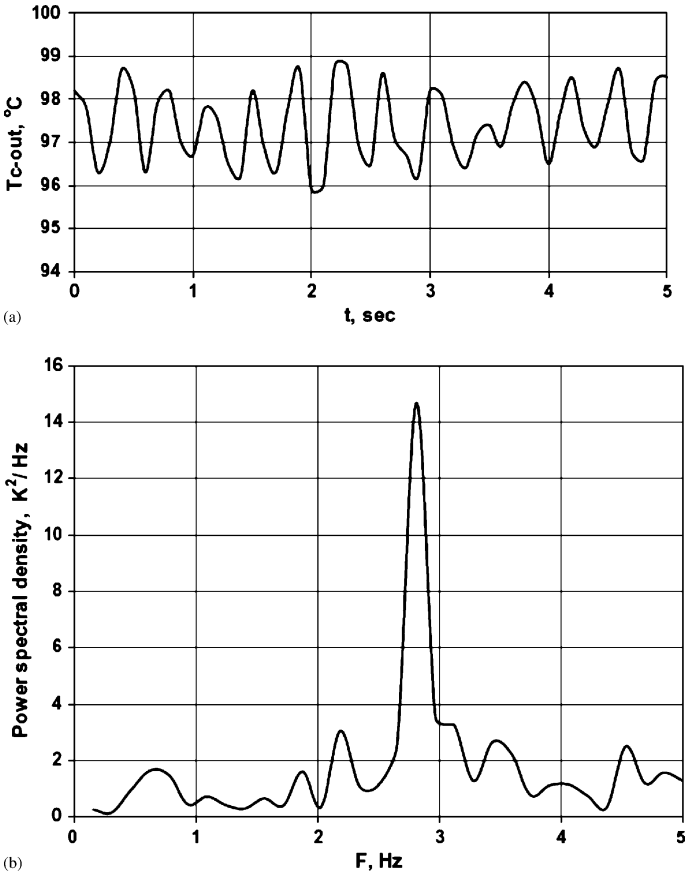

Fig. 6.38 Time variation of fluid temperature at the outlet manifold $q = 200\,\mathrm{kW/m^2}$: (**a**) temperature fluctuations, (**b**) temperature amplitude spectrum. Reprinted from Hetsroni et al. (2006b) with permission

periments, the mass flow rate was independent of pressure drop fluctuations, and the oscillation periods are very much different from those recorded by Wu and Cheng (2004).

The pressure drop fluctuation provides insight into the temperature behavior of the fluid in the outlet manifold. The pressure drop fluctuation frequency is representative of the oscillations in the system. Figure 6.38a,b shows time variation and FFT of the fluctuation component of the fluid temperature. From Fig. 6.38a one can see that the average fluid temperature at the outlet manifold is less than the saturation temperature. This results in the fact that only single liquid comes to the outlet manifold through some of the parallel micro-channels.

The time variation of the mean and maximum heater temperature is presented in Fig. 6.39. The mean heater temperature (i.e., the average temperature of the whole heater) changed in the range of $\Delta T_{av} = 10\,\mathrm{K}$. The maximum heater temperature changed in the range of $\Delta T_{max} = 6\,\mathrm{K}$. Comparison between Figs. 6.37, 6.38 and 6.39, shows that the time period (frequency) is the same for the pressure drop, the fluid temperature at the outlet manifold, and the mean and maximum heater temperature fluctuations. It also allows one to conclude that these fluctuations are in phase.

When the heat flux is increased, at constant value of mass flux, the oscillation amplitudes of the pressure drop, the fluid and the heater temperatures also increase.

6.5.4 Average Heat Transfer Coefficient

It was observed that at the same boiling number and inlet temperature, an increase in diameter shifts the ONB further from the inlet. The region of the local dryout decreases and the average heated surface temperature decreases as well. Under this condition the heat transfer coefficient increases with increased hydraulic diameter.

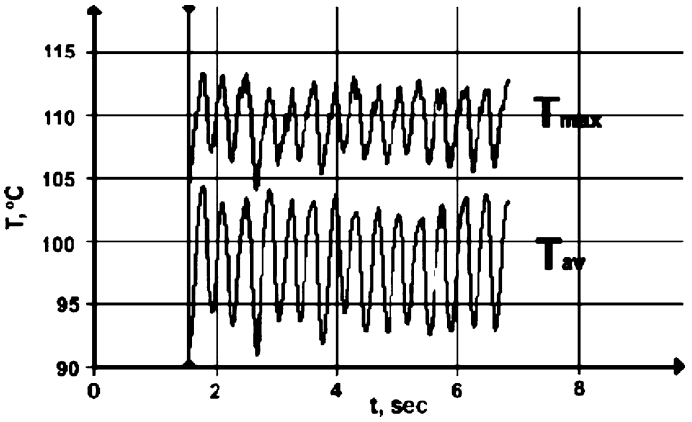

Fig. 6.39 Time variation of average and maximum heater temperature at $q = 200\,\mathrm{kW/m^2}$. Reprinted from Hetsroni et al. (2006b) with permission

In order to take into account the effect of surface tension and micro-channel hydraulic diameter, we have applied the Eotvos number $\mathrm{Eo} = g(\rho_\mathrm{L} - \rho_\mathrm{G})d_\mathrm{h}^2/\sigma$. Figure 6.40 shows the dependence of the Nu/Eo on the boiling number Bo, where $\mathrm{Nu} = hd_\mathrm{h}/k_\mathrm{L}$ is the Nusselt number, h is the heat transfer coefficient, and k_L is the thermal conductivity of fluid. All fluid properties are taken at the saturation temperature. This dependence can be approximated, with a standard deviation of 18%, by the relation:

$$\mathrm{Nu/Eo} = 0.030\mathrm{Bo}^{-1.5} \tag{6.66}$$

Simultaneous measurements of temporal variations of pressure drop, fluid and heater temperatures show the boiling instability in parallel micro-channels. The channel-to-channel interactions may affect pressure drop between the inlet and the outlet manifold, as well as associated temperature of the fluid in the outlet manifold and the temperature of the heater. The frequency is the same for the pressure drop, the fluid temperature at the outlet manifold, and for the fluctuations of the mean and maximum temperature of the heater. All these fluctuations are in phase. When the heat flux increases, at a constant value of mass flux, the oscillation amplitudes of the pressure drop, the fluid and the heater temperatures also increase.

The large heated wall temperature fluctuations are associated with the critical heat flux (CHF). The CHF phenomenon is different from that observed in a single channel of conventional size. A key difference between micro-channel heat sink and a single conventional channel is the amplification of the parallel channel instability prior to CHF. As the heat flux approached CHF, the parallel channel instability, which was moderate over a wide range of heat fluxes, became quite intense and should be associated with a maximum temperature fluctuation of the heated surface. The dimensionless experimental values of the heat transfer coefficient may be correlated using the Eotvos number and boiling number.

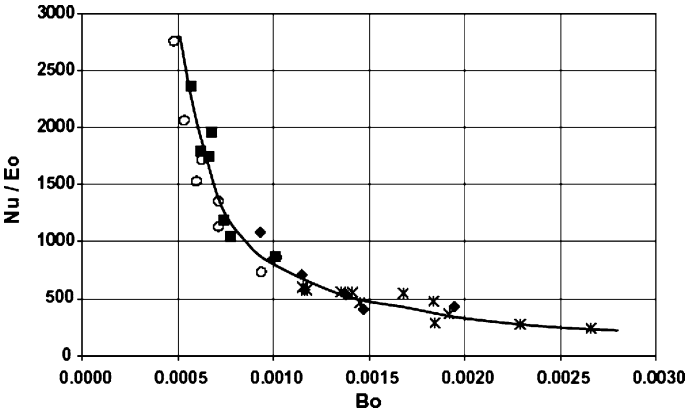

Fig. 6.40 Dependence of Nu/Eo on Bo: *circles* (○) represent $d_\mathrm{h} = 100\,\mu\mathrm{m}$, water, *triangles* (▲) represent $d_\mathrm{h} = 130\,\mu\mathrm{m}$, water, *diamonds* (♦) represent $d_\mathrm{h} = 220\,\mu\mathrm{m}$, water, *star* (∗) represents $d_\mathrm{h} = 220\,\mu\mathrm{m}$, ethanol. Reprinted from Hetsroni et al. (2006b) with permission

Summary

1. Incipience boiling

Wall superheat

Significant differences in boiling inception phenomena have been reported in micro-channels compared to conventional size channels. Phase-change processes, particularly boiling incipience, are important in the micro-scale as well in the macro-scale, but relatively little work has been done to compare the experimental results in this area. Most of the studies on this phenomenon in conventional size channels ($d_h = 1-20$ mm) were carried out in a single channel. Heat exchangers with micro-channels (d_h less than about 0.5 mm) are generally subject to two problems. The first of these is flow distribution among parallel channels. The second is conjugate effects, circumferential and axial heat conduction in the material forming the channel, so that the actual heat flux and temperature distributions at the channel wall are difficult to estimate. Typical micro-channels studied in the literature had one unheated side wall (usually a transparent cover plate in the experimental apparatus) and heat was applied from the bottom, with the result that the heat flux and wall temperature distribution may be circumferentially non-uniform.

There is significant disagreement between experimental results for conventional size channels due to different experimental conditions. For example, the wall has to be superheated to a relatively great extent to initiate the nucleate boiling in the experiments by Hapke et al. (2000) compared to those reported by Sato and Matsumura (1964) and by Bergles and Rohsenow (1964). Moreover, a mass flux dependence of the wall superheat was reported by Hapke et al. (2000). Measurements of incipient boiling heat flux performed by Qu and Mudawar (2002) in a heat sink containing rectangular parallel micro-channels showed that $q_{ONB} \sim \Delta T_{S,ONB}$ whereas measurements by Bergles and Rohsenow (1964) showed that heat flux depends on the wall superheat as $q_{ONB} \sim \Delta T_{S,ONB}^2$ and is independent of mass flux.

For qualitative analysis of the conditions at which the boiling incipience was studied experimentally the parameter $D = \Delta T_{sub,ONB}/T_S$ may be used. Depending on the value of D, the channels can be subdivided into two groups: $D < 1$ and $D \ll 1$. When $D < 1$ ($D = 0.125-0.25$) the onset of nucleate boiling occurred at a bulk temperature significantly less than saturation. When $D \ll 1$ ($D = 0.011-0.043$) the onset of nucleate boiling occurred at values of the bulk temperature close to saturation.

Incipient boiling heat flux

When $D < 1$ ($T_{in} \ll T_S$) incipient boiling heat flux increases with increasing mass velocity. When $D \ll 1$ ($T_{in} \sim T_S$) incipient boiling heat flux weakly depends on mass velocity. For micro-channels boiling incipient heat flux may weakly depend on inlet temperature. This case corresponds to flow boiling in parallel micro-channels, in which vapor penetrates the inlet manifold.

Surfactant solutions

For some kind of surfactant solutions boiling incipience was accompanied with hysteresis and the wall superheat up to 24 K was observed.

Effect of dissolved gases

Desorption of the dissolved gases formed bubbles of gas and a limited amount of bubbles containing gas–water vapor mixture. Under these conditions, during flow boiling of water boiling incipience occurred at channel wall temperatures below that of saturation temperature. Addition of surfactants led to an increase in wall temperature. In this case the boiling occurred in the range of heat flux of 5.2–21 $\mathrm{W/cm^2}$ at wall temperatures of 107–121 °C.

2. Bubble dynamics in a confined space

Dimensional analysis shows that the behavior of the bubble radius with time depends on the parameter $\Pi = q/(\rho_{\mathrm{L}} U c_{\mathrm{pL}} \Delta T_{\mathrm{S}})$. In the range of $\Pi = 0.0079{-}0.026$, linear behavior was observed, and when $\Pi > 0.026$ exponential bubble growth took place.

3. Pressure drop

The complexity of steam–liquid flow in a micro-channel is the result of interactions between liquid inertia, the liquid viscous force, and surface tension. The approach developed by Lee and Mudawar (2005a) may be used to calculate the pressure drop in micro-channels. Two key measures of these interactions are the Reynolds and Weber numbers based on liquid properties.

4. Heat transfer in two-phase flow boiling

The extent to which an incoming liquid will be vaporized is a design variable that depends on the intended application. In micro-scale refrigeration systems, the change in vapor quality may be substantial, on the order of 0.8 for example. In electronics cooling applications, the equilibrium vapor quality may remain at 0, or be very small; in those designs, the aim is to capture the high-heat transfer coefficients of subcooled flow boiling, without the added complexities of net vapor generation (e.g., the need to incorporate a condenser). The distinction between low and high-quality outflow affects heat transfer coefficients. Experiments by Lee and Mudawar (2005b) revealed the range of parameters at which heat transfer was controlled by nucleate boiling or annular film evaporation. The first of this process occurred only at low qualities ($x < 0.05$), the second one at moderate ($0.05 < x < 0.55$) or high

($x > 0.55$) qualities. New correlations were suggested by Lee and Mudawar (2005b). They are based on the Martinelli parameter and may be used for two-phase flow boiling of water and refrigerant R-134a.

5. Critical heat flux

Several thousand CHF points have been reported in the boiling literature of the past 50 years. Most of these data were obtained with stable flow in single conventional size circular tubes and conventional size channels. The tubes were usually of uniform wall thickness, and direct electrical heating was utilized to simulate the constant heat flux. The correlation suggested by Zhang et al. (2006) gives the best agreement with experimental data on saturated CHF in the channels of 0.33–6.22 mm. As discussed in detail in Chap. 2, there is significant difference between experimental results of CHF obtained in a single micro-channel of $d_h = 0.5$ mm and in the block that contained twenty-one 0.215×0.21 mm channels.

The study of CHF in micro-channels has not received much attention in the literature. Single-tube CHF data are not available for micro-channels with hydraulic diameters less than 0.3 mm. Under conditions of explosive boiling, Hetsroni et al. (2006b) suggested that the initial thickness of the liquid film may by considered as a key parameter that affects CHF in the system containing a number of parallel micro-channels of $d_h = 0.1-0.22$ mm. New experiments should be performed to validate the dimensionless groups caused by the evaporating interface near the heated wall and CHF for single micro-channels, as well as for blocks that contain parallel micro-channels.

6. Flow instability

The channel-to-channel interactions may affect pressure drop between the inlet and the outlet manifold, as well as associated temperature of the fluid in the outlet manifold and temperature of the heater. The frequency and the phase are the same for all these fluctuations. They increase at a constant value of mass flux with increasing heat flux. The large heated wall temperature fluctuations are associated with the CHF. As the heat flux approached CHF, the parallel-channel instability, which was moderate over a wide range of heat fluxes, became quite intense and should be associated with maximum temperature fluctuation of the heated surface.

References

Agostini B, Revellin R, Thome J (2008) Elongated bubbles in micro-channels. Part I: Experimental study and modeling of elongated bubble velocity. Int. J. Multiphase Flow 34:590–601

Bankoff SG, Haute T (1957) Ebullition from solid surfaces in the absence of pre-existing gaseous phase. Trans ASME 79:735–740

Becker KM, Hernborg G, Bode M, Eriksson O (1965) Burnout data for flow of boiling water in vertical round ducts, annuli and rod clusters, AE-177. Aktiebolaget Atomenergi, Stockholm, Sweden

Becker R, Doring W (1935) The kinetic treatment of nuclear formation in superheated vapors. Ann Phys 24:719–752

Bergles AE, Rohsenow WW (1964) The Determination of Forced-Convection Surface-Boiling Heat Transfer. Trans ASME J Heat Transfer 86:365–372

Blander M, Katz JL (1975) Bubble nucleation in liquids. AIChE J 21:833–848

Bowers MB, Mudawar I (1994) High flux boiling in low flow rate, low pressure drop mini-channel and micro-channel heat sinks. Int. J. Heat Mass Transfer 37:321–332

Bowring RW (1972) A simple but accurate round tube uniform heat flux, dryout correlation over the pressure range 0.7–17 MN/m2 (100–2500 psia), AEEW-R 789. United Kingdom Atomic Energy Authority, Harwell

Brutin B, Tadrist L (2004) Pressure drop and heat transfer analysis of flow boiling in micro-channel: influence of the inlet condition on two-phase flow stability. Int J Heat Mass Transfer 47:2367–2377

Carey van P (1992) Liquid–vapor phase-change phenomena. An introduction to the thermophysics of vaporization and condensation processes in heat transfer equipment. Hemisphere, New York

Celata GP, Cumo M, Mariani A (1997) Experimental evaluation of the onset of subcooled flow boiling at high liquid velocity and subcooling. Int J Heat Mass Transfer 40:2979–2885

Celata GP, Cumo M, Mariani A (1993) Burnout in highly subcooled water flow boiling in small diameter tubes. Int J Heat Mass Transfer 36:1269–1285

Chen JC (1966) Correlation for boiling heat transfer to saturated fluids in convective flow. Ind Eng Chem Process Des Develop 5:322–329

Cole R (1974) Boiling nucleation. In: Advances in Heat Transfer 10. Academic, New York, pp 86–166

Cole R, Shulman HL (1966) Bubble growth rates at high Jacob numbers Int J Heat Mass Transfer 9:1377–1390

Collier G, Thome J (1994) Convective Boiling and Condensation, 3rd edn. Oxford University Press, Oxford

Davis EJ, Anderson GH (1966) The incipience of nucleate boiling in forced convection flow. AIChE 12:774–780

Dhir VK (1998) Boiling heat transfer. Ann Rev Fluid Mech 30:365–401

Farkas L (1927) The velocity of nucleus formation in superheated vapors. Z Phys Chem 125:236–240

Fritz WW (1936) Ende über den Verdampfungsvorgang nach kinematographischen Aufnahmen an Dampfblasen. Phys Z 37:391–401

Geld C (2004) Prediction of dynamic contact angle histories of a bubble growing at a wall. Int J Heat Fluid Flow 25:74–80

Ghiaasiaan SM, Chedester RC (2002) Boiling incipience in microchannels. Int J Heat Mass Transfer 45:4599–4606

Griffel J (1965) Forced convection boiling burnout for water in uniformly heated tubular test sections. USAEC Report NYO 187-7, TID-4500, Columbia University

Grohmann S (2005) Measurement and modeling of single-phase and flow-boiling heat transfer in micro-tubes. Int J Heat Mass Transfer 48:4072–4089

Hall DD, Mudawar I (2000) Critical heat flux (CHF) for water flow in tubes – II. Subcooled CHF correlations. Int J Heat Mass Transfer 43:2605–2640

Han CH, Griffith P (1965) The mechanism of heat transfer in nucleate pool boiling. Part I: Bubble initiation, growth and departure Int J Heat Mass Transfer 8:887–904

Hapke I, Boye H, Schmidt J (2000) Onset of nucleate boiling in micro-channels. Int J Therm Sci 39:505–513

Helden W, Geld C, Boot P (1995) Forces on bubbles growing and detaching in flow along a vertical wall. Int J Heat Mass Transfer 38:2075–2088

Hetsroni G, Mosyak A, Pogrebnyak E, Sher I, Segal Z (2006a) Bubble growth in saturated pool boiling in water and surfactant solution. Int J Multiphase Flow 22:159–182
Hetsroni G, Mosyak A, Pogrebnyak E, Segal S (2006b) Periodic boiling in parallel micro-channels at low vapor quality. Int J Multiphase Flow 32:1141–1159
Hetsroni G, Mosyak A, Pogrebnyak E, Segal S (2007) Natural convection boiling of water and surfactant in narrow horizontal annular channels. Int J Multiphase Flow 33:469–483
Hetsroni G, Mosyak A, Pogrebnyak E, Segal Z (2005) Explosive boiling of water in parallel micro-channels. Int J Multiphase Flow 31:371–392
Hetsroni G, Mosyak A, Segal Z, Pogrebnyak E (2003) Two-phase flow pattern in parallel micro-channels. Int J Multiphase Flow 29:344–360
Hetsroni G, Mosyak A, Segal Z, Ziskind G (2002a) A uniform temperature heat sink for cooling of electronic devices. Int J Heat Mass Transfer 45:3275–3286
Hetsroni G, Gurevich M, Mosyak A, Rozenblit R, Yarin LP (2002b) Subcooling boiling of surfactant solutions. Int J Multiphase Flow 28:347–361
Hino R, Ueda T (1985) Studies on heat transfer and flow characteristics in subcooled flow boiling. Part 1: Boiling characteristics. Int J Multiphase Flow 11:269–281
Hsu YY (1962) On size range of active nucleation cavities on a heating surface. J Heat Transfer 84:207–216
Hsu YY, Graham RW (1961) An analytical and experimental study of the thermal boundary layer and ebullition cycle in nucleate boiling. NASA TN D-594
Hwan YW, Kim MS (2006) The pressure drop in micro-tubes and correlation development. Int J Heat Mass Transfer 49:1804–1812
Inasaka F (1993) Critical heat flux of subcooled flow boiling in water under uniform heating conditions. Papers Ship Res Inst 30(4):1–69
Inasaka F, Nariai H (1987) Critical heat flux and flow characteristics of subcooled flow boiling in narrow tubes. JSME Int J 30:1595–1600
Inasaka F, Nariai H (1989) Critical heat flux of subcooled flow boiling with water. Proc NURETH-4 1:115–120
Jens WH, Lottes PA (1951) Analysis of heat transfer burnout drop and density data for high pressure water. US ANL Rep 4627
Kakac S, Bon B (2008) A review of two-phase flow dynamic instabilities in tube boiling systems. Int. J. Heat Mass Transfer 51:399–433
Kandlikar SG (2002) Fundamental issues related to flow boiling in mini-channels and micro-channels. Exp Thermal Fluid Sci 26:389–407
Kandlikar SG, Steinke ME, Tian S, Campbell LA (2001) High speed photographic observation of flow boiling of water in parallel mini-channels. In: 35th Proceeding of National Heat Transfer Conference, ASME, New York
Kandlikar SG, Balasubramanian P (2004) An extension of the flow boiling correlation to transition, laminar and deep laminar flows in mini-channels and micro-channels. Heat Transfer Eng 25:86–93
Kandlikar SG, Mizo V, Cartwright M, Ikenze E (1997) Bubble nucleation and growth characteristics in subcooled flow boiling water. National Heat Transfer Conference HTD-342. ASME, New York, pp 11–18
Kandlikar SG (2006) Nucleation characteristics and stability considerations during flow boiling in micro-channels. Exp. Thermal and Fluid Science 30:441–447
Katto Y, Ohno H (1984) An improved version of the generalized correlation of critical heat flux for the forced convective boiling in uniformly heated vertical tubes. Int J Heat Mass Transfer 27:1641–1648
Kays WM, Krawford ME (1993) Convective heat and mass transfer. McGraw-Hill, New York
Kennedy JE, Roach GM, Dowling ME, Abdel-Khalik SI, Chiaasiaan SM, Jeter SM, Quershi ZH (2000) The onset of flow instability in uniformly heated horizontal micro-channels. Trans ASME J Heat Transfer 122:118–125
Klausner JF, Mei R, Bernard D, Zeng L (1993) Vapor bubble departure in forced convection boiling. Int J Heat Mass Transfer 36:651–661

Klein D, Hetsroni G, Mosyak A (2005) Heat transfer characteristics of water and APG surfactant solution in a micro-channel heat sink. Int J Multiphase Flow 31:393–415

Kosar, A, Kuo, CJ, Peles, Y (2005) Boiling heat transfer with reentrant cavities. Int. J. Heat Mass Transfer 48:4867–4886

Kuo, CJ, Peles, Y (2007) Local measurements of flow boiling in structured surface micro-channels. Int. J. Heat Mass Transfer 50:4513–4526.

Kureta M (1997) Critical heat flux for flow boiling of water in small diameter tubes under atmospheric pressure. Dissertation, Kyoto University (in Japanese)

Kutateladze SS (1963) Fundamentals of heat transfer. Edward Arnold, London

Lazarek GM, Black SH (1982) Evaporative heat transfer, pressure drop and critical heat flux in a small vertical tube with R-113. Int J Heat Mass Transfer 25:945–959

Lee HC, Oh BD, Bae SW, Kim MH (2003) Single bubble growth in saturated pool boiling on a constant wall temperature surface. Int J Multiphase Flow 29:1857–1874

Lee HJ, Lee SY (2001a) Pressure drop correlations for two-phase flow within horizontal rectangular channels with small heights. Int J Multiphase Flow 27:782–796

Lee HJ, Lee SY (2001b) Heat transfer correlation for boiling flows in small rectangular horizontal channels with low aspect ratios. Int J Multiphase Flow 27:2043–2062

Lee J, Mudawar I (2005a) Two-phase flow in high-heat-flux micro-channel heat sink for refrigeration cooling applications. Part I: pressure drop characteristics. Int J Heat Mass Transfer 48:928–940

Lee J, Mudawar I (2005b) Two-phase flow in high-heat-flux micro-channel heat sink for refrigeration cooling applications. Part II: heat transfer characteristics. Int J Heat Mass Transfer 48:941–955

Lee PC, Tseng FC, Pan C (2004) Bubble dynamics in microchannels. Part 1: single microchannel. Int J Heat Mass Transfer 47:5575–5589

Lezzi AM, Niro A, Beretta GP (1994) Experimental data on CHF for forced convection water boiling in long horizontal capillary tubes. In: Hewitt GF (ed) Heat Transfer 1994: Proceedings of the 10th International Heat Transfer Conference, vol 7, Institution of Chemical Engineers, Rugby, pp 491–496

Li HY, Tseng FC, Pan C (2004) Bubble dynamics in micro-channels. Part II: two parallel microchannels. Int J Heat Mass Transfer 47:5591–5601

Li J, Cheng P (2004) Bubble cavitation in a micro-channel. Int J Heat Mass Transfer 47:2689–2698

Liu D, Lee PS, Garimella SV (2005) Prediction of the onset of nucleate boiling in microchannel flow. Int J Heat Mass Transfer 48:5134–5149

Liu Z, Winterton RHS (1991) A general correlation for saturated and subcooled flow boiling in tubes and annuli, based on a nucleate pool boiling equation. Int J Heat Mass Transfer 34:2759–2766

Lockhart RW, Martinelli RC (1949) Proposed correlation of data for isothermal two-phase two-component flow in pipes. Chem Eng Prog 45:39–48

Lowdermilk WH, Lanzo CD, Siegel BL (1958) Investigation of boiling burnout and flow stability for water flowing in tubes, NACA TN 4382. National Advisory Committee for Aeronautics, Washington, DC

Mei R, Chen W, Klausner JF (1995a) Vapor bubble growth in heterogeneous boiling Int J Heat Mass Transfer 38:909–919

Mei R, Chen W, Klausner JF (1995b) Vapor bubble growth in heterogeneous boiling. Part I: growth rate and thermal fields. Int J Heat Mass Transfer 38:921–934

Mikic BB, Rohsenow WM, Griffith P (1970) On bubble growth rates. Int J Heat Mass Transfer 13:657–666

Mishima K, Hibiki T (1996) Some characteristics of air–water two-phase flow in small diameter vertical tubes. Int J Multiphase Flow 22:703–712

Moriyama K, Inoue A (1996) Thickness of the liquid film formed by growing bubble in a narrow gap between two horizontal plates. J Heat Transfer Trans ASME 118:132–139

Mudawar I, Bowers MB (1999) Ultra-high critical heat flux (CHF) for subcooled water flow boiling. I: CHF data and parametric effects for small diameter tubes. Int J Heat Mass Transfer 42:1405–1428

Nakoryakov VE, Pokusaev BG, Shreiberg IR (2000) Wave propagation in gas–liquid media, 2nd edn. CRC, Boca Raton

Nariai H, Inasak F, Uehara K (1989) Critical heat flux in narrow tubes with uniform heating. Heat Transfer Jpn Res 18:21–30

Nariai H, Inasaka F, Shimura T (1987) Critical heat flux of subcooled flow boiling in narrow tube. ASME JSME Thermal Eng Joint Conf Proc 5:455–462

Nigmatulin IR (1991) Dynamics of multiphase media and 2. Hemisphere, London

Ory E, Yuan H, Prosperetti A, Popinet S, Zaleski S (2000) Growth and collapse of vapor bubble in a narrow tube. Phys Fluids 12:1268–1277

Ozawa M, Akagawea K, Sakaguchi T (1989) Flow instabilities in parallel-channel flow systems of gas-liquid two-phase mixtures. Int J Multiphase Flow 15:639–657

Peles YP (1999) VLSI chip cooling by boiling-two-phase flow in micro-channels. Dissertation, Faculty of Mechanical Engineering, Technion–Israel Institute of Technology, Haifa

Peles YP, Yarin LP, Hetsroni G (2001) Steady and unsteady flow in heated capillary. Int J Multiphase Flow 22:577–598

Peng XF, Hu HY, Wang BX (1997) Boiling nucleation during liquid flow in micro-channels. Int J Heat Mass Transfer 41:101–106

Plesset MS, Zwick SA (1954) The growth of vapor bubbles in superheated. J Appl Phys 25:474–478

Prodanovic V, Fraser D, Salcudean M (2002) On transition from partial to fully developed subcooled flow boiling. Int J Heat Mass Transfer 45:4727–4738

Qu W, Mudawar I (2003a) Measurement and prediction of pressure drop in two-phase micro-channel heat sinks. Int J Heat Mass Transfer 46:2737–2753

Qu W, Mudawar I (2003b) Flow boiling heat transfer in two-phase micro-channel heat sink. I: Experimental investigation and assessment of correlation methods. Int J Heat Mass Transfer 46:2755–2771

Qu W, Mudawar I (2002) Prediction and measurement of incipient boiling heat flux in micro-channel heat sinks. Int J Heat Mass Transfer 45:3933–3945

Qu W, Mudawar I (2004) Measurement and correlation of critical heat flux in two-phase micro-channel heat sinks. Int J Heat Mass Transfer 47:2045–2059

Quiben JM, Thome JR (2007a) Flow pattern based two-phase pressure drop model for horizontal tubes. Part I. Diabatic and adiabatic experimental study. Int. J. Heat and Fluid Flow. 28(5):1049–1059

Quiben JM, Thome JR (2007b) Flow pattern based two-phase pressure drop model for horizontal tubes. Part II. New phenomenological model. Int. J. Heat and Fluid Flow. 28(5):1060–1072

Rayleigh JWS (1917) On the pressure developed in a liquid during the collapse of a spherical cavity. Phil Mag 34:94–98

Revellin R, Thome J. (2008) A theoretical model for the prediction of the critical hat flux in heated micro-channel. Int. J. Heat and Mass Transfer 51:1216–1225

Roach GM, Abdel-Khalik SI, Ghiaasiaan SM, Dowling MF, Jeter SM (1999) Low-flow critical heat flux in heated microchannels. Nucl Sci Eng 131:411–425

Robinson AJ, Judd RL (2001) Bubble growth in a uniform and spatially distributed temperature field. Int J Heat Mass Transfer 44:2699–2710

Sato T, Matsumura H (1964) On the conditions of incipient subcooled-boiling with forced convection. Bull Jpn Soc Mech Eng 7:392–398

Sedov LI (1993) Similarity and dimensional methods in mechanics, 10th edn. CRC, Boca Raton

Shah MM (1982) Chart correlation for saturated boiling heat transfer: equation and further study. ASHRAE Trans 88:185–196

Shah MM (1987) Improved general correlation for critical heat flux during upflow in uniformly heated vertical tubes. Int J Heat Fluid Flow 8:326–335

Shah RK, London AL (1978) Laminar flow forced convection in ducts: a source book for compact heat exchanger analytical data. Advances in Heat Transfer, suppl 1. Academic, New York

Sher I, Hetsroni G (2002) An analytical model for nucleate pool boiling with surfactant additives. Int J Multiphase Flow 28:699–706

Shuai J, Kulenovic R, Droll M (2003) Heat transfer and pressure drop for flow boiling of water in narrow vertical rectangular channels. In: Proceedings for 1st International Conference on Micro-channels, Rochester, New York, 24–25 April 2003, ICMM 2003-1084

Staniszewski BE (1959) Nucleate boiling bubble growth and departure MIT DSR Project N7-7673, Technical Report N16

Steinke ME, Kandlikar SG (2004a) Control and effect of dissolved air in water during flow boiling in micro-channels. Int J Heat Mass Transfer 47:1925–1935

Steinke M, Kandlikar SG (2004b) An experimental investigation of flow boiling characteristics of water in parallel micro-channels. Trans ASME J Heat Transfer 126:518–526

Stoddard RM, Blasick AM, Ghiaasiaan SM, Abdel-Khalik SI, Jeter SM, Dowling MF (2002) Onset of flow instability and critical heat flux in thin horizontal annuli. Exp Thermal Fluid Sci 26:1–14

Su S, Huang S, Wang X (2001) Study of boiling incipience and heat transfer enhancement in forced flow through narrow channels. Int J Heat Mass Transfer 31:253–260

Revellin R, Agostini B, Thome J (2008) Elongated bubbles in micro-channels Part II: Experimental study and modeling of bubble collisions. Int. J. Multiphase Flow 34:602–613

Thom JRS, Walker WM, Fallon TA, Reising GFS (1965) Boiling in subcooled water during flow up heated tubes or annuli. In: Symposium on Boiling Heat Transfer in Steam Generating Units and Heat Exchangers, Manchester, 15–16 September 1965. IMechE London

Thome JR, Dupont V, Jacobi AM (2004) Heat transfer model for evaporation in micro-channels. Part I: Comparison with database. Int J Heat Mass Transfer 47:3375–3385

Thompson B, Macbeth RV (1964) Boiling water heat transfer – burnout in uniformly heated round tubes: a compilation of world data with accurate correlations, AEEW-R 356. United Kingdom Atomic Energy Authority, Winfrith, UK

Thorncroft GE, Klausner JF, Mei R (1998) An experimental investigation of bubble growth and detachment in vertical upflow and downflow boiling. Int J Heat Mass Transfer 41:3857–3871

Thorncroft GE, Klausner JF, Mei R (2001) Bubble forces and detachment models Multiphase Sci Technol 13:35–76

Tran TN, Chyu M-C, Wambsganss MW, France DM (2000) Two-phase pressure drop of refrigerants during flow boiling in small channels: an experimental investigation and correlation development. Int J Multiphase Flow 26:1739–1754

Tran TN, Wambsganss MW, France DM (1996) Small circular and rectangular channel boiling with two refrigerants. Int J Multiphase Flow 22:485–498

Unal HC (1975) Determination of the initial point of net vapor generation in flow boiling system. Int J Heat Mass Transfer 18:1095–1099

van Stralen SJD (1966) The mechanism of nucleate boiling in pure liquids and in binary mixtures. Int J Heat Mass Transfer 9:995–1046

Vandervort CL, Bergles AE, Jensen MK (1994) An experimental study of critical heat flux in very high heat flux subcooled boiling. Int J Heat Mass Transfer 37:161–173

Volmer M, Weber A (1926) Nucleus formation in superheated systems. Z Phys Chem 119:277–281

Wang G, Cheng P, Bergles AE 2008 Effects of inlet outlet configurations on flow boiling instability in parallel micro-channels. Int. J. Mass Transfer 51:2267–2281

Warrier GR, Pan T, Dhir VK (2002) Heat transfer and pressure drop in narrow rectangular channels. Exp Therm Fluid Sci 26:53–64

Wojtan L, Revellin R, Thome J (2006) Investigation of critical heat flux in single uniformly heated micro-channels. Exp. Therm, Fluid Sci. 30:765–774

Wu HY, Cheng P (2004) Boiling instability in parallel silicon micro-channels at different heat flux. Int J Heat Mass Transfer 47:3631–3641

Wu HY, Cheng P (2003a) Liquid/two-phase/vapor alternating flow during boiling in micro-channels at high heat flux. Int Comm Heat Transfer 39:295–302

Wu HY, Cheng P (2003b) Visualization and measurements of periodic boiling in silicon microchannels. Int J Heat Mass Transfer 46:2603–2614
Wu WT, Yang YM (1992) Enhanced boiling heat transfer by surfactant additives. In: Proceedings Engineering Foundation Conference On Pool and External Flow Boiling, Santa Barbara, California, 1992, pp 361–366
Yang YM, Maa JR (2003) Boiling heat transfer enhancement by surfactant additives. In: Proceedings of the 5th International Conference Boiling Heat Transfer, ICBHT, Montego Bay, Jamaica, 4–8 May 2003
Ye H, Naguib N, Gogotsi Y (2004) TEM study of water in carbon nanotubes. JEOL News 39:2–7
Yen T-H, Shji M, Takemura F, Suzuki Y, Kasagi N (2006) Visualization of convective boiling heat transfer in single micro-channels with different shaped cross-sections. Int J Heat Mass Transfer 49:3884–3894
Yen T-H, Kasagi N, Suzuki Y (2003) Forced convective boiling heat transfer in micro-tubes at low mass and heat fluxes. Int J Multiphase Flow 29:1771–1792
Yu W, France DM, Wambsganss MW, Hull JR (2002) Two-phase pressure drop, boiling heat transfer, and critical heat flux to water in a small-diameter horizontal tube. Int J Multiphase Flow 28:927–941
Zel'dovich YaB (1943) On the theory of new phase formation: cavitation. Acta Physicochim URSS 18:1–7
Zeng LZ, Klausner JF, Mei R (1993) A unified model for the prediction on bubble detachment diameters in boiling system. Part I: Pool boiling. Int J Heat Mass Transfer 36:2261–2270
Zhang W, Hibiki T, Mishima K, Mi Y (2006) Correlation of critical heat flux for flow boiling of water in mini-channels. Int J Heat and Mass Transfer 49:1058–1072
Zhang J, Manglik RM (2005) Additive absorption and interfacial characteristics of nucleate pool boiling in aqueous surfactant solutions. J Heat Transfer 127: 684–691
Zhang L, Koo J-M, Jiang L, Asheghi M, Goodson KE, Santiago JK (2002) Measurements and modeling of two-phase flow in micro-channels with nearly constant heat flux boundary conditions. J Microelectromech Syst 11: 12–19
Zuber N (1961) The dynamics of vapor bubbles in non-uniform temperature fields. Int J Heat Mass Transfer 2:83–98

Nomenclature

a	Half of channel height
b	Half of channel width
c_p	Heat capacity at constant pressure
C	Parameter C (Eqs. 6.39, 6.50)
Co	Convection number (Eqs. 6.57, 6.58)
d	Diameter
d_0	Initial diameter of bubble
d_*	Characteristic size
D	Subcooling parameter at ONB point
G	Mass flux, mass velocity of liquid plus vapor
g	Acceleration due to gravity
h	Heat transfer coefficient
h_LG	Latent heat
k	Thermal conductivity, Boltzman constant
k_s	Surface roughness

L	Channel length
m	Mass flow rate
M	Mass, constant (Eqs. 6.9, 6.13)
MAE	Mean absolute error
No	Molecular number per unit volume
P	Pressure
P_s^*	Pressure 1 bar
P_s^+	Dimensionless pressure
q	Heat flux
r	Bubble radius
r_b	Radius of bubble embryo
r_c	Radius of cavity
r_{max}^*	Largest cavity radius
t	Time
t^*	Dimensionless period
T	Temperature
T_f	Fluid temperature in annular space
T_∞	Temperature of surrounding fluid
u	Streamwise velocity
U	Average flow velocity in micro-channel, uncertainty
U_b	Velocity of bubble tail
U_{LS}	Superficial liquid velocity
U_{GS}	Superficial gas velocity
v	Spanwise velocity
x	Vapor quality
X	Martinelli parameter
x, y, z	Cartesian coordinates
$\mathrm{Bn} = \delta\sqrt{\frac{g(\rho_L - \rho_G)}{\sigma}}$	Bond number
$\mathrm{Bo} = \frac{q}{Gh_{LG}}$	Boiling number
$\mathrm{Eo} = \frac{\delta^2 g(\rho_L - \rho_G)}{\sigma}$	Eotvos number
$\mathrm{Fo} = \frac{2\alpha t}{\delta^2}$	Fourier number
$\mathrm{Ja} = \frac{(T_\infty - T_s)\rho_L c_{pL}}{\rho_G h_{LG}}$	Jacob numer
$\mathrm{Nu} = \frac{h d_h}{k}$	Nusselt number
$\mathrm{Po} = \lambda \cdot \mathrm{Re}$	Poiseuille number
Pr	Prandtl number

$\mathrm{Re} = \dfrac{U d_\mathrm{h}}{\nu}$	Reynolds number
$\mathrm{St}_\mathrm{ONB} = \dfrac{q_\mathrm{ONB}}{\rho_\mathrm{L} u_\mathrm{in} c_\mathrm{p} (T_\mathrm{s} - T_\mathrm{in})}$	Stanton number at ONB point
$\mathrm{We} = \dfrac{G^2 d_\mathrm{h}}{\sigma \rho}$	Weber number

Greek symbols

α	Thermal Diffusivity, exponent
β	Ratio of channel depth to width, exponent
ΔP	Pressure drop
ΔT	Temperature difference
ΔT^*_ONB	Wall superheat at pressure of 1 bar
δ	Gap size, liquid thickness, thermal boundary layer
δ^*	Dimensionless liquid thickness
η	Dimensionless distance from the wall
θ	Temperature difference, contact angle
μ	Dynamic viscosity
ν	Kinematic viscosity
Π	Dimensionless parameter (Eqs. 6.43, 6.44)
ρ	Density
σ	Surface tension
τ_w	Wall shear stress
Φ_L	Two-phase pressure drop multiplier
ψ	Parameter (Eqs. 6.5, 6.7)

Subscripts

av	Average
B	Bubble, bulk
c	Cavity, circular, center
CHF	Critical heat flux
CMC	Critical micelle concentration
crit	Critical
exp	Experimental
G	Gas
h	Hydraulic, heated
heat	Heat
het	Heterogeneous
hom	Homogeneous

in	Inlet
L	Liquid
LG	Liquid/gas
max	Maximum
min	Minimum
n	Spanwise
out	Outlet
ONB	Onset of nucleate boiling
p	Streamwise
pred	Predicted
s	Saturation
s,B	Saturation in the bubble
sub	Subcooled
sub,ONB	Subcooled at ONB point
tp	Two-phase
tp,a	Acceleration component
tp,cor	Uniform circumferential heating
tp,f	Friction component
vt	Laminar liquid–turbulent vapor
vv	Laminar liquid–laminar vapor
w	Wall
w,ONB	Wall at ONB point
3	Three sides heating
4	Four sides heating